Author:
Hartley, Jamie W

Title:
Crashworthiness Improvements to Automotive Sandwich Composites Using Tufting

Author:
Hartley, Jamie W

Title:
Crashworthiness Improvements to Automotive Sandwich Composites Using Tufting

Crashworthiness Improvements to Automotive Sandwich Composites Using Tufting

By

Jamie William Hartley

Department of Aerospace Engineering

UNIVERSITY OF BRISTOL

A dissertation submitted to the University of Bristol in accordance with the requirements of the degree of Doctor of Philosophy in the Faculty of Engineering

September 2018

Word count: 50,211

ABSTRACT

With the growing demand for battery electric vehicles (BEVs), a focus within the automotive industry is ensuring vehicle performance can meet customer demands. Electric powertrains are inevitably much heavier than existing internal combustion systems, which severely limits the range of the vehicle. To compensate for this, automotive manufacturers are now looking to exploit fibre-reinforced composites (FRPs) to reduce the structural weight of the vehicle.

One route to achieving this is using lightweight composite sandwich structures, which show great potential because of their good mechanical performance and low density, as well good damping properties. However, relatively poor interfacial properties render these structures unreliable when it comes to the demanding safety requirements that must be in place to protect the vehicle occupants during a crash. Through-thickness tufting has recently been demonstrated to be a promising method for reinforcing dry sandwich preforms, showing improvements in the crash performance whilst offering improvements in processability over more conventional through-thickness reinforcement methods. However, while promising results have been demonstrated there is still much to be understood of the failure behaviour of these structures, as well as the influence that design and manufacturing variables can have on this.

This work aims to develop a deeper understanding in this field, to help influence and improve the future design of these structures. This is achieved using several novel experimental techniques designed to capture the behaviour of these structures at a level of detail not seen before. Testing has looked at the failure mechanics of tufted sandwich structures, as well as the influence of the tuft structure and material selection from an automotive-focused viewpoint. The output of this work proposes desired design choices and failure behaviour for high energy absorption, as well as possible design improvements for increased structural efficiency, and offering suggestions for the future direction of research.

DEDICATION AND ACKNOWLEDGEMENTS

First and foremost, I would like to thank my project supervisors, James Kratz, Ivana Partridge and Carwyn Ward for providing me the opportunity to take up this research project, and for their valued support, advice, technical input and opportunities throughout.

Secondly a thank you to my fellow cohort members, Jon, Giampaolo, Laura, Bradley, Shash, Manu, Mamat, Jakub, Emily, Xun, and Evangelos, as well as the other students, academics and support staff of both the CDT and the wider ACCIS community, for creating an environment in which it has been a joy to work in for the past five years. A special thank you must also go to Ian Chorley who frequently went out of his way to support all lab-based work, and to Harry Clegg for the countless hours operating the tufting equipment at the NCC.

Finally, a thank you to my family for all your support and encouragement for the past five years. Without you this wouldn't have been possible.

This work was made possible through funding from the *EPSRC Centre for Doctoral Training in Advanced Composites for Innovation and Science* (Grant: EP/G036772/1) and the *EPSRC Centre for Innovative Manufacturing in Composites (CIMComp)* (Grant: EP/IO33513/1). Elements of this work were also conducted within the framework of a G8-2012 project on "*Material efficiency: A first step towards sustainable manufacturing*", between the University of Southern California, McGill University, the Technische Universitat Munchen, and the University of Bristol. Funding for this work was provided by the EPSRC, under grant no. EP/K025023/1. Additional financial support to present the results of Chapter 7 at the SAMPE USA Technical Conference 2016 was provided by the University of Bristol Alumni Association.

AUTHOR'S DECLARATION

I declare that the work in this dissertation was carried out in accordance with the requirements of the University's Regulations and Code of Practice for Research Degree Programmes and that it has not been submitted for any other academic award. Except where indicated by specific reference in the text, the work is the candidate's own work. Work done in collaboration with, or with the assistance of, others, is indicated as such. Any views expressed in the dissertation are those of the author.

SIGNED: ..... DATE: .....

TABLE OF CONTENTS

LIST OF TABLES

LIST OF FIGURES

ABBREVIATIONS

ACCIS	Bristol Composites Institute (ACCIS)
ANOVA	Analysis of Variance
ASTM	American Society for Testing and Materials
BEV	Battery Electric Vehicle
BIW	Body-in-White
CAI	Compression After Impact
CFE	Crush Force Efficiency
CFRP	Carbon-Fibre Reinforced Polymer
DCB	Double Cantilever Beam
DIC	Digital Image Correlation
DoE	Design of Experiments
ELV	End-of-Life Vehicle
EU	European Union
FRP	Fibre Reinforced Polymer
GFRP	Glass-Fibre Reinforced Polymer
GTR	Global Technical Regulation
HPRTM	High-Pressure Resin Transfer Moulding
NCAP	New Car Assessment Programme
NCC	(UK) National Composites Centre
NCF	Non-Crimped Fabric
PAN	Polyacrylonitrile

PHEV	Plug-in Hybrid Electric Vehicle
PMI	Polymethacrylimide
PVC	Polyvinylchloride
RTM	Resin Transfer Moulding
SEA	Specific Energy Absorption
TTR	Through-Thickness Reinforcement
VARTM	Vacuum-Assisted Resin Transfer Moulding

ASSOCIATED PUBLICATIONS

Journal Articles

Hartley, J.W., Kratz, J., Ward, C. and Partridge, I.K., 2017. Effect of tufting density and loop length on the crushing behaviour of tufted sandwich specimens. Composites Part B: Engineering, 112, pp.49-56.

Conference Publications

Hartley, J, Kratz, J, Ward, C & Partridge, I, 2015, 'Observing process parameter effects in tufted sandwich structures'. In: The International Conference on Manufacturing Advanced Composites (ICMAC). Bristol, UK. (Presentation Only)

Tan, G, **Hartley, J**, Withers, E, Kratz, J & Ward, C, 2015, 'Towards the development of an instrumented test bed for tufting visualisation'. in: Proceedings of the SAMPE Europe Conference 2015. Amiens, France.

Hartley, J, Bogucki, P, Snudden, JP, Withers, EM, Ward, C & Kratz, J, 2016, 'Reclaiming in-process composite waste for use in energy absorbing sandwich structures'. in: Proceedings of the SAMPE Technical Conference 2016. Long Beach, USA.

Hartley, J, Tse, G, Kratz, J, Ward, C & Partridge, IK, 2016, 'Column Interaction in Tufted Sandwich Structures Under Edgewise Loading'. in: 17th European Conference on Composite Materials (ECCM17). Munich, Germany.

Hartley, J, Dyson, M & Ward, C, 2017, 'Improving the Performance of Tufted Composite Sandwich Structures'. in: 21st International Conference on Composite Materials (ICCM21). Xi'an, China.

Hartley, J & Ward, C, 2017, 'Improving the Understanding of Tufted Energy Absorbing Sandwich Structures'. in: Proceedings of the thirty-second technical conference of the American Society for Composites (ASC), pp. 2260-2273. West Lafayette, USA.

RELATED WORKS

Crash Simulation of Tufted Sandwich Components for Automotive Applications

Jamie Hartley – Extended Research Project 2014

Abstract

A finite element model based at the unit-cell level was created in LS-DYNA to investigate the behaviour of an individual tuft within a sandwich structure under edgewise compression. Optical microscopy was carried out on tufted panels to observe the geometry and dimensions to generate inputs for the model. In conjunction to this, several highly novel small-scale specimens were created, based around individual tufts with varying input parameters and tested in static compression. These were used to explore the effect of changing the tufting parameters as well as being used to validate modelling results. Initial results of the model demonstrated a correlation of the initial peak loading of the individual cell, but no significant impact of the tuft. Experimental testing showed good consistency of results but no clear differences between the varied parameters.

Exploring the effect on the tufting quality by the manufacturing characteristics in the tufting process

George Tan Chee Tong – MEng Final Year Project Student 2015

Abstract

This paper presents a study to investigate the effect of the tufting needle insertion speed on the perceived tufting quality by observing the cross section of a dry sandwich panel. A test frame was developed to simulate the tufting process using a test machine to provide a simple yet effective research platform. The dry skins and core could be observed directly at the cross section and the damage caused could be studied. Sandwich specimens were penetrated by a tufting needle within a speed range of 100 to 1000 mm/min and the resulting tufting results were then rated with a quality matrix to produce a tufting quality rating. The overall results revealed a trend where the tufting quality is better at a higher penetration speed. There was no significant difference between the reaction forces of the needle, recorded using a load cell attached to the needle, at different speeds.

Reclaiming in-process composite waste for use in energy absorbing sandwich structures

Philip Bogucki - MEng Final Year Project Student 2016

Abstract

Two types of carbon fibre in-process waste were considered in this investigation looking at their use in sandwich structures for energy absorption. The first was strips of unidirectional dry fibre scrap taken directly off the ply cutter forming a component in patches. The second was a mat made from those scraps after being extensively reprocessed. Quasi-static and dynamic edgewise crushing tests were performed on four different types of house shaped sandwich structures using these materials, where it was found that the lower quality of material of the face sheets due to reprocessing, led to worse energy absorption characteristics. The main reason for this was the skin and core de-bonding in the sandwich specimens, which was attempted to be solved using tufting. This led to promising results with all the specimens showing similarly good energy absorption characteristics, higher than the control un-tufted specimen.

Exploring tufted sandwich structures in edgewise compression by novel failure control

Gavin Tse - MEng Final Year Project Student 2016

Abstract

This paper investigates the progressive failure mechanisms in sandwich panels reinforced through thickness via tufting, to develop an understanding of the energy absorption mechanism. A detailed test of tufted and untufted sandwich structures demonstrated the importance of Through-Thickness Reinforcement (TTR). Sandwich coupons of varying length and number of tufts were loaded uniaxially in static compression. Test results indicated that the inclusion of tufts in sandwich coupons allowed the stable progressive collapse of the structure and confirmed the existence of column drift and column rotational recovery. This enabled an element of controllability in the collapse of tufted structures as the failure mechanisms become more predictable, significantly improving energy absorption capabilities compared to its untufted equivalent.

Exploring the effects of column interaction in tufted sandwich cores

Matthew J. Dyson - MEng Final Year Project Student 2017

Abstract

This paper explores the use of a test method for observing the effects of resin column drift within a foam core and the results obtained from these tests. The results allow for further investigations into other components of a tufted panel to design and predict the performance of an optimal tufting configuration. A test method has been developed which has been used on several different column configurations with an acceptable coefficient of variation. Further improvements in the test method by providing more constraint to the foam sample and inserting the pins with more accuracy have been identified. The results reiterate previous test results which show an increase in energy absorption with the addition of additional tufts (columns). Furthermore, the results showed that reducing the gap between columns causes high levels of stress between them.

Chapter 1 Introduction

1.1 Background

To date, the development of alternative, cleaner power systems for automotive vehicles has been slow, but the industry is now coming under renewed pressure to make vehicles more environmentally friendly and efficient. For instance, the European Union has ruled that CO_2 emissions need to be reduced below 95 g/km (new vehicles averaged 118.5 g/km in 2017 [1]) by 2021, while in the US it is hoped that vehicles will achieve an efficiency target of 54.5 mpg (currently averaging 28.9 mpg) by 2025 [2]. The threat of complete bans on petrol and diesel cars in the near future is also quickly becoming a reality [3,4], and has begun to drive automotive manufacturers towards developing alternative powertrains. Early attempts at the deployment of plug-in hybrids (PHEV) and battery electric vehicles (BEV) have proven successful and uptake has grown rapidly year-on-year (Figure 1-1) [5]. There is now a clear drive within the industry to move towards electric power for forthcoming generations of vehicles [6].

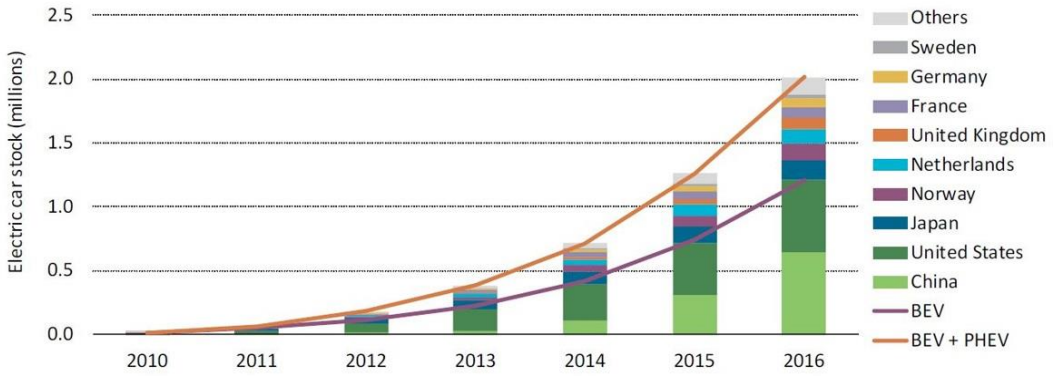

Figure 1-1: The worldwide growth in production of plug-in hybrid (PHEV) and battery-powered electric (BEV) vehicles between 2010-2016 [5].

However, such a substantial change to the industry will bring many significant challenges which are not easily overcome. On the one hand, significant upgrades to infrastructure are needed to meet rapidly increasing charging demands, whilst at a design level one of the greatest problems that needs to be overcome is delivering vehicle performance to an acceptable level that rivals existing combustion engines. Whilst lithium-ion battery technology is gradually maturing, weight increases of 100 kg over combustion-based powertrains are typical, which has a significant knock-down on the vehicle efficiency. Poor energy efficiency leads to lower vehicle ranges and more frequent 'refuelling' stops, with

only a very few BEVs capable of achieving a range of 300 miles, well below that of an average combustion-powered vehicle. This does not sit well in the eyes of the consumer, creating a negative image of electric vehicles over their less environmentally friendly counterparts.

Consequently, reducing vehicle weight becomes a very important factor in the design of electric vehicles. What must be overcome is the negative weight spiral that is created by the integration of a relatively heavy powertrain into the vehicle. To support this additional weight, the vehicle structure must be strengthened, which in turn increases the overall weight of the vehicle. To be able to move this increased mass, an increase in power is required which means a larger power supply must be integrated, and so the negative spiral continues. If either the vehicle weight or battery performance could be improved then this effect can be reversed, and a more optimised vehicle performance is possible.

Whilst improving the performance of existing battery technology is currently a key area of research [7–9], major breakthroughs are not anticipated in the near future. This emphasises the need for designers to focus on reducing structural weight to meet performance requirements. Simply retrofitting electric motors in existing vehicles will not be effective, and will instead require a major shift in how future vehicles are designed and manufactured [10].

1.2 Automotive Composites

To achieve lighter-weight vehicle structures it is becoming increasingly likely that automotive manufacturers will look to exploit advanced composite materials in future designs. Fibre-reinforced polymer composites (FRPs) are rapidly becoming the material of choice across many engineering sectors. In the aerospace sector for example, next generation aircraft now feature as much as 50% of their structural weight as composite materials [11], whilst in the renewable energy sector, composites have provided a near exponential growth in size and performance of wind turbine blades, reaching as much as 90 metres in length [12]. The use of these materials is also seeing rapid growth in other sectors, such as in the civil engineering sector for the construction of bridges and buildings [13,14], as well as many high performance space applications [15].

Figure 1-2: Composite materials play a major role in the manufacture of current generation aircraft, such as the Airbus A350. (Left [16]**, Right** [17]**).**

In contrast, whilst these materials are present within the automotive industry, there has up until now existed a barrier to their widespread use. Instead manufacturers have made a conscious decision to rely on tried and tested metallic structures for all but the most expensive, high-performance and low-production rate vehicles. Currently composite use is dominated by racing applications, where a "win at all costs attitude" dictates that performance is crucial and lightweight structures are the necessary means to achieving this.

For some time Formula 1 teams have been at the forefront of composite development [18], where composite materials are almost exclusively used to reach the highest possible performance. Composite use in Formula 1 originates in the 1960s, when glass reinforced plastic combined with aluminium was used to build the vehicle chassis. The introduction of the first ever carbon fibre chassis to the McLaren MP4 in 1981 began a rapid increase in the use of the material, with teams quickly realising the benefits attainable. In the 1990s, McLaren developed composite suspension members, which are now used by every team, the improved fatigue properties of composites combined with their low weight made these components a significant improvement over the steel counterparts they replaced [18]. Carbon fibre composites now make up as much as 85% of the total volume of a Formula 1 vehicle, including components such as the chassis, bodywork, cooling ducts, crash structures, suspension, gearbox, and the steering wheel and column [18].

Figure 1-3: High-performance composites have become the dominant materials within Formula 1 racing cars. Left: McLaren MP4 (1981) [19]**. Right: McLaren MCL32 (2017)** [20]**.**

Despite the growth in technology in the motorsport industry, high performance composites have not seen such widespread use on the road. The very first production car body manufactured from fibre-reinforced composite materials was the Chevrolet Corvette, which was manufactured using a glass fibre reinforced polymer composite (GFRP) in 1953. Similarly, the Dodge Viper released in 1992 used fibreglass panels to form the body of the vehicle. Aside from these, use in production vehicles have been very much limited to the supercar market, through manufacturers such as McLaren, Bugatti, Lamborghini and Pagani. In the early 90s, the McLaren F1 demonstrated the first carbon fibre monocoque seen on a production road vehicle [21]. This development led to a series of descendants, including the 12C and 650s models, which also feature a single piece carbon fibre chassis (pressed in a single step process) called the MonoCell, and the P1 model which includes a carbon fibre roof structure too (MonoCage). Lamborghini has followed a similar development timeline, beginning with its Countach prototype in 1983 through to the fully carbon fibre monocoque found in the Aventador today [22]. Lamborghini recently adopted the Forged Composite process [23], a discontinuous fibre sheet moulding process capable of producing composite parts in a matter of minutes and increasing production rates to the order of 2,000 per year.

A more recent development within the industry is BMW's breakthrough use of composites in the development of the i-series BEVs. Both the BMW i3 and i8 models feature extensive use of carbon fibre, including a full carbon fibre passenger cell. The i3 model has a current production volume of approximately 30,000 vehicles per year and is the largest-volume production car to make such extensive use of carbon fibre [24]. For BMW to be able to achieve numbers on this scale it has had to create one of the largest and most complex supply chains for composites in the automotive industry, from the basic precursors, right through to the fabrication and assembly of the structures themselves [25]. Manufacture of the polyacrylonitrile (PAN) precursor takes place in Japan through a joint venture between Mitsubishi Rayon and SGL. This is then sent to a facility in the USA, jointly owned by

BMW and SGL, which produces carbon fibre tows. At an SGL facility in Germany, the raw carbon fibre is converted into several fabric forms, which are then cut, kitted and stacked ready for manufacture. Primary part manufacture takes place in Leipzig, Germany, using high pressure resin transfer moulding (HP-RTM). The incoming ply kits are stapled, preformed in a mould using thermoplastic binder, and then trimmed to near net-shape. The preforms are placed into a mould and resin injected at pressures of up to 40 bars. A hydraulic press is used to apply pressure to the part during cure, which can be achieved in under 10 minutes if an elevated temperature is used. The cured parts are then assembled into the final full passenger cell structure using adhesive bonding. An example of preparation of the preform as well as the final assembled structure are shown in Figure 1-4.

Figure 1-4: Manufacturing process of the BMW i3. Left: positioning of assembled ply kits within a mould [25]**. Right: The fully assembled carbon fibre passenger cell** [26]**.**

Despite the breakthroughs made with both the i3 and i8, the future development of composite vehicle manufacture is not clear, with BMW now working with hybrid solutions that reduce the amount of carbon fibre used to keep costs low. The latest BMW 7-series, for example, features a 'carbon core', a predominantly steel framework with discrete carbon reinforcement integrated in key locations [27]. Whilst new electric vehicles are in the pipeline it remains to be seen how BMW will approach the structural design of these in the future.

Aside from BMW's success, there is a current trend of innovation and novel processing techniques within the industry to try to increase process efficiency and enable the use of composites to grow. For example, the iStream® programme developed by Gordon Murray Design [28] features hybrid metallic frames with composite sandwich panels as shown in Figure 1-5. The resulting lightweight structure meets the demands of a modern automotive vehicle, but the streamlined process can achieve this at a fraction of the cost and with a

single automated production line. The technology can produce composite parts with a cycle time of just 100 seconds, allowing annual production volumes up to 350,000 units per year.

Figure 1-5: An example of a vehicle chassis produced using the iStream® process [28]**. A metallic frame is supported by composite sandwich panels.**

Another example is Bright Lite Structures, who use a patented press process to form complex carbon sandwich structures with cycle times under 5 minutes [29]. A novel polycarbonate honeycomb structure is used for the sandwich core, onto which the carbon skins are press formed (Figure 1-6). The process integrates recycled carbon fibre into the skins of the sandwich, whilst the low pressures required enable larger components to be manufactured and for a lower cost than high pressure methods. The method also enables self-joining components to be produced, eliminating the need for jigging and simplifying assembly.

Figure 1-6: Recycled carbon facesheets and polycarbonate honeycomb core used by Brite Lite Structures (left). Press formed sandwich structure after cure (right) [29]**.**

1.3 The Challenges of Using Composite Materials:

As the development of the BMW i-series has shown, transferring composite technology to the mass market is an incredibly difficult undertaking for the industry. For automotive manufacturers to seriously consider FRPs as the material of choice for future vehicle structures there are still several significant challenges that must be overcome. At present, the complex and expensive manufacturing processes required to mass produce, the high costs relative to metallic structures, and the often-unpredictable mechanical behaviour of composite materials are heavily restricting the use of these materials on a larger scale.

1.3.1 Manufacturability

One area in which the automotive industry stands out when compared to other engineering fields is the rapid production rates that must be achieved to maintain profitability and meet customer demand. With global vehicle production rates measured in millions of units per year, vehicles need to be continuously rolling off the production line to meet demand, making every step of the manufacturing process time critical. In Formula 1, like the aerospace industry, the preference is to use autoclave cured parts to maximise performance, but the substantial costs as well as long cycle times make this process unfeasible in a mass-production environment [30]. Road-car manufacturers must therefore look to alternative methods that deliver suitable performance but fit within the tight production windows imposed. Recent developments such as snap-curing resins, out-of-autoclave processing and thermoplastics have gone some way towards driving down cycle times [24]. High-pressure injection methods are proving popular, delivering fast cycle times, tight geometrical tolerances, as well as the high-quality finish that automotive surfaces require [31].

Whilst the manufacturing process is one critical aspect that must be considered, the raw materials that feed this must also be taken into consideration. The first and foremost issue is the raw material cost, with CFRP costing more than ten times that of traditional automotive materials such as aluminium and magnesium, as well as high strength steels and other fibre-reinforced plastics [24]. The other challenge is being able to develop an adequate supply chain to meet the increased demand. As of 2016 the global market demand for carbon fibre totalled 70,000 metric tonnes, but with an increase in automotive manufacture, amongst others, this is expected to grow to as much as 125,000 metric tonnes by 2025 [32]. Material suppliers are thus rapidly expanding their production capacity to meet this expected growth.

1.3.2 Sustainability and Recycling

Whilst the industry is coming under increasing pressure to reduce emissions, there are also new rules in place to ensure vehicle manufacture is more sustainable. The recent European Union (EU) end-of-life vehicle directive (ELV) has dictated that from 2015, 85% of a vehicle's weight must be reusable or recyclable [33]. One area in which composite materials do not perform well is end-of-life recycling, and with the growing need for composites in the industry, there is now added pressure for the maturation of recycling technologies to meet these targets [34]. Until now, landfill disposal has been the favoured method for dealing with composite waste. However, the cost of landfill has risen to as much as 130 £/tonne [35], and is even banned in some countries, such as Germany, to encourage the development of better processes. As current composite parts predominantly feature thermoset resin systems, they cannot simply be melted down and reprocessed like metals or thermoplastics. Instead more complex techniques such as chemical (solvolysis), thermal (pyrolysis) or mechanical (grinding) processes must be used [36]. These methods are often energy intensive and can have a significant detrimental effect on the material properties of the resultant by-products. Because of this, closed-loop recycling of composite parts is still relatively underutilised, with the recycled products preferred for low value applications such as secondary structural parts and fillers.

Recycling of thermoplastic matrices can be much easier, through initial mechanical chopping followed by remoulding of the material into a new part [37]. Whilst a reduction in fibre length as well as some degradation of the polymer matrix is possible, mechanical performance has still been shown to meet automotive requirements [38] and retain value. However, the downside of thermoplastics is that due to high processing viscosities they

require very high temperatures and pressures to be manufactured successfully, meaning that currently they are very difficult and costly to work with.

Aside from recycling of end-of-life components, of further concern is the relatively high waste content produced during manufacture. This scrap results from material off-cuts and trimming operations, as well as out-of-date feedstocks, and has been reported to be as much as 50% of the input material [34]. One technique for dealing with this is waste reduction, the principle of ensuring the minimum amount of waste is produced through careful considerations at the design and manufacturing stages. However ultimately process waste cannot be avoided, leaving a large amount of dry or uncured scrap material that isn't used. This has led to a rise in the reforming of composite waste into more useful forms that allows their reuse. Provided the scrap material is not mistreated once it is separated from the cut preforms, it will not require any additional cleaning and should retain its high mechanical properties, potentially making it more valuable than material recycled from end-of-life components [24]. Whilst this waste material is typically only available in smaller fragments after cutting and trimming, these could be directly reapplied as patches within a preform [39]. Another method for reclaiming the scrap is to collect it, break it down into small pieces and reform the fibres into a discontinuous random mat, simplifying its reuse in future parts. Several manufacturers, such as Sigmatex (sigmaRF) and SGL (Recatex™) have already begun to commercialise this process, and BMW currently use this material to manufacture the roof panel in its i-series vehicles [25].

1.3.3 Structural Performance

A further barrier to the uptake of composites within the automotive industry is that whilst the performance benefits of increased strength and stiffness are well understood, fatigue performance and failure predictions are still very difficult to account for [31]. Currently, material models and failure criteria have not yet reached a mature enough level, and so to compensate for this, designers must over-engineer the vehicle structure to ensure adequate safety margins exist, meaning the full potential of these materials is not realised. In fact, this is a concern across many industries where composite materials are used. One reason this is a problem is that automotive composites are currently often not laminate-based but are instead short-fibre bulk materials that do not correspond well with existing damage and failure models. Of further concern is the lack of standardised material systems and test methods, which makes reliable design data scarce.

The lack of failure predictability is particularly of concern when designing for vehicle crash events, as the vehicle structure plays a key role in protecting the occupants. During an impact event, the vehicle structure must absorb the impact energy in a controlled way, to ensure high acceleration forces are not transferred to the occupants. Unlike metals which achieve this by folding, composites absorb energy through several brittle failure mechanisms [40,41]. Whilst composite materials have been shown to offer better energy absorbing performance than metals, if this behaviour cannot be well predicted, then concerns for safety and the potential for the structure to be overdesigned mean that the full potential of the material is not reached. As a result, current vehicle passive safety systems are dominated by metallic structures.

1.4 Project Background

With ever changing performance requirements and increasingly stricter legislation, predicting the future of the automotive industry is incredibly difficult. Nevertheless, current momentum within the industry is focused on the development of electric vehicles and considering research and design cycle times, this is unlikely to change. Unless there is a sudden step-change in battery performance, designers will be expected to meet performance requirements through more efficient aerodynamic and structural designs, and composite materials are going to be at the forefront of this movement.

But bringing composite materials into a mass production environment is a significant undertaking. For almost a century the automotive industry has invested heavily in production lines based around metallic components, and it will be very difficult, and costly, to steer away from this. As a result, there is a clear need to bring solutions to the table that can either be easily integrated into existing production lines or have a value that greatly outweighs the cost to implement them. A key advantage of using composite materials is that they present designers with the opportunity to develop solutions that not only solve one problem, but that are able to solve multiple issues concurrently. One area that could be exploited is the development of passive safety systems using composites. Not only would this enable improved crash performance, but also simplify vehicle assembly, by removing the need for complex joining methods between metallic and composite components.

It is highly likely that any forthcoming structural developments will see an increase in the use of sandwich structures. These are ideal for the design of automotive structural components, such as the floor panel of the passenger cell, as they provide a significant increase in stiffness as well as noise and vibration damping to meet driving performance

demands, whilst at the same time maintaining a low weight. However, one area in which sandwich structures do not excel is there response to dynamic loading, particularly when loaded at a free edge, as would be expected during a crash. This is due to the inherent weakness of the resin-rich adhesive interface between skin and core, which limits the load carrying capability of the structure. If the interface fails, then the skins and core separate leading to an unstable, and therefore unsafe collapse of the structure.

In the aerospace industry, through-thickness reinforcement (TTR) has been shown to be effective at resisting delamination between prepreg layers in composite laminates, however as aerospace methods vastly exceed the cost limitations of the automotive industry, dry fibre and liquid resin infusion methods must be accounted for. Recently, tufting has taken on a renewed interest as a TTR method that is suited for use in dry preforms. Originally developed as an ancient carpet manufacturing process, tufting is an alternative stitching method that uses a single needle to insert a reinforcing yarn through the preform, relying on friction alone to hold the reinforcement in place. This makes it an ideal process for reinforcing complex preforms quickly prior to subsequent resin infusion. Until now, tufting has been demonstrated primarily in monolithic structures, and its capabilities in sandwich structures are still relatively unknown. However, recent studies have indicated promising results, demonstrating the potential for incorporating tufted sandwich structures into vehicle design [42].

1.5 Research Question

The aim of this research is to understand how tufted sandwich structures behave under automotive-type impact load cases. Over the past 5 years, a collection of works between BMW, TU Delft and the University of Bristol have explored the use of composite sandwich panels in automotive crash events, with a focus on the application in a vehicle floor assembly in a Global Technical Regulation (GTR) 14 impact case, as shown in Figure 1-7 [43]. This load case involves the impact of the vehicle against a rigid pole, which is considered a particularly violent and therefore dangerous load case. The worst-case scenario is if the impact occurs centrally to the vehicle meaning that all the kinetic energy must be absorbed by the vehicle structure, and thus involves a significant impact force against the floor panel. The advantage of a sandwich structure for this load case is that unlike aligned crash tubes they can act as energy absorbing structures in multiple loading directions, making them a much more robust crash management structure.

Figure 1-7: Global Technical Regulation 14 side pole impact test [43]**.**

Early work in this area was carried out by Lukaszewicz et al. [44], who tested sandwich coupons in edgewise compression to screen several effective core types. Testing showed that polymethacrylimide (PMI) and polyvinylchloride (PVC) foams offered the best specific energy absorption of the materials tested. More recently Blok et al. extended this work to test similar sandwich coupons but with the addition of kevlar tufts to provide through-thickness reinforcement [45]. The results of these tests showed that tufted sandwich panels were very effective at absorbing energy during edgewise impact and so were transferred to a full scale structural demonstrator [42]. The demonstrator component was designed to match in scale a typical automotive floor panel, using NCF carbon facesheets, a Rohacell foam core and Kevlar tufts as demonstrated in the two previous tests. The test setup was designed to replicate the GTR 14 impact standard, using a pole impactor of diameter 254 mm, and an impact speed of 32 km/h (8.9 m/s) (Figure 1-8). The simulated vehicle weight for impact was 1520 kg resulting in an impact energy of 60 kJ. A maximum intrusion depth into the panel of 200 mm was targeted and the facesheet layups were chosen to be $[+45/-45,0,\underline{0}]_s$. Testing of the panel under dynamic loading conditions showed a progressive crushing mechanism of the central region of the panel, with the movement of the pole impactor effectively arrested at a length of 197 mm (Figure 1-9).

Figure 1-8: Overview of the test panel geometry and impact site for a side pole impact test of a tufted sandwich panel [42]**.**

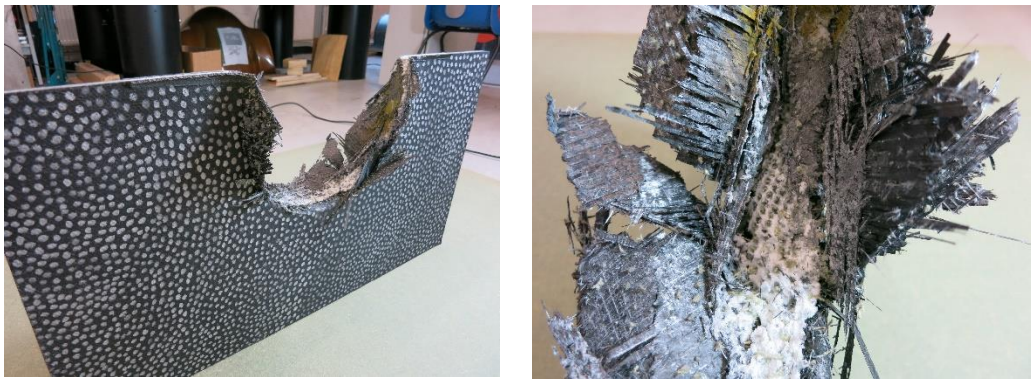

Figure 1-9: Post-failure images of the tested panel. Left, overall panel showing arrested damage at a crushing distance of 197 mm. Right, localised view of failure site highlighting the complex nature of the mechanisms involved.

However, whilst the overall result of this testing has proven to be successful, there is still a lack of understanding regarding how these structures are behaving under load. If a typical testing pyramid is considered (Figure 1-10), there is a significant jump from the basic known mechanical properties of the constituents involved, to larger sub-component level structures. Whilst several of the levels have been covered, the intricacy of a reinforced sandwich structure, coupled with the complexity of the load case under consideration demands an additional level of testing to capture the behaviour of the entire system.

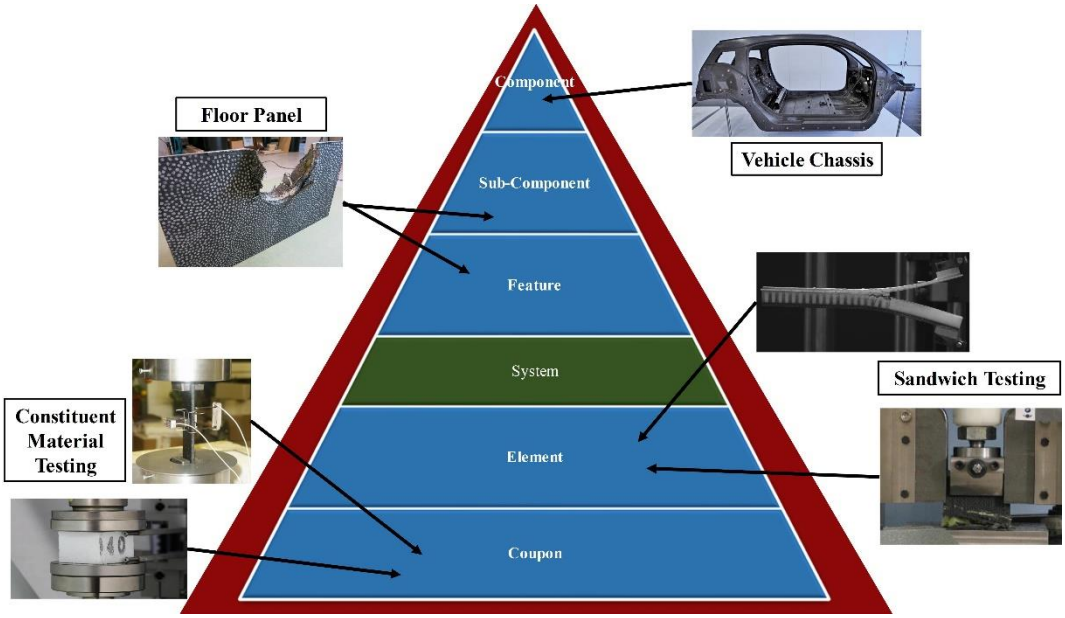

Figure 1-10: Typical structural testing pyramid with relevant examples included for each level.

Currently, due to the complex and destructive nature of the crushing mechanism that takes place, as demonstrated in Figure 1-9, no clear evidence is available to deduce what takes place within the structure as it fails. What is not yet clear are the failure mechanisms that take place and the influence these have towards the energy absorption of the structure. There is also no clear link between the traits observed during testing and the manufacturing process used to insert the tufts. Improving the understanding of both the manufacturing process and its effects on performance, and the role the tufts play on failure will enable better design methodologies to be used, improving both manufacturing processability and structural efficiency, allowing the full potential of these structures to be realised.

1.6 Thesis Outline

The focus and challenge of this research is to characterise and optimise the failure mode and energy absorption of composite sandwich structures for automotive crashworthiness. More specifically the focus will be on developing an understanding of the manufacturing and design parameters of tufted sandwich panels and connecting these to the mechanical behaviour of these structures.

Whilst previous work has demonstrated performance improvements in macro-scale structures, this work will focus on a range of experimental methods carried out at a local level, necessary to capture the finer details required.

It is important to highlight that testing within this work has been predominantly carried out under quasi-static loading conditions. Wherever possible, low velocity dynamic impact testing has been used to supplement the quasi-static data and explore differences in the results, however the maximum velocities achievable in the lab scale testing presented here are in the order of 2-3 m/s, an approximate order of magnitude below what a typical automotive structure would be subjected to under a typical crash type load case.

In Chapter 2, a literature review is carried out introducing the concept of vehicle crashworthiness. This will also cover the behaviour of sandwich structures under these types of load cases, as well as the use of TTR methods in sandwich structures for improving performance under these types of conditions. Chapter 3 will introduce the general materials and methods used throughout this research project. It will introduce the tufting process and outline the design variables and process parameters that are the focus of this project. Chapter 4 introduces a novel coupon design to explore the failure of individual tufts. The aim of this investigation is to test the effect of varying both the thickness and length of the tufting yarn, two variables that can be controlled during the tufting process. The test shows that whilst tuft length has a negligible effect, the increased thickness of adding multiple yarns improves the energy absorption. Also highlighted is the tendency of tuft failure to occur at the skin-core interface, resulting in the ability for tufts to slide through the foam core after failure. In Chapter 5, the tuft failure mechanism is explored in more detail, using test coupons designed to allow observations of the tufts as crushing progresses. It is believed that for the first time, this test has been able to capture the progressive drifting and stacking of resin columns (formed due to the void left by needle insertion) within the foam core and which appear to play a role in the overall energy absorption of the structure. Alongside this, other notable features, such as column fracture, skin fracture and tuft pull-out are also detailed. The aim of Chapter 6 is to gain an understanding of the relative contributions of the failure mechanisms present to the overall performance of the structure. Currently the interaction of the resin columns with the foam core has been explored, demonstrating a small amount of energy absorbed for isolated tufts. Chapter 7 aims to bring this work together through a novel demonstrator project. This is carried out using tufting in reclaimed short fibre laminates, a relevant automotive topic aimed at addressing the need for improved sustainability. Chapter 8 is a discussion of the results and lessons learned from the various tested outline previously. Finally, Chapter 9 outlines the conclusions of the work, with Chapter 10 offering some suggestions for future studies in this area.

Chapter 2 Literature Review

The aim of this chapter is to review the concept of vehicle crashworthiness, and how this links to the topics of composite sandwich structures and TTR to setup this research project. Automotive crashworthiness is the aspect of automotive structural design that manages the impact loads experienced during a crash, with the aim of protecting the vehicle occupants. This review covers existing crashworthiness design philosophies for metallic structures as well as introducing the current and potential future uses of composite materials in this area. The use of sandwich structures is also presented, covering the failure mechanisms from edgewise impact loads and the challenges associated with designing for these load cases. Finally, the use of through-thickness reinforcement in sandwich structures is discussed, outlining the benefits to crashworthiness performance if TTR is used.

2.1 Automotive Crashworthiness

Passenger safety is an important design criterion that must be considered from the outset of any new vehicle programme. Vehicle safety systems can normally be assigned to one of two categories, active or passive. Active safety systems are those which are designed to avoid collisions happening altogether, typically using a system of onboard sensors and devices that can override the driver's actions in the event of an impending crash. Passive systems on the other hand takeover when crashes cannot be avoided. Passive systems are those that are designed to reduce the severity of a crash for the vehicle, its occupants, as well as any potential third parties such as other vehicles or pedestrians. These can take the form of seatbelts, headrests and airbags, but predominantly this role is carried out by the vehicle structure, or body-in-white (BIW), which must be capable of protecting the passengers whilst reducing the severity of the impact through controlled energy dissipation from structural deformation [46].

2.1.1 Structural Design

Over many decades of vehicle design, the BIW (Figure 2-1) has become somewhat standardised across many different manufacturers and models. The individual components that make up this structure are designed to serve two purposes during the vehicle's lifetime. During normal service they serve to maintain the passenger cell, where the passengers of the vehicle as well as all necessary systems to control the vehicle are located, as well as providing the necessary strength and stiffness to meet driving performance requirements. However, during a crash scenario these components are also responsible for protecting the

vehicle from a wide variety of impact cases, depending on the object that the collision occurs with as well as the region on the vehicle where it strikes. In Europe, the New Car Assessment Programme (NCAP) is tasked with producing safety reports assessing the crashworthiness of new vehicles entering the market. Whilst not compulsory, new vehicles are subjected to a range of tests, focusing on various colliding objects at different locations of the vehicle, and these are considered a benchmark of vehicle crash performance. These crash scenarios can broadly be divided into two groups, a front crash and a side crash, as summarised by Lukaszewicz [46].

Figure 2-1: Locations of structutral safety features on a typical automotive BIW [47]**.**

In frontal impact (Figure 2-2a), the role of the structure depends on the nature of the event. Under low-speed impact the energy to be dissipated is low, so the primary role is to offer protection to pedestrians if struck and to allow repair of the structure after the event. Under high-speed impact energy management becomes more important. Firstly, the front longitudinal beams will deform, from which the load then travels into the front bulkhead and then onto the 'A-pillar', undercarriage and the door sill. Depending on the severity of the impact, if the impact barrier reaches the engine then it too can be pushed towards the forward bulkhead to provide additional energy absorption. If this happens the steering rack and front axle module must deform to dissipate energy but not allow penetration into the passenger cell. Under rear impact loading the vehicle structure behaves in a similar manner, with the rear longitudinal beams providing much of the energy dissipation through controlled deformation before transferring the loads into the rest of the vehicle structure.

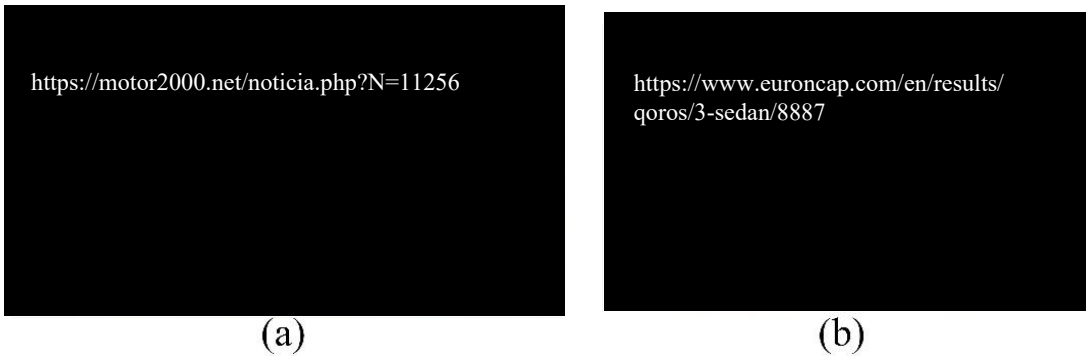

Figure 2-2: Euro NCAP crash testing examples demonstrating typical vehicle crash load cases, a) frontal barrier impact, b) side pole impact.

In a side impact event (Figure 2-2b), as before, the role the structure plays will depend largely on the type of impact. The structural behaviour is somewhat different to frontal impact due to the absence of a sacrificial volume outside of the passenger compartment that can be exploited for a controlled structural collapse. Under barrier impact loading it is the 'B-pillar' that takes the initial impact load and deforms into the passenger cell. As this occurs the roof cross members and door sill are loaded in tension, whilst the 'A-pillar' is also deformed dissipating further energy.

A particularly extreme case of a side impact is when the vehicle strikes a narrow object such as a pole, as was introduced in Chapter 1. For a pole impact into the side of the vehicle the loaded area is much smaller and so energy management is more challenging. Research by the Global Registry of the United Nations demonstrated that whilst these types of load cases are not as common, levels of serious injuries and fatalities are disproportionately high [43]. This emphasises the particularly challenging safety design aspect around this load case, as well as the need for stricter regulations to ensure it is dealt with in the future. In this load case, the load is continuously introduced into the door sill, which is supported underneath the vehicle by cross members as well as the vehicle undercarriage. Meanwhile the roof structure is loaded, carrying load through its cross members to the other side of the vehicle. With increasing intrusion into the passenger cell, the load is directed into the 'A'- and 'B'- pillars for further support. Ultimately the key design driver is to maintain a required survival space within the vehicle throughout the crash event.

This load case is expected to take on even more importance in coming years with the rapidly growing use of electric vehicles. Lithium ion batteries that are typically used in BEVs are highly susceptible to fire, and can burn uncontrollably if damaged [48]. As there is currently a strong design tendency to storing the batteries within the passenger cell (Figure 2-3), it is highly likely that design criteria for side impact events will come under increasing scrutiny.

Figure 2-3: Cutaway of a BMW i3, showing battery cells located underneath the passenger cell [49]**.**

2.1.2 Measuring Performance

For a vehicle structure to be deemed ‘crashworthy` it must effectively dissipate the associated impact energy from a crash throughout the structure, whilst avoiding sudden decelerations that could prove fatal to the occupants. This performance level is derived using the force-displacement relation of the load case, as shown in Figure 2-4.

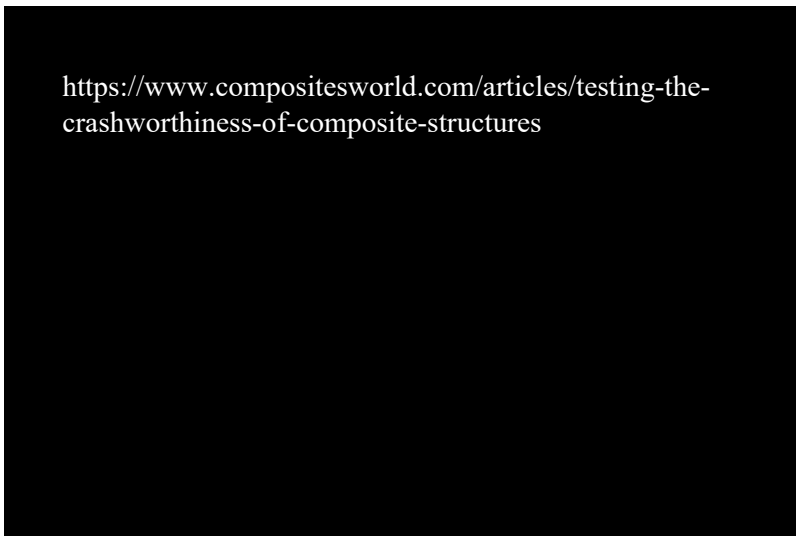

Figure 2-4: Typical load-displacement response of a component failing by crushing. Load response consists of an initial peak failure load, followed by a sustained crushing load [50]**.**

Sudden decelerations are shown by a sharp drop in load from the initial peak, which means that for a crash structure to be operating successfully it must be able to maintain a relatively high average crushing load as the controlled failure takes place, through a stable failure

mechanism. A metric to measure this performance is the 'crush force efficiency (CFE)' which is defined in Equation 1.

$$CFE = \frac{Average\ Crush\ Load}{Peak\ Force} \tag{1}$$

The energy dissipated by the structure can also be found using this data and is calculated by integrating the area under the force-displacement curve. The typical metric used to define this is the 'specific energy absorption' (SEA), which is the overall energy absorption relative to the mass of the material loaded. This allows for comparisons between dissimilar materials and is defined in Equation 2 where W is the work done during crushing, and ρAδ represents the mass of the crushed material assuming a constant cross-section.

$$SEA = \frac{W}{\rho A \delta} = \frac{\int_0^\delta F d\delta}{\rho A \delta} \tag{2}$$

2.2 Energy Absorption in Composites

Even though roadworthy cars predominantly featuring composite materials exist today, those that do still feature passive safety systems that are metallic. This is despite composite materials having the advantage of being able to absorb more energy for a given mass when crushed [41], as shown in Figure 2-5. Experimental studies have been carried out that demonstrate composites can absorb as much as 3-4 times the SEA compared to steel, or aluminium structures. With the greater demand for improved efficiency in road vehicles, the exploitation of increased energy absorption in composite components has taken on a renewed interest. This is evidenced by the growth of this particular area of research, such as the formation of the ICONIC project (Improving the Crashworthiness of Composite Transportation Structures) [51], as part of the wider Horizon 2020 research programme.

Figure 2-5: Typical values of SEA for materials commonly used in automotive structural design. Adapted from [41]**.**

2.2.1 Monolithic Laminates

Unlike metals, which absorb energy through a progressive plastic folding mechanism, composite laminates can achieve much higher amounts of energy absorption through brittle failure mechanisms (Figure 2-6), which vary depending on how the load is applied, as well as the composition of the structure tested. Because of this obvious advantage, the use of composites as safety features has been an area of research interest for some time.

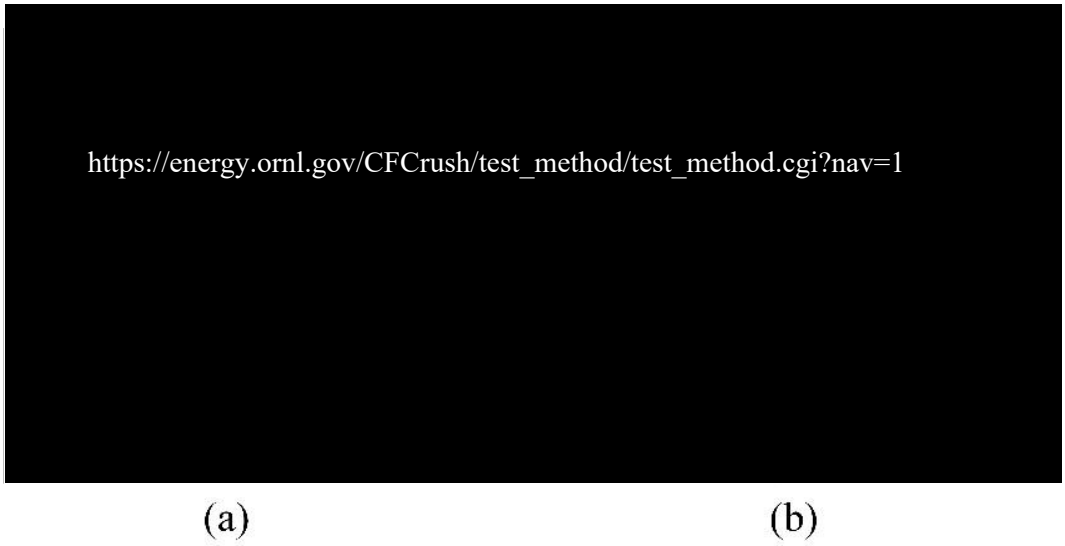

Figure 2-6: Characteristic crushing failure mechanisms of tubes manufactured using a) Metal, b) Composites [52]**.**

One of the earliest accounts of the energy absorption of composite materials was by Thornton in 1979 [53]. In this study, the author investigated the axial collapse of a series of tubular specimens reinforced by glass, carbon or Kevlar fibres. Energy absorbing components are typically tubular, to help maintain stability during compressive loading. The author observed that failure of the composite tubes occurred initially by interlaminar shear followed by fibre fracture, unlike high-strength metal tubes which failed by buckling. It was noted that the crush forces for the composite tubes were much higher and thus a greater amount of energy was absorbed. Following this, one of the earliest authors to actually characterise these failure modes was Hull in 1982 [54]. At this time the failure mechanisms were identified as fibre splaying and bending, fibre splaying and axial tearing, as well as micro-fragmentation. This was followed up by Farley in 1987 [55], Hull again in 1991 [56] and Jones and Farley in 1992 [57], who all generally observed similar failure mechanisms. More recently, composite crushing failure modes are classified by three key groups, fibre splaying, fragmentation, and brittle fracture, shown in Figure 2-7 [40,41].

Figure 2-7: The three typical failure mechanisms observed during the crushing of composite tubes [50]**. A) Fibre splaying. B) Fragmentation. C) Brittle Fracture.**

Because of the increased energy absorption through numerous interacting failure mechanisms, coupled with the low density of composite materials, the resulting SEA will be much higher than that of metallic structures, as was illustrated in Figure 2-5. However, whilst the performance is higher, the brittle behaviour means that design strategies must be adapted to compensate. Whilst externally mounted crushable tubular composite designs are effective for deployment as the longitudinal beams for front and rear impact cases, under a side impact load case the passive safety features must be integrated directly into the passenger cell, and so must fit seamlessly within the surrounding structure.

Whilst the use of continuous fibre composites in in-plane energy absorbing applications has been explored to some depth, short-fibre composites are less well known. In theory, the shorter fibre lengths of reused fibre could help to promote energy absorbing failure mechanisms through increased fracture sites. Previous studies by Jacob et al. [58,59], looked at the energy absorption of chopped fibre composites. Whilst no direct comparisons to continuous fibre composites were made, the authors were encouraged by the results seen, with values of specific energy absorption (SEA) close to that reported for a continuous glass-fibre reinforced mat. However, the relationship to fibre length is less clear, with tests showing SEA both decreased [58], and increased [59], with fibre length. It was suggested that whilst the mechanical properties are higher at longer fibre lengths, the larger number of fibre-ends in short fibre composites act as stress concentrations points, resulting in a larger number of fracture initiation sites and thus a greater amount of energy absorbed. Generally it is accepted that due to the lower level of alignment of the reinforcement in short fibre composites, they tend to show reduced mechanical properties when compared to continuous fibre laminates [60]. However static strength is not usually the primary driver in the design of the component, as instead the SEA of the material, combined with the deceleration times required will dictate the design requirements [34].

2.2.2 Sandwich Structures

One configuration in which composite materials are yet to be truly exploited for crashworthy components is using sandwich structures. Composite sandwich structures involve separating two thin laminates using a relatively lightweight core material such as a foam or honeycomb (Figure 2-8) [61]. By doing so the effective thickness of the laminate is increased, and thus the bending stiffness of the assembled structure can be increased substantially, with only a small penalty in weight. An adhesive bond between the faces and core is required to allow loads to be transferred between them, which can be achieved by co-curing the elements together or using a separate adhesive compound. Under loading, each component carries out a separate role, with the facesheets acting together to counter external bending moments, the core acts to resist shear loading as well as stabilise the facesheets from wrinkling or buckling, whilst the adhesive bond resists the tensile and shear stresses at the interface.

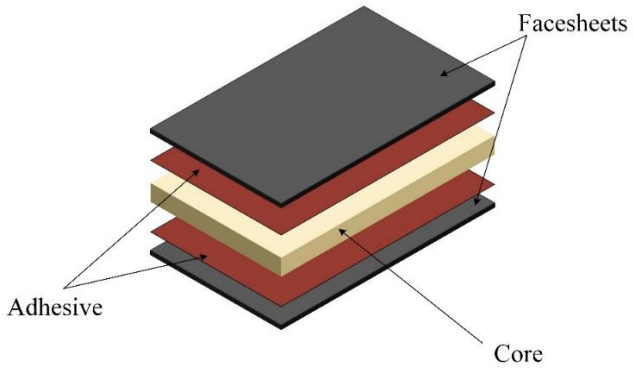

Figure 2-8: Typical components and configuration of a composite sandwich structure.

Sandwich structures have primarily seen use in the aerospace industry, however as well as the increased structural efficiency, sandwich structures can offer numerous other benefits, such as good vibration damping properties, thermal and acoustic insulation, greater energy absorption, and even buoyancy [61], expanding the range of applications to include the marine, aerospace, rail and construction industries [62,63].

Due to the highly compressible nature of typical sandwich core types, there is also the capacity to absorb a relatively large amount of energy during crushing as shown in Figure 2-9 [64,65], with varying results depending on core type and structure. However, the stability of a core under edgewise loading in isolation would typically lead to a significant reduction in these figures.

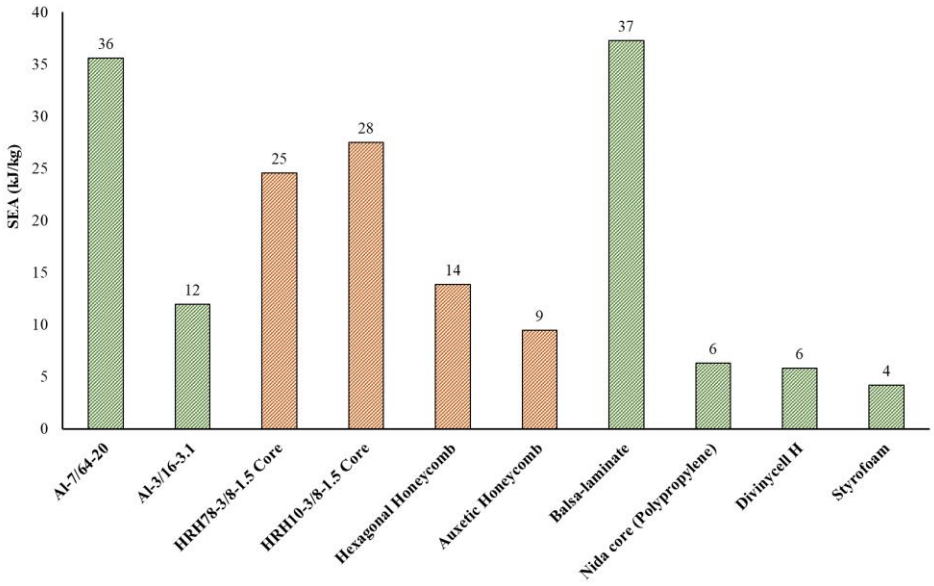

Figure 2-9: Energy absorption of typical sandwich cores. Green bars show results from continuous crushing [64]**, orange bars show cores tested to failure** [65]**.**

2.2.2.1 Dynamic Behaviour and Crashworthiness

Some of the earliest work on the impact behaviour of honeycomb-cored sandwich panels was reported by Kassapoglou et al. in 1988 [66]. In this work, various impactor sizes and energy levels were used to test out-of-plane impact loading and subsequent compression-after-impact (CAI) strength. The impact load led to delaminations in the facesheet which changed the compression failure mechanism from global buckling to cracking away from the flaw site. A reduction in the load carrying capability of as much as 33% was reported after impact, however a proposal for locally applying adhesive between plies at likely delamination sites led to a recovery in the static strength. Later work by Sun and Wu [67] explored the impact behaviour of both foam and honeycomb cored sandwich panels in more detail. Both static indentation and dynamic impact were used to characterise the contact behaviour and subsequent failure modes, including intraply matrix cracking and delamination. In a similar area to the work by Kassapoglou et al., Minguet [68] presented a modelling technique for predicting CAI of sandwich structures. Results from simulation showed good correlation with experimental testing, with failure occurring as unstable crack propagation away from the impact site as shown before. A key observation was that core crushing strength played an important role in the sandwich performance. In 1992, Goldsmith and Sackman [69] reported the firing of projectiles at the surface of various sandwich panels, as well as carrying out corresponding static crush tests on the core materials used. Primarily aluminium materials were considered for both the facesheets and honeycomb core, however Nomex honeycomb and fibreglass facesheets were also investigated. The authors noted that the energy absorbing mechanisms consisted of bending and stretching of the facesheet, as well as crushing of the core, however they also noted that weak bonding between facings occasionally led to separation of the facesheets and lower energy absorption. It was suggested that maximising plastic deformation, as well as densification of the core would maximise energy absorption. Borazjani and Belingardi proposed a design for sandwich based vehicle roof structures [70], particularly for protection during a roll-over of the vehicle. In this load case the roof panel undergoes transverse crushing as the weight of the vehicle compresses it against a rigid surface. By optimising the sandwich design the authors were able to achieve a comparable performance to steel whilst reducing the weight of the panel by as much as 70%.

A more realistic loading condition for sandwich structures, particularly in automotive design, would be edgewise loading of the panel. The most prolific author in this area is Mamalis, who initially published the edgewise performance of sandwich structures in 2001 [71]. In this initial study, the authors considered thick-walled tubular structures formed

using foam-cored sandwich structures. As an additional level of energy absorption, the sandwich facings were reinforced using perpendicular fibreglass cylindrical tubes, embedded within the foam core. These tubes were loaded axially under quasi-static loading conditions and failed in a progressive end-crushing mode. After an initial elastic load response, axial cracks developed at the four corners of the specimen. These split the facesheets into "two continuous fronds" which curved away from the core in either direction. Brittle fracture occurred within the facesheets whilst crushing of the foam core began to take place. Further energy absorption was observed to have taken place through friction between interacting surfaces, as well as the progression of a debris wedge driving through the foam core. Follow up work investigated similarly designed sandwich panels in both edgewise and flatwise compression loading [72]. One modification that was made was the addition of a single fibreglass tube within the foam core aligned in the direction of loading. During edgewise testing it was observed that the facesheets buckled and separated from the foam core. Buckling of the reinforcing tube aligned to the load also occurred, whilst the foam core primarily fractured. It was concluded that separation of the facesheets was not ideal for energy absorption, and the use of the internal reinforcing tubes tied to the facesheets did not do much to affect this behaviour. More recent works by the authors aimed to fully characterise the behaviour of sandwich structures under edgewise loading [73]. This time the authors conducted a series of tests on simple unreinforced sandwich structures, using fibreglass facesheets and several foam cores. Observations during testing led the authors to the conclusion that, analogous to the crushing of monolithic laminates, there are three distinct crushing modes for sandwich structures, shown in Figure 2-10.

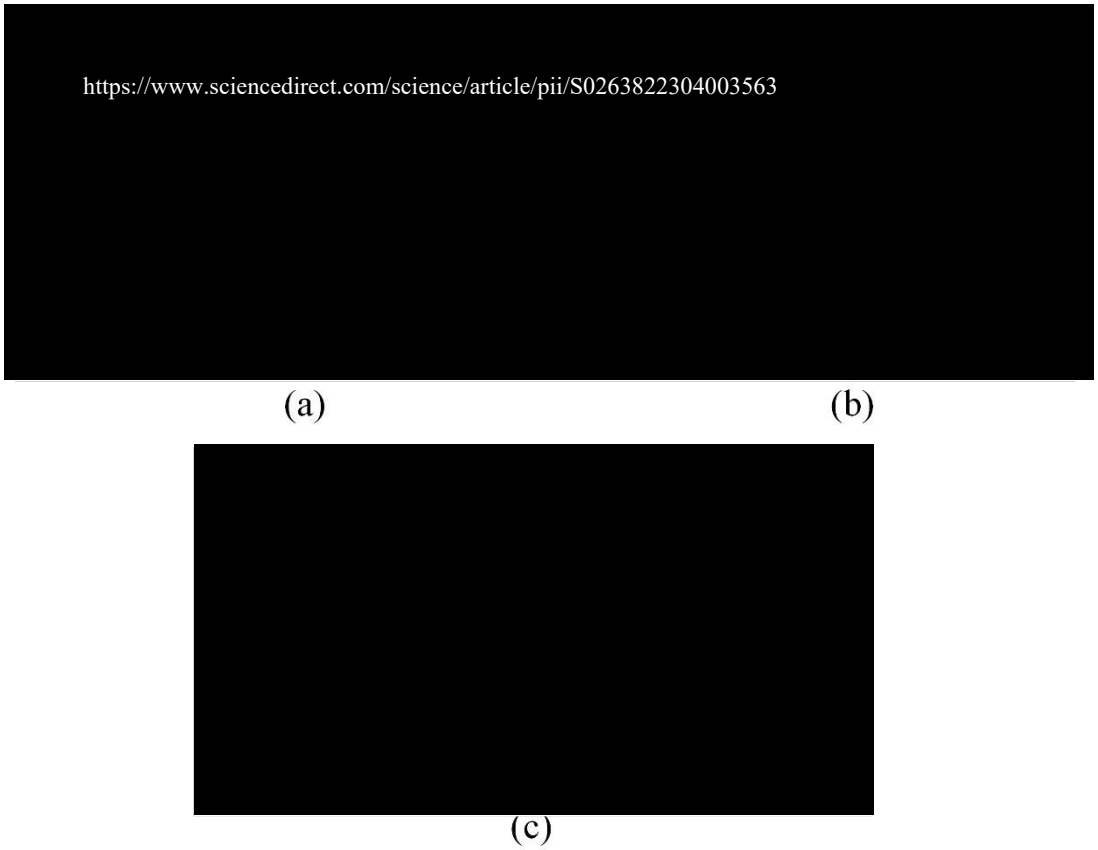

Figure 2-10: The three failure mechanisms observed in sandwich structures loaded in edgewise compression [73]**. A) Facesheet separation and local buckling. B) Global column buckling. C) Progressive crushing.**

The first of these is unstable column buckling of the overall sandwich panel, featuring shear failure within the foam core. This also led to separation of the facesheet on the compression side during bending of the panel. It was noted that this was the most frequent failure mode observed, occurring as much as 50% of the total specimens tested. The second mode involves complete separation of the facesheets, followed by buckling, with the now unsupported foam core also collapsing under compressive loading through shear failure. As with the first failure mode, very little fracture of the facesheets takes place, except some localised crushing at the ends, as well as failure due to bending at the mid-section after buckling. The final failure mode is stable progressive end crushing of the sandwich structure, which is the mechanism desired for high energy absorption. Throughout this crushing mode, a series of failure mechanisms take place that directly contribute to energy absorption. These include:

- Elastic compression of the facesheets and core
- Ply delamination
- Bending of the facesheets

- Friction due to sliding of the plies
- Local separation of the facesheets from the foam core
- Crushing of the foam core

It was found that, in general, the foam core played a key role in determining which failure mode would take place. From the range of foam cores tested, the one with the highest stiffness, strength and elongation at break was the one that was consistently capable of exhibiting the stable crushing mode. In contrast, the specimens with the most brittle foam core typically failed by facesheet separation and collapse.

In a further study, Mamalis and Papapostolou [74] considered the effects of strain rate on the crushing behaviour and performance. Whilst no clear trend was observed between strain rate and the observed collapse mode, it was noted that all cases of stable crushing occurred under dynamic loading. It was also noted that in general the initial peak load was higher under higher strain rates, whilst the overall energy absorption was also generally higher.

The tendency for sandwich structures to separate under edgewise loading limits their ability to be effective crashworthy structures, and often this is due to the way the failure initiates. A number of authors have therefore focused on developing suitable 'trigger' features to help initiate failure and produce a stable crushing failure [71,75–77], examples of which are shown in Figure 2-11. The purpose of a trigger is to create a stress concentration, or inherent weakness at the impact surface, reducing the initial failure load and thus producing a more stable collapse of the structure. Several different trigger forms have been investigated, including tulip [76], chamfer [71], as well as external mechanisms [78]. However, whilst trigger mechanisms play a key role in obtaining a desirable and efficient failure mechanism, as noted by Mamalis et al. [71] they have a tendency to limit the load carrying capability of the structure. As such it is necessary to focus on ensuring the interface of the sandwich structure remains intact as the structure fails.

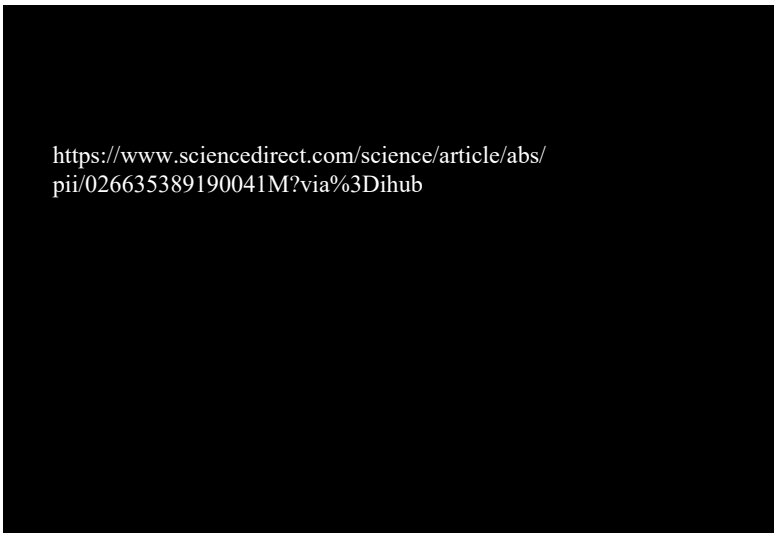

Figure 2-11: Examples of typical trigger mechanisms used in composite structures. Left, Chamfer/Bevel type. Right, Tulip type [79]**.**

2.3 Through-Thickness Reinforcement in Sandwich Structures

Efforts to reinforce composite laminates through-thickness have been going on for some time [80–82], however similar work in sandwich structures is more limited. Early attempts to provide additional reinforcement in sandwich structures used rigid z-pins to tie the facesheets together, whilst providing a rigid support within the core. Palazotto et al. achieved this using steel reinforcing pins, and showed effective performance in low energy face impact [83]. Similar work was carried out by Marasco, who investigated the development of pin-reinforced sandwich structures using resin impregnated z-pins [84]. These pins were produced using a continuous pultrusion method and inserted into the foam core using a robotic insertion head. Once inserted into the foam, the pins could either be left exposed, to allow them to mechanically lock on to the facesheets when placed afterwards (X-Cor, Figure 2-12) or be deliberately folded flush with the foam surface (K-Cor). A series of different tests were carried out on these structures, but of most interest was a set of edgewise crushing tests to determine the energy absorption. Following the development of a novel coupon design, samples were tested under quasi-static loading conditions and exhibited a stable progressive crushing failure. Both pin configurations showed similar levels of performance, however the X-Cor configuration with direct contact between pin and facesheet was more reliable overall. Rice et al. also focused on X-Cor sandwich structures, this time considering 3-point bending of sandwich beams [85]. The authors noted that whilst the failure mode by indentation was observed in both pinned and unpinned samples, the peak load and flexural stiffness of the X-Cor samples was much higher than regular foam and presented a similar level of bending performance to aluminium honeycomb. Du et al. investigated the effect of pin angle on the shear properties of the foam core [86]. They showed through a parametric study that the out-of-plane shear

strength increased with an increase in angle of the pins, as the pins were more aligned to the loading direction. They also showed an increase in strength with increasing pin diameter and density. Haldar and Bruck [87] have proposed a scaling effect on the results of testing such structures. They proposed that testing specimens of different sizes varies the number of active pins and thus will lead to different results. To account for this, they tested a series of specimens in flatwise compression and developed a scaling factor for the stress and stiffness to account for variations in size.

Figure 2-12: Example of a reinforced sandwich core (X-Cor) [88]**.**

On a different scale to Z-pinning, some researchers have focused on the use of more significant reinforcement within the core of sandwich structures. For example, Laurin investigated the use of strips of a carbon fibre laminate embedded within a foam core, aligned to a flatwise crushing load [64]. It was noted that energy absorption improved compared to the baseline unreinforced foam core samples, however the results were not as promising when compared to other core types such as balsa wood, which had a comparable performance. A recent study by Pitarresi et al. [78] recognised the need to improve the interfacial performance of sandwich structures to maximise the energy absorbing potential. In this study the authors created a series of structural 'ties' embedded within the foam core that remained connected to the facesheets. The test specimens were thick-walled sandwich tubular sections and tested under quasi-static edgewise compression. Through testing it was shown that tying the facesheets helped to stabilise the failure mechanism and improve energy absorption. It was noted by the authors that the most effective tie configuration was a corrugated one, as the contact area between tie and facesheet was much larger. Martakos et al. [89,90] demonstrated the use of a unique 'crack stopper' for controlling peeling failure propagation at the sandwich interface. A glass fibre reinforced polyurethane resin 'C-section' was created and embedded within the foam core. The bond between crack stopper

and facesheet was strong enough to redirect the crack path around the crack stopper and into the foam core. This led to a significantly enhanced fatigue life of the structure.

Whilst promising methods of reinforcing sandwich structures have been demonstrated, these methods are not always suitable for high processing rates or low-cost processing methods due to the use of pre-assembled components or prepreg parts. Of more suitable use are dry reinforcement methods that are better suited to resin infusion processing and can easily be incorporated into a preform as part of a production line. One method that falls into this category and has seen use for some time in the composites industry is through-thickness stitching (Figure 2-13).

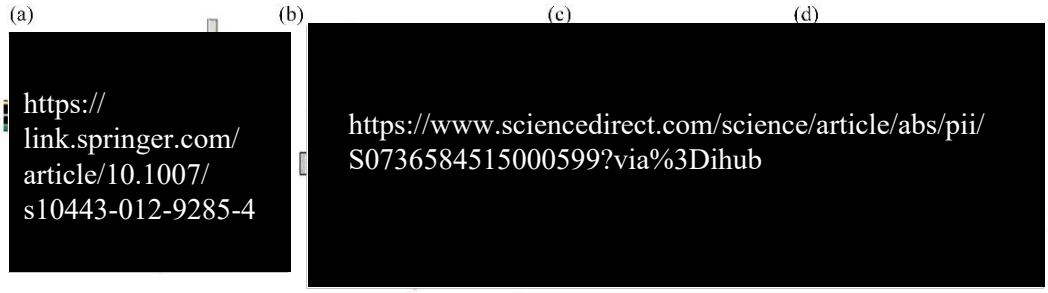

Figure 2-13: A comparison of typical stitching methods used in composite laminate manufacture. A) Lock-stitching method [91]**. B-D) Dual thread, single thread and blind stitch variants of one-sided stitching** [92]**.**

Potluri et al. developed a novel stitching technique to use for sandwich structures [93]. A stitch-bonding machine was developed capable of inserting through a relatively thick section as well as for penetrating through a relatively hard foam core. By carrying out quasi-static indentation tests it was shown that the stitching process helped reinforce the interface and reduce the debonding area significantly. Reducing the spacing between stitches led to a reduction in the debond area, ultimately leading to transverse shear failure of the panel rather than debonding, as well as a greater peak load to initiate failure. Later, Lascoup et al. used a similar technique to reinforce sandwich structures for testing under bending, shearing, and compression load cases [94]. They observed that the stitches reduced inter-laminar shearing which often leads to separation at the skin-core interface. They also observed improvements in the through-thickness properties of the structure. Whilst the weight of the panel was increased by the process, the specific performance was still of a high level. The same authors also carried out low-velocity impact testing on the surface of stitched panels [95]. They again observed a significant decrease in the bonding area of the panels, observing failure of the internal reinforced structure as the primary energy absorbing mechanism. As before it was observed that reducing the spacing between stitches

had an improvement in the debonding area but led to an increase in mass due to the increased reinforcement present. In similar work, Xia and Wu et al. also tested the impact behaviour of stitched sandwich structures and made similar observations on the reduction of damage with increasing stitch density [96,97]. Ma et al. tested the CAI strength of impacted stitched sandwich panels [98]. Failure would initiate from the damage site, however the stitch reinforcement helped to reduce the size of this and thus led to a greater CAI strength of the panel. Wang et al. explored stitched sandwich panels under flexural loading [99]. They concluded that stitching increases the flexural rigidity and strength of the panels tested, however increasing the stitching density led to a decrease in the in-plane rigidity of the panel. It was also observed that thicker foam cores led to an increase in diameter of the resin columns formed around the stitches. Shigang et al. investigated the effect stitch angle has on performance [100]. It was noticeable from their work that stitching angle can have a significant effect on mechanical properties of the sandwich structure, with perpendicular stitches not necessarily the optimum design. From the array of tests carried out it was suggested that a reinforcement angle of 60° was a good compromise across multiple load cases. The optimum angle for interlaminar shear of the sandwich was 45°.

2.4 Tufting

An alternative method to traditional stitching techniques is tufting. Originally developed as an ancient carpet making technique, tufting has recently started to garner interest as a method for reinforcing composite structures [92]. Originally introduced by Sickinger and Herrmann in 2001 [101], tufting is a method of TTR for dry preforms, which unlike more conventional stitching methods, requires only a single threaded needle to insert the reinforcement and requires access to only one side of the preform (Figure 2-14). This gives it numerous advantages over other reinforcement methods that can lead to increased efficiency and performance [102,103]. For example, the need for only single-sided access enables more complex and thicker preform sections to be used, and with a suitable sacrificial layer underneath, reinforcement can even take place in the mould prior to resin infusion. Furthermore, the use of only a single reinforcing yarn means friction alone keeps the reinforcement in place within the preform. The lack of applied tension reduces crimp of the preform and thus better maintains the in-plane mechanical properties of the final cured part. However as shown in Figure 2-15, the nature of this process means that defects such as fibre waviness and damage can still occur.

Figure 2-14: Outline of the tufting process [92]**. A) Reinforcement insertion stages of the tufting process. B) Comparison of partial and fully inserted tufts.**

Figure 2-15: Defect formation in tufted laminates. A) Resin pockets and voids [104]**. B) Fibre crimping and waviness** [105]**. C) Broken filaments** [92]**.**

Cartié et al. outlined the use of tufting for reinforcing a skin-stringer T-joint [106]. It was observed that the S-glass tufts provided effective reinforcement at resisting delamination in the joint, changing the failure mode to flexure, as well as significant improvements in both the static and fatigue performance. The authors did however note that the T-joint preform had to be tufted out of the mould to enable complete needle penetration, before moving it into the RTM tool. In a related study, Harman et al. investigated the economic implications of using tufting for a T-section [107]. Using some simple approximations, a cost model was derived to compare tufted and untufted parts, alongside a benchmark prepreg equivalent. Although the model was based on lab-scale manufacturing processes, it was shown that the tufted part was more economical than the typical aerospace prepreg part. The untufted RTM part was significantly cheaper than both options, however structural properties were not fully considered at this stage. Based upon a structural index derived by the authors, it was revealed that of the three options the tufted part was the most weight efficient. In further work by Harman [108], it was shown that for the example of an aircraft rib post, the lifetime cost per part for the tufted component was 14% lower than an untufted component, and as much as 61% less than the prepreg equivalent. Wang and Soutis attempted to model the performance of tufted T-joints [109]. As expected, they were able to demonstrate the increased load carrying capacity, but also showed a higher deflection capability and thus improved energy absorption of the structure. It was however noted that

the presence of non-linearities made it difficult to accurately capture the load-deflection response. Further work on the reinforcement of T-joints by tufting was carried out by Kratz et al. [110]. Glass fibre stringers were manufactured, incorporating a region of carbon tufts at the transition from the stringer flange to the skin, as shown in Figure 2-16. The use of tufting helped to restrict delamination at this transition region, providing a moderate increase in initial failure load, by as much as 16%, whilst also increasing stiffness and damage of the structure. However, the relative weakness of the interface at the web-to-flange transition led to delamination occurring there instead, meaning that tufting was not able to fully mitigate failure in the joint. In further work by Clegg et al. efforts were made to address this failure mechanism by incorporating tufts within the web-flange interface transition also [110]. Additional tufted regions were positioned perpendicularly to the preform either side of the radius at the transition point, as well as diagonally through the radius across the 'noodle' region. It was observed that these additional regions of tufts further helped to restrict delamination propagation and increased the failure load over the untufted baseline. Later work by Clegg et al. has looked to eliminate the noodle transition region completely, through the use of 3D-woven 'π-shaped' connectors [111]. The use of 3D preforms simplified the manufacturing process, whilst eliminating the stress concentration at the noodle helped increase the failure load over traditional designs. The use of tufting further helped by restricting delamination and thus improving damage tolerance of the structure.

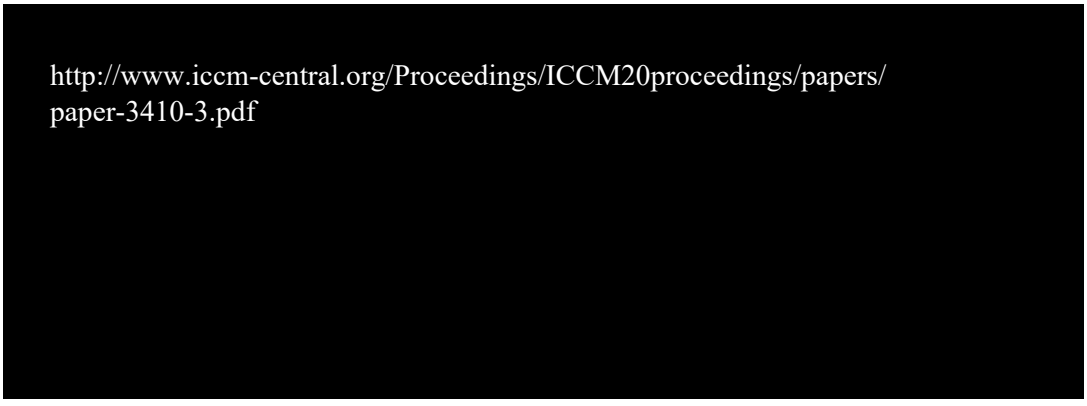

Figure 2-16: Four-point bend test of a glass fibre stringer reinforced by tufting [112]**.**

Further work has been carried out on flat monolithic laminates. For example, Scarponi et al. demonstrated very good compression after impact properties of kevlar tufted laminates, particularly when compared to other TTR methods such as high-tension stitching and z-pinning [113]. Similarly Colin de Verdiere et al. carried out a series of mechanical tests on tufted laminates using carbon threads, where they demonstrated a reduction of in-plane

strength and stiffness of around 10-15%, which they attributed to fibre crimping as well as resin rich zones around the tufts [114,115], as shown in Figure 2-15. It was shown through C-scanning that under cyclic loading the damage distribution was more uniform up until failure, while mode I and mode II testing indicated an improvement in the interlaminar properties of the laminate. Further interlaminar testing at higher loading rates also demonstrated superior out-of-plane properties as a result of tufting [116,117]. At the same time Dell'Anno et al. also investigated tufted laminates and made very similar observations of performance [104]. In this work manufacturing considerations were also made, such as what could be done with the exposed loops on one surface. It also raised the question of other manufacturing variables, such as material type and tuft layout, and the effects these have on performance.

In the area of manufacturing, Wang et al. explored the forming behaviour of dry preforms after tufting [118,119]. A hemispherical mould was used to simulate the drape of a preform. It was observed that tufting increased the rigidity of the preform with increasing tuft density, thus requiring higher compressive forces to drape the material. However, it was also observed that interlaminar slippage of the plies was reduced, resulting in a reduction in wrinkles. In another study, the authors focused on the effect of the tuft length through the thickness of a preform [120]. Carbon tufts were inserted to various depths ranging from 6 mm to 14 mm within a glass fibre preform approximately 20 mm thick. Through-thickness tensile testing was then carried out on the laminate. It was observed that at the upper end of the tuft length range, the failure mode would change from pull-out of the tuft yarn to fracture. The authors proposed that partially inserted tufts performed better due to less degradation of the tufting yarn from a full insertion. However, what was not fully clear was the effectiveness of the two different failure modes observed. In another study, glass preforms were tufted with carbon threads with varying densities and orientations [121]. Tensile testing demonstrated that each of the tufted coupons tested exhibited greater failure strains, but lower maximum failure loads than the untufted baseline. It was shown that aligning the seams of tufts in the loading direction resulted in greater failure strengths than those perpendicular. Flexural stiffness on the other hand was largely driven by the density of the tufting pattern, with the highest density pattern having the greatest increase in flexural stiffness. Préau et al. conducted flexural tests on an omega shaped stiffener [122]. They concluded that full insertion of the tufts through the preform led to a resin rich layer on the surface of the preform, which reduced the flexural properties of the part. In addition, they tested the effect of thread-less needle insertions and observed no noticeable drop in performance, indicating the tufting yarn is what gives the primary in-plane mechanical

knock-down. In similar work by Martins et al., tufting was demonstrated to greatly increase the fracture toughness by as much as five times of omega stiffeners [123]. However, it was observed that due to compaction of the plies in the transition region due to tufting, the stiffener radius is reduced and a strain concentration in this region is created. This led to a reduction in the ultimate load due to premature failure at this point. Scott et al. explored the effect that varying tuft insertion parameters can have on the manufactured component [124]. The authors noted that under flexible tooling such as a vacuum bag, the geometry of the component can change compared to the untufted state. Areal density, tuft size, loop length, tuft angle and compaction pressure were all varied, with the final component measured to explore the effects. Of the variables considered, areal density had the greatest influence on the preform thickness, with an increase in density from 0.5% to 2% resulting in a thickness increase of 27%.

Deconinck et al. explored the variation of tuft density on a panel subjected to ballistic impact loading [125]. By varying the pitch of the tufts, as well as the tow density, different areal densities were obtained. High velocity testing was carried out using a gas-gun at velocities up to 110 m/s. It was revealed that the smaller the pitch depth, the greater the delamination resistance, however the increased tufting density would lead to a greater knock-down in the in-plane mechanical properties and so a balance must be found. Similarly, French explored the use of tufting for reinforcing the armour of military vehicles against ballistic impact [126]. It was shown that the presence of tufts significantly reduced the damage area after ballistic impact, however the panels still showed a similar level of resistance to impact because of the energy absorbed from failure of the tufts themselves.

In the field of sandwich structures, the use of tufting is far more limited. Henao et al. conducted a series of tests on tufted sandwich structures, including bending and compression [127], as well as impact [128]. Under compression loading the failure mechanism changed from facesheet disbonding to column buckling and the failure load was increased for both carbon and glass fibre facesheets. Reducing the density of tufts by increasing the spacing led to a reduction in the force increase. Similarly, under flexural loading a significant increase in load carrying capability is observed in both carbon and glass samples after tufting. The failure mechanism changed from primarily indentation before tufting to shear failure of the core after. Impact loading of 40 Joules was carried out on the faces of a set of sandwich coupons. As before, the tuft spacing was varied to generate a change in density, and an increase in energy absorption was observed as the tuft density

increased. The bending deflection under impact decreased with increasing density, as the flexural stiffness of the panel was improved.

Lukaszewicz et al. identified the potential use of sandwich structures for stabilising the crushing behaviour of composite laminates for automotive crash scenarios [45]. However, facesheet separation is the limiting factor for these types of structures and so the use of aramid tufts to reinforce the facesheets was investigated. Several facesheet configurations and two different foam cores were tested, in both static and dynamic edgewise crushing load cases. It was observed that the addition of tufts increased the initiation failure load, as well as the sustained crushing load, which led to an improvement in the energy absorption of the test samples. Facesheet layup and core type did play a significant role in the results, with thinner facesheets and the more brittle foam core having lower energy absorption before tufting. The addition of tufting led to a much greater improvement in performance for these configurations. Comparative results of this study are shown in Figure 2-17.

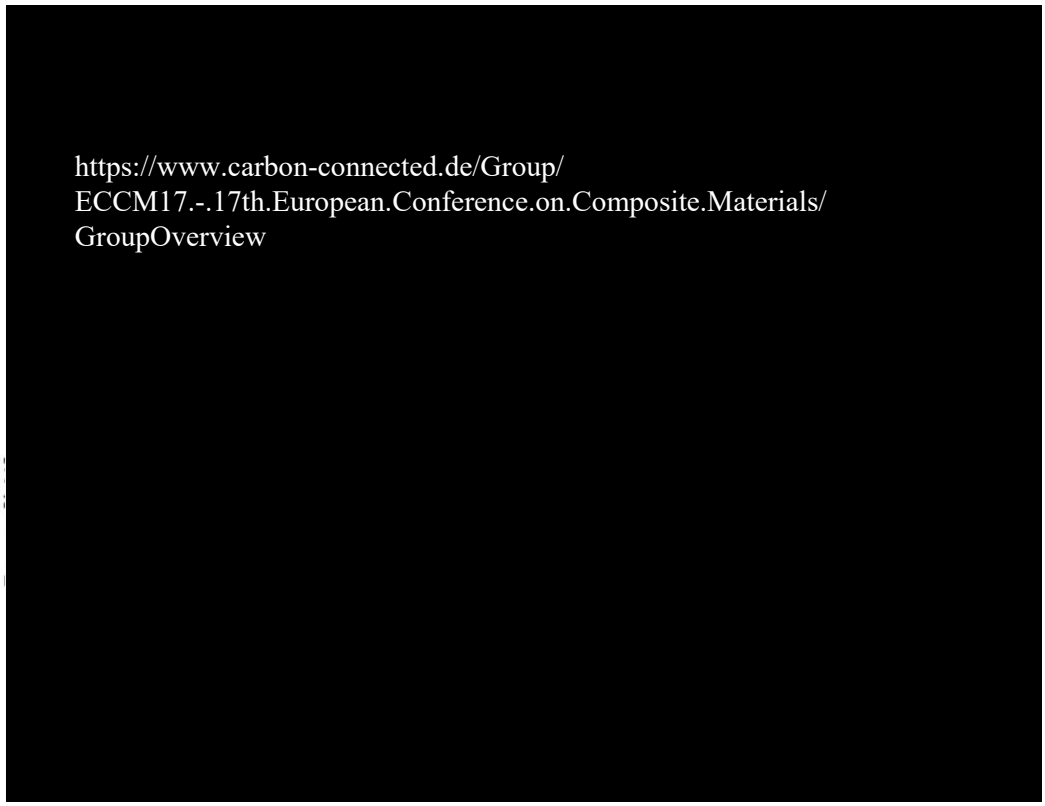

Figure 2-17: A comparison of the failure behaviour and force output for an untufted and tufted sandwich panel during crushing [129]**.**

In a follow-up study, these tests were scaled up to a sub-assembly level, through the development and testing of a crashworthy component for an automotive vehicle [42]. A demonstrator floor sandwich panel modelled on a BMW i3 was tufted and tested in

edgewise compression to represent a typical pole-side impact automotive safety test. Aramid tufts were used to reinforce the sandwich structure, with a target crush distance of 200 mm set for design. Testing of the panel showed a stable crushing behaviour as the pole cut through the panel. The final crush distance was 197 mm, meeting the requirement set in design, and supporting the design methodology used.

2.5 Summary

This literature review has shown that for road vehicles to withstand high-energy impacts during a crash and protect the occupants within, key structural elements must be designed to fail in a controllable manner to maximise energy absorption. Composite materials can achieve very high energy absorption but can be susceptible to unstable collapse, particularly in the case of composite sandwich structures. Methods of through-thickness reinforcement, such as pinning or stitching help stabilise this interface, and it has now been shown that tufting offers great potential to improve the energy absorption of a sandwich panel in the event of a crash.

However, research around tufting of sandwich structures is currently very limited, with a limited understanding of the manufacturing process and failure behaviour of components, particularly under dynamic impact loading. Current design philosophies see very high density TTR patterns used, which would lead to low process rates and poor structural efficiency. Improving the understanding of this technology will lead to better design strategies which will help optimise performance.

Chapter 3 Materials and Methods

In this chapter, an overview of the general materials and processing methods used throughout this study is provided. To remain consistent with closely matched previous works on this subject [42,44,45], the same set of materials and processing methods was maintained. Where it was necessary to introduce new materials or methods, further information is provided in the relevant chapter.

3.1 Materials

Due to the decision to match the materials used in previous work no down selection of materials took place. Instead a single set of materials was used for the manufacture and characterisation of all test samples. These included the reinforcing fibre and resin materials to form the facesheets, the sandwich core material, and the tufting yarns to provide through-thickness reinforcement, as outlined in the following sections.

3.1.1 Reinforcement

Reinforcement for the facesheets of the sandwich panels was provided by a 50K tow (SIGRAFIL C T50-4.0/240-E100) dry uniweave carbon fibre non-crimped fabric (NCF), SIGRATEX C U320/ST (with polyester stitching yarn) from SGL Automotive (320 gsm). The NCF was supplied from SGL in 0° and 45° rolls and was cut to size using an automated ply-cutting machine with a cutting-wheel blade tool. The properties of both the tow and NCF are provided in Table 3-1.

Table 3-1: Carbon fibre reinforcement tow specific properties [130]

Number of Filaments	Fineness of yarn (dry)	Density	Tensile Strength	Tensile Modulus	Elongation at Break	Sizing Type	Sizing Level
-	*Tex (g/km)*	*g/cm³*	*GPa*	*GPa*	*%*	-	*%*
50k	3300	1.80	4.0	240	1.70	Epoxy	1.0

Table 3-2: Carbon fibre reinforcement fabric specific properties [131]

Fibre Orientation	Fineness of yarn	Weight per layer	Weight of stitching thread	Areal Weight	Width	Stitching Thread
-	*Tex*	*g/m²*	*g/m²*	*g/m²*	*cm*	-
0°	3300/68 G	300	7	320	126	Polyester Yarn

In addition to a standard NCF product, a roll of reclaimed carbon fibre was supplied by SGL, under the brand name RECATEX™. The specific material was a type 62 nonwoven complex (400 gsm), with a constituent breakdown as shown in Table 3-3. This material is formed from dry fibre waste, which is put through a carding process, reformed and then sewn together to create a useful product. The use of this material in the context of this project is discussed in Chapter 7.

Table 3-3: Physical Properties of SGL RECATEX Type 62 [132]

Areal Weight	*g/m²*	400 (±15%)
Carbon Fibre Content	*%*	75
Glass Fibre Content	*%*	11
Polymer Fibre Content	*%*	11
Binder Content	*%*	3

3.1.2 Resin

For the matrix, an EPIKOTE® Resin MGS RIMR 935 and EPIKURE® Curing Agent MGS RIMH 936 low viscosity two-part liquid epoxy system was used, supplied by Momentive Speciality Chemicals (now Hexion). The basic physical properties of the resin system are provided in Table 3-4.

Table 3-4: RIMR 935/RIMH 936 Resin Properties [133]

		Resin (RIMR 935)	Hardener (RIMH 936)
Density	*g/cm³*	1.14 - 1.20	0.92 – 0.97
Viscosity	*mPas*	300 - 600	10 - 50
Mixture Ratio (By Weight)	*Parts*	100	29 (±2)

3.1.3 Core

The core of the sandwich panels is formed using a 10 mm thick Rohacell® 110 IG-F closed-cell foam (110 kg/m^3), supplied by Evonik. The foam is a polymethacrylimide (PMI), with a strain to failure of 3%. The mechanical properties of the foam core are shown in Table 3-5.

Table 3-5: Mechanical Properties of Rohacell® 110 IG-F Foam [134]

Density (ASTM D1622)	*kg/m³*	110
Compressive Strength (ASTM D1621)	*MPa*	3.0
Tensile Strength (ASTM D638)	*MPa*	3.5
Shear Strength (ASTM C273)	*MPa*	2.4
Elastic Modulus (ASTM D638)	*MPa*	160
Shear Modulus (ASTM C273)	*MPa*	50

To further characterise the properties of the foam core, compression testing of the foam core was carried out to ASTM standard C365. Square sections of the foam core were cut (50 x 50 mm) and tested in flatwise compression between two rigid flat platens in a Zwick electromechanical test machine using a loading rate of 2 mm/min. The typical stress-strain response of this testing is shown in Figure 3-1, confirming the manufacturer's data of a compression strength of 3 MPa, and highlighting the densification response that occurs at compressive strains around 0.65.

Whilst high variation in properties can sometimes be expected from foam cores, this was not explored in any more detail in this work. It is believed that due to the relative significance of the foam core compared to the other material constituents within the load cases considered here, that variation in properties of the foam core is not critical to behaviour and performance of the sandwich coupons. In addition, the results presented in Figure 3-1 show a good level of agreement between foam test samples, and thus indicate a lower than expected level of scatter of the material properties.

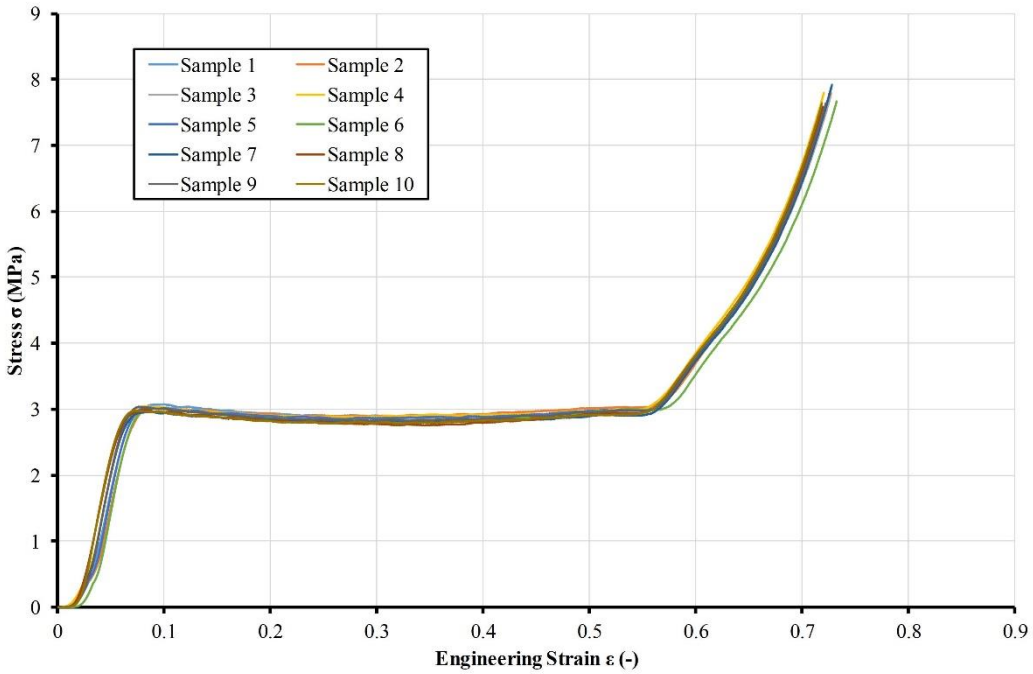

Figure 3-1: Stress-strain response of a Rohacell 110 IG-F foam in flatwise compression.

3.1.4 Tufting Yarn

A tkt-20 Kevlar thread was used to form the tufting yarns of the sandwich panels, supplied by Somac Threads. Kevlar reinforcement was used by necessity, as previous works had shown the difficulty of maintaining the integrity of other threads when tufting through the relatively tough foam core.

Table 3-6: Physical Properties of Kevlar Tufting Thread

Ticket Size	-	20
Thread Construction	*D'tex/ply*	220/6
Final Tex	-	132
Turns per metre	-	308
Final Twist	-	Z
Metres per kg	*m/kg*	6,400
Material Density	g/cm^3	1.44
Thread Diameter	*mm*	0.37
Breaking Strength	*kg*	22
Extension	*%*	4

3.1.5 Laminate Properties

The cured laminate properties of the sandwich panel facesheets were tested and reported in a separate study [135], and are provided for reference in Table 3-7.

Table 3-7: Mechanical Properties of Sandwich Facesheet Fibre/Resin System [135]

Cured Ply Thickness	*mm*	0.37
Average Fibre Volume Fraction	*%*	54.6
Tensile Strength (1-1)	*MPa*	1140
Tensile Strength (2-2)	*MPa*	36.8
Compressive Strength (1-1)	*MPa*	813 [136]
Compressive Strength (2-2)	*MPa*	160
Young's Modulus (1-1)	*GPa*	119
Young's Modulus (2-2)	*GPa*	7.42
Shear Strength	*MPa*	76.3 [136]
Shear Modulus	*GPa*	2.41 [136]
Poisson Ratio	-	0.27

3.2 Methods

This section introduces the manufacturing and analysis processes used across all experimental work. Due to the variation in test methods used throughout the study, specific testing methods are covered in their relevant chapters.

3.2.1 Sandwich Panel Assembly and Manufacture

All sandwich panels and laminates tested were produced in-house using a vacuum assisted resin infusion manufacturing process. The process used features several key stages as outlined in the following sections.

3.2.1.1 Tool Preparation

All test panels manufactured were done so using a 1200 x 600 mm aluminium tool plate. Prior to infusion the tool plate was covered with a self-adhesive PTFE coated glass fabric tape to facilitate part release. Furthermore, a single layer of unperforated FEP release film was placed over the tool and held down with high-temperature PET flash tape.

3.2.1.2 Preform Assembly

All preforms were assembled by hand in a climate-controlled clean room at the University of Bristol (UoB). Cut plies (typically 600 x 500 mm) were placed sequentially on to the tool with no intermediate debulk process carried out. The foam core was cut to the required size using a jigsaw and cleaned using a vacuum cleaner and a brush end-connector to remove any traces of dust from the cutting process. The foam core was then placed on the stacked plies and the remaining plies laid up on top to complete the layup process.

Following assembly of the dry sandwich preform, a hot debulk cycle was carried out. Firstly, an additional layer of FEP release film was placed over the top of the preform, followed by a single layer of breather. The preform would then be sealed within a vacuum bag against a rigid tool plate (Figure 3-2) and held at temperature under vacuum to stabilise it. The NCF fabric used contains within it a thermoplastic binder and upon heating this binder melts allowing the neighbouring plies and foam core to bind together. Upon cool down, the bound preform can be handled easier, avoiding slipping of the plies. This benefit also extends to the tufting process itself, providing better resistance to slipping as the tufting needle is inserted. The heating cycle used to activate the binder was a 2-hour dwell at 90°C under vacuum pressure. After cooling, the panel would be sealed to keep it protected from dust and moisture prior to tufting.

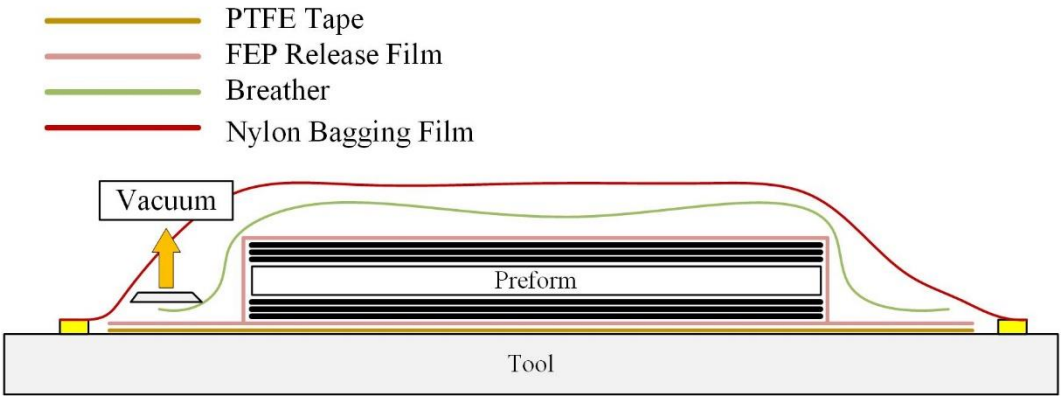

Figure 3-2: Vacuum bagging scheme for performing a debulk cycle on a sandwich preform.

3.2.1.3 Tufting

Tufting of all sandwich preforms was carried out using the through-thickness reinforcement facilities based at the UK National Composites Centre (NCC). The tufting unit comprises of a six-axis KUKA robotic arm, with an end-mounted KSL tufting head (Figure 3-3).

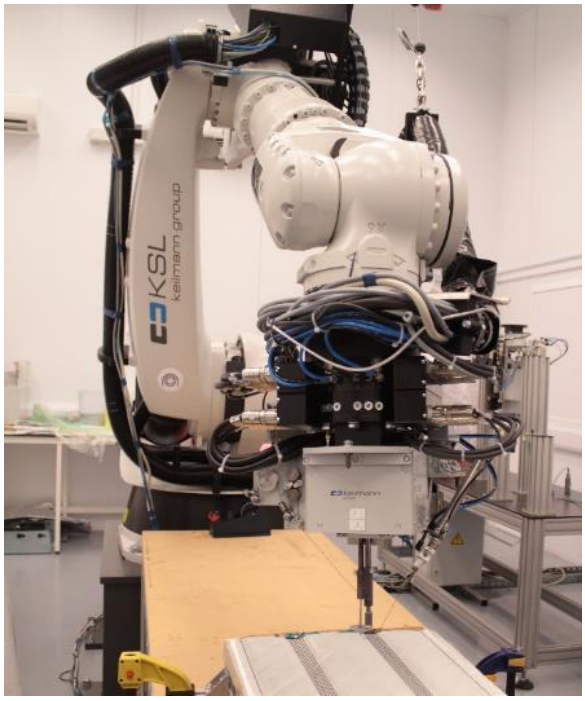

Figure 3-3: Overview of the tufting setup located at the UK NCC.

The tufting head is a pneumatic system that contains a needle and presser foot mounted on the underside (Figure 3-4). The needle acts independently of the tufting head and can insert and retract to drive the reinforcing yarn through the preform. The tufting needle used is specifically designed for the process (Figure 3-5), featuring an embedded channel along the length of the needle to protect the thread during insertion. The tufting needle used for this process was approximately 2 mm in diameter. The presser foot acts in conjunction with

the needle to apply local pressure to hold the material down as the needle is inserted and then retracted.

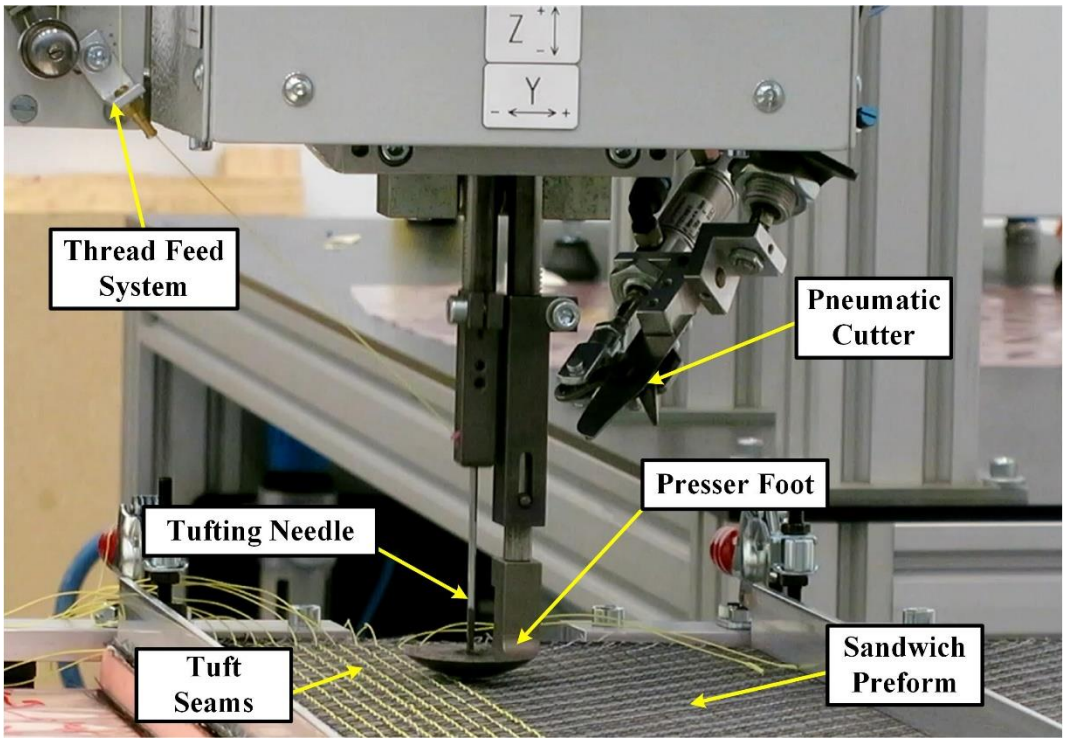

Figure 3-4: Close-up view displaying the key components of the tufting head.

To carry out the tufting process the dry preform is first placed on to a level tool surface within reach of the robotic arm. A sacrificial block of thick polystyrene (or similar) foam is placed beneath the preform to allow the tufting needle to pass completely through the preform during insertion. A nylon film is also placed between the backing foam and the preform to help enable release when the process is finished. Metal bars are then clamped down on to the surface of the preform to hold it in place.

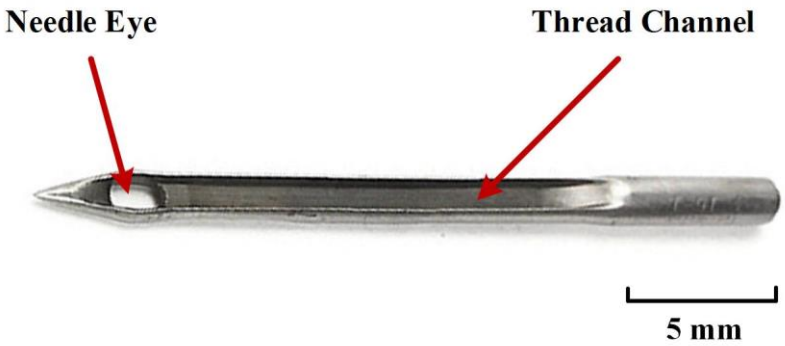

Figure 3-5: Example of a typical tufting needle.

Control of the tufting process is carried out using a CNC programme, which allows control of both the robot arm positioning as well as independently the operation of the tufting head. Controllable parameters include the tuft position and insertion angle, insertion rate, and insertion depth of the needle relative to the total thickness of the preform (Figure 3-6). Whilst the location, angle and spacing of the tufts can be defined with some certainty, the depth of insertion is dependent on the type of preform to be tufted, as the compressibility of the preform will affect needle penetration depth. To overcome this, nominal values are typically defined for the material thickness and penetration depth followed by a process of trial and error to ensure adequate penetration of the needle, and suitable formation of the tuft loops on the back face of the preform. The tufting setup is capable of penetration depths up to 33 mm, at which point clearance between the equipment and preform are no longer adequate. Once these parameters have been chosen the system can be set to run automatically, inserting seams of tufts at the desired locations. At the end of each seam, the tufting yarn is cut using an automated pneumatic cutter and the head moves to the next location.

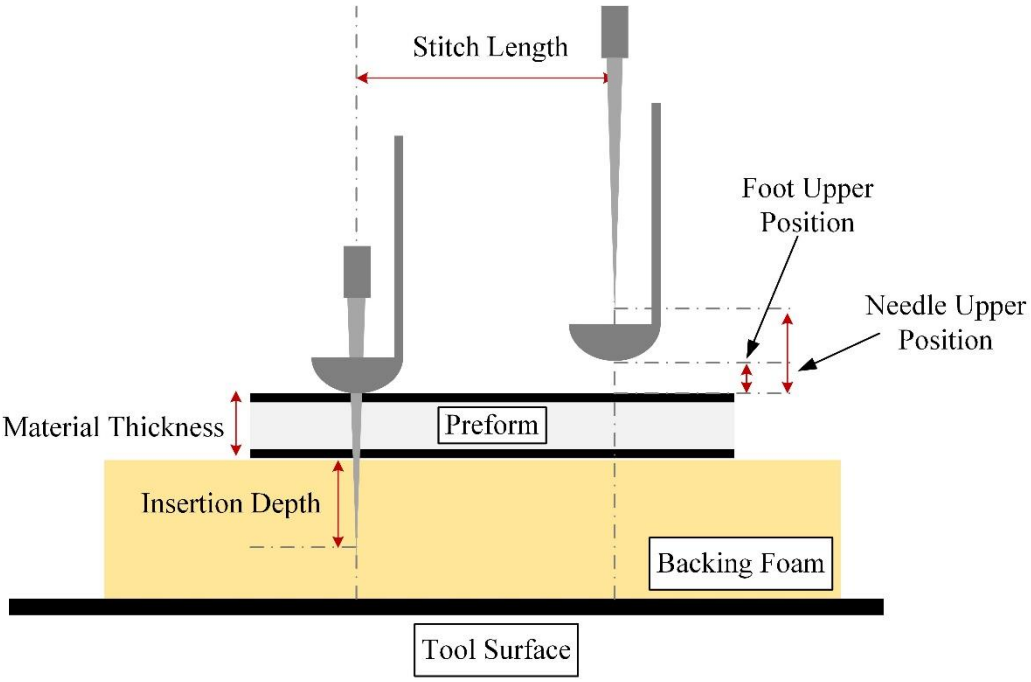

Figure 3-6: Schematic showing the manufacturing parameters that can be adjusted.

The mechanism of tuft insertion relies on friction of the preform to hold the tufting thread in place as the needle retracts. An inherent problem of TTR methods, is that the surrounding preform conceals the mechanisms that are taking place. To be able to observe this mechanism, and for later use in observing process variables in defects, a tool was developed that could allow the process to be captured. To simulate the tufting process, a custom-made

rectangular box was manufactured from transparent acrylic, as shown in Figure 3-7. Further detail of the development and use of this tool can be found in [137] and [138].

The box was designed to hold a sandwich preform whilst representing the boundary conditions of a full-scale panel. Holes were cut into the top of the box to enable a tufting needle to pass through, with the remaining upper surface covered provide the constraining effect of the presser foot as the needle is retracted. The transparent face allows the full path of the needle as well as the development of the tuft within to be tracked.

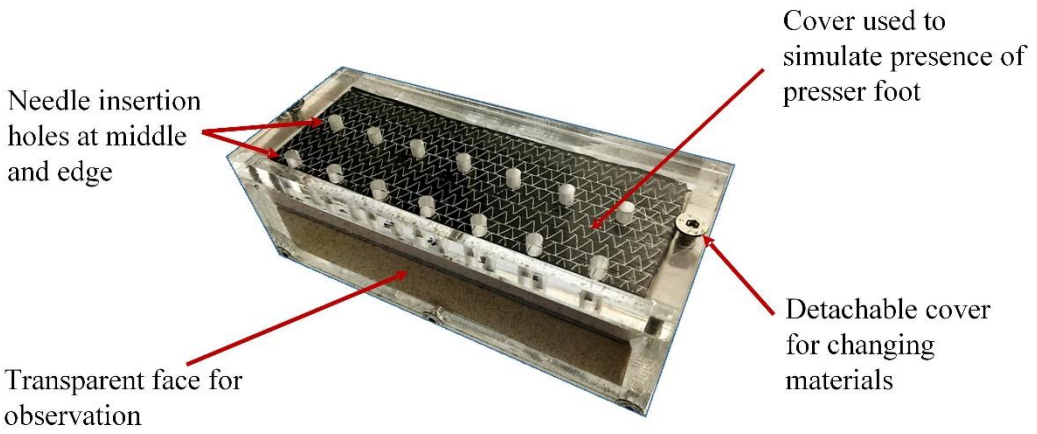

Figure 3-7: Prototype tufting observation tool.

To generate the motion of the tufting needle through the preform, an Instron 3343 desktop electromechanical test machine was used. The upper grip of the test machine was modified to allow the needle to be attached (Figure 3-8), whilst the lower grip was removed completely to allow positioning of the tool in line with the load path. A temporary frame was assembled around the box to prevent it from slipping under the force of the needle and to hold it in place as the needle was retracted (Figure 3-9).

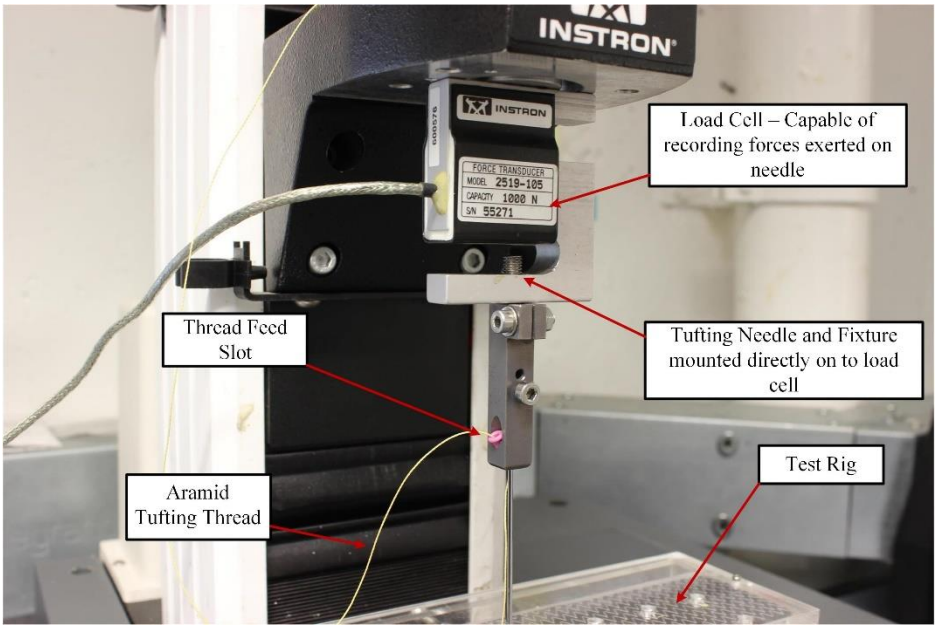

Figure 3-8: Experimental set-up for preliminary tufting trials using the Instron 3343 test machine.

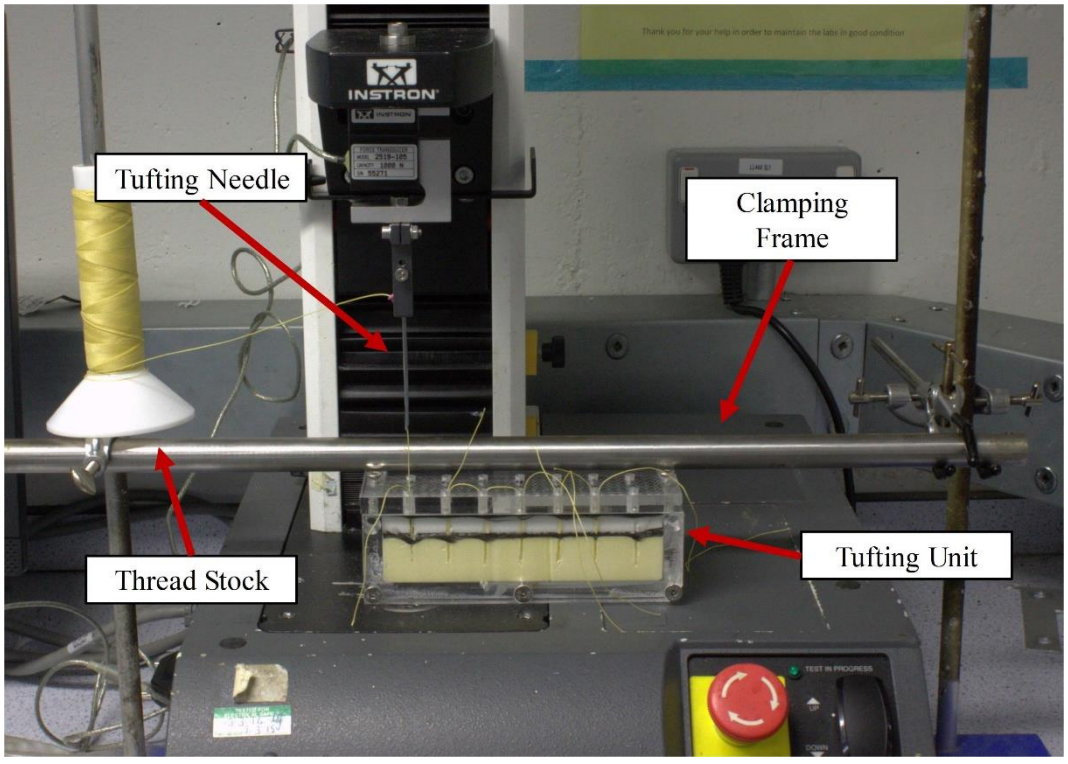

Figure 3-9: Close view of the tufting needle attachment to the test machine and load cell.

Control of the insertion and retraction process was carried out using a simple 'compression-tension' load profile. Control of the test machine allowed rates ranging from 100 mm/min to 1,000 mm/min to be tested.

Figure 3-10 shows the full process of the formation of a tuft within a sandwich panel preform as captured using the tufting tool. Initially the needle passes through the various elements of the sandwich preform; the upper skin (1), foam core (2) and lower skin (3), before penetrating the foam backing material beneath (4). At this point the needle reverses direction and retracts from the preform. The tufting thread remains locked in place by the friction of the facesheets of the preform and remains in place while the needle can freely slide by (5). After complete retraction of the tufting needle, the full extent of the tuft within the preform can be seen (6).

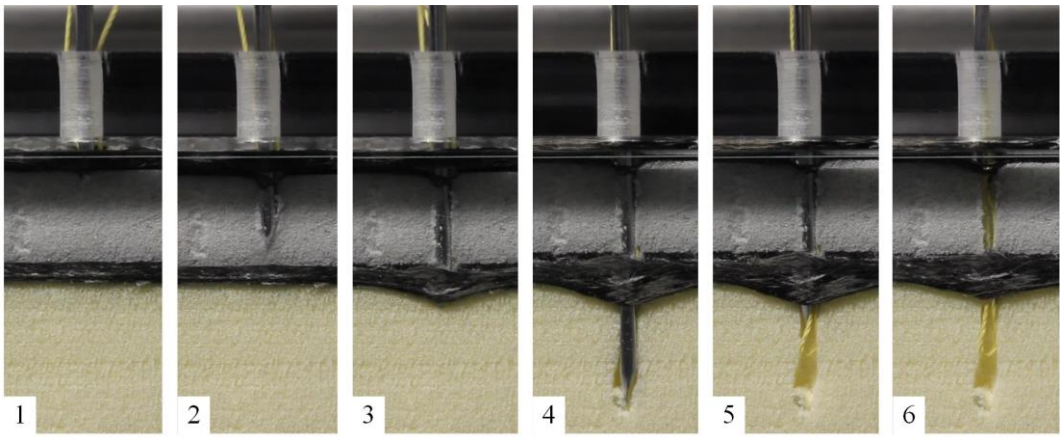

Figure 3-10: Step-by-step process of tuft formation. Stages 1-4 show the stages of needle insertion through the preform. Stages 5 & 6 show the formation of the tuft as the needle is retracted.

Using the tufting rig, several insertion trials were carried out to determine observable defects that can occur as a result of needle insertion and retraction. As an initial feasibility study, commonly occurring observable defects were grouped together into three measurable parameters; carbon debris, core collapse, and channel dimension and scored based upon a "quality matrix". It should be noted that by selecting and grouping measurable defects in this way, a design of experiments (DoE) methodology has not been followed. Future work in this area would look to incorporate DoE, along with a detailed "failure modes and effects analysis" to provide a stronger link between quality and performance. Further detail and the results of this set of experiments are covered in Section 8.6.

3.2.1.4 Infusion and Cure

Following tufting of the preform, the sandwich panel is then prepared for resin infusion. The vacuum-assisted resin transfer moulding (VARTM) method is used for all panels manufactured. The sandwich preform is placed on a flat tool plate, and a layer of peel ply and infusion mesh placed on each surface of the sandwich to aid resin flow across the preform. A 13 mm diameter steel helical spring is placed along one edge of the panel to distribute the resin and create an even flow front across the panel. A double vacuum bagging method is used to seal the part. The inner bag forming a chamber around the part for the resin to flow into, with the outer bag providing vacuum pressure onto the part during cure. The complete bagging scheme for infusion is shown in Figure 3-11.

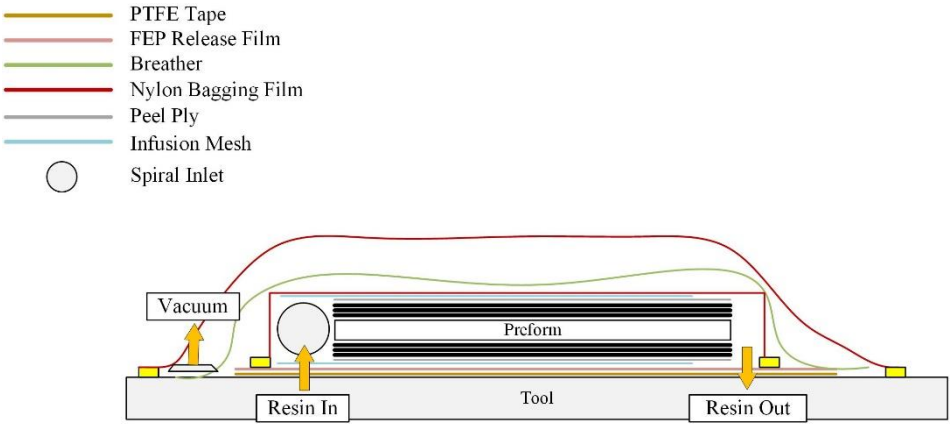

Figure 3-11: Vacuum bag scheme required to carry out an infusion on a sandwich preform.

After setup and leak testing of the vacuum bag, the plate is placed within an oven and heated to a temperature of 35°C, for a dwell time of 1 hour, to allow uniform heating of the preform and tool. The resin is then mixed and degassed for a period of 15 minutes until any trapped air bubbles had cleared from the surface of the resin. The resin feed line is then unclamped, and the resin allowed to flow into the part. Resin infusion could continue until the resin reached the vacuum outlet pipe, at which point both inlet and outlet pipes are clamped, and the resin allowed to cure. The cure cycle used is 2 hours at 60°C, followed by a 2-hour post-cure at 90°C. After cure the part is cooled before removing from the oven. The tool can then be stripped down, and the peel ply and mesh removed from the surfaces of the panel.

3.2.1.5 Moisture Uptake

It is important to highlight that whilst Rohacell foam is susceptible to moisture uptake, no direct measurements of relative humidity of the manufacturing environment or change in mass of the foam cores was carried out in this work. In order to reduce the possibility of

moisture uptake within the panels, manufacturing processes were carried out in environmentally controlled areas wherever possible. Both the layup and tufting phases were carried out in “clean” rooms, whilst panels were sealed within nylon film to transport between sites.

3.2.2 Foam Core Removal

As the tufts are primarily shrouded by the foam core it was necessary to be able to remove the core to allow the tuft structure to be observed, particularly after failure. As discussed by Marasco [84], Rohacell foam cannot withstand an alkaline media. The author successfully used a sodium hydroxide solution to break down the chemical bonds within the core to allow successful removal. They reported a solution concentration of 20-30% in water formed from caustic soda pellets. Warm water and occasional stirring were also used to speed up the reaction. Once the foam reacts it takes on a viscous consistency and can then be washed away using running water.

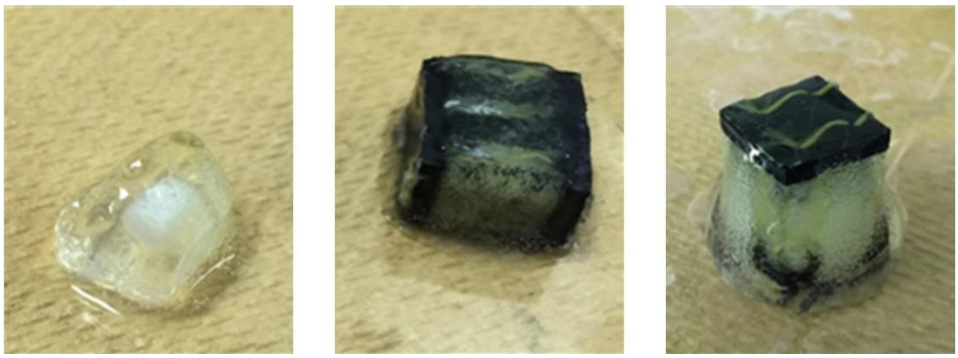

Figure 3-12: Viscous form of Rohacell foam after reaction with Sodium Hydroxide solution.

Several attempts were made to replicate this technique, using 20-30% wt. solutions of differing volumes. Leaving pieces of core within the solution for extended periods of time softened the core significantly but no significant loss of volume was observed. Layers of material could be scraped away using mechanical input, however the very centre of the part typically remained quite brittle suggesting the alkaline solution had not penetrated deep enough. The action of running water also did little to remove any of the softened material.

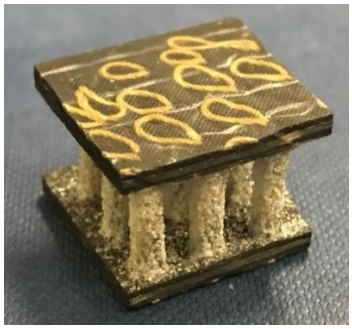

Figure 3-13: Sample part after core removal, showing rough surface finish on the resin columns.

To improve the process, an ultrasonic bath at elevated temperature was used. The bath temperature could not be controlled, but could reach a temperature of approximately 50°C. To achieve full removal of the core, it was necessary to carry out the process in stages, first by placing within the heated sodium hydroxide solution to soften the material, followed by soaking in clean water to dislodge the viscous residue. Running water and mechanical scraping were then used to separate the dissolved foam from the part. After completely clearing the foam it was observed that a fuzzy white material remained on the resin columns (Figure 3-13). This material is hard and cannot be removed by scraping which implies it is the resin that has infiltrated the open cells at the core boundary.

3.2.3 Specific Energy Absorption

Much of the work presented in this thesis required the determination of the specific energy absoprtion of a coupon after testing. Whilst SEA for this work has been determined using the standard mathematical definition (Equation 2 in Section 2.1.2), a decision still had to be made regarding the crushing length over which the metric was calculated. A logical method would be to use the full crushing distance occurring in the trial for each individual test coupon, however an alternative thinking is to normalise the crushing distance, to remain consistent across each test coupon. The issue with the first approach is that treating each coupon individually can lead to large scatter in results due to dissimilar behaviour. However, by normalising each coupon to a fixed length can hide variations as a result of failure mechanisms that may occur at different locations. Within this work, both methods have been used due to their suitability for different test cases and the design intent. Justifications for both will be presented in the relevant chapters.

Chapter 4 Single Tuft Testing

4.1 Introduction

As tufting is a relatively new manufacturing process for composite parts, one area that has not been clearly defined is the influence that the manufacturing process has on the performance of tufted components. As was introduced in Chapter 3, control of the tufting process is driven by several variables that need to be chosen by the machine operator to define the pattern to be inserted into the preform. Due to the consistent nature of CNC control, the absolute positions of the tufts within the preform can be defined with a high level of accuracy, ensuring consistency across different preforms. This would likely be driven by design and would therefore typically be fixed in advance of manufacture. On the other hand, what is less well understood, is the control of insertion depth (and therefore the resulting loop length) and type of thread, with regards to material and density, used to form a successful tufted preform. As a result, these variables are currently heavily reliant on the experience of the operator, rather than being specific design choices. In addition, as the tufting process relies on friction alone to hold the reinforcement in place within the preform, there is the distinct possibility that the reinforcement can slide, either during the needle insertion and retraction process, or during subsequent preform handling. The result of this is the presently unreliable nature of the tufting process with regards to a consistently defined and replicated tuft geometry. In the interest of understanding the implications of these potential variations and for improving future design, it is necessary to understand the role that loop length and thread type play in mechanical performance of tufted sandwich structures. This chapter details an edgewise crush test method using a novel coupon design to characterise the influence of these variables. The foundation of the work presented in this chapter was originally produced as part of an extended research project [139], and has been published externally in [140].

4.1.1 Manufacturing Variability

The loop of thread that is formed at the end of a tuft is dependent on several factors. Primarily the influencing factor is the depth of needle penetration, although this is also influenced by the local compaction of the preform provided by the presser foot. Whilst the way the tufting yarn is threaded through the needle will naturally always cause a loop to form at the end, if the needle does not push deep enough through the preform then the loop will not be exposed, thus denying the opportunity for it to anchor on the surface. In addition to this, a suitable backing material is required that can allow the needle to penetrate through

the full depth of the preform and then hold the loops in place as the needle is retracted, with empirical results showing variation across different backing materials.

Loop formation can be sensitive to other factors, such as inadequate calibration of the tufting bed causing misalignment between the preform and the needle, or the preform itself, where factors such as variations in thickness or flexing of the preform can change the path the needle follows and result in variations in tuft length. This is shown in Figure 4-1, where loop formation varies across the surface of the preform, whilst also exhibiting regions of incomplete tuft formation.

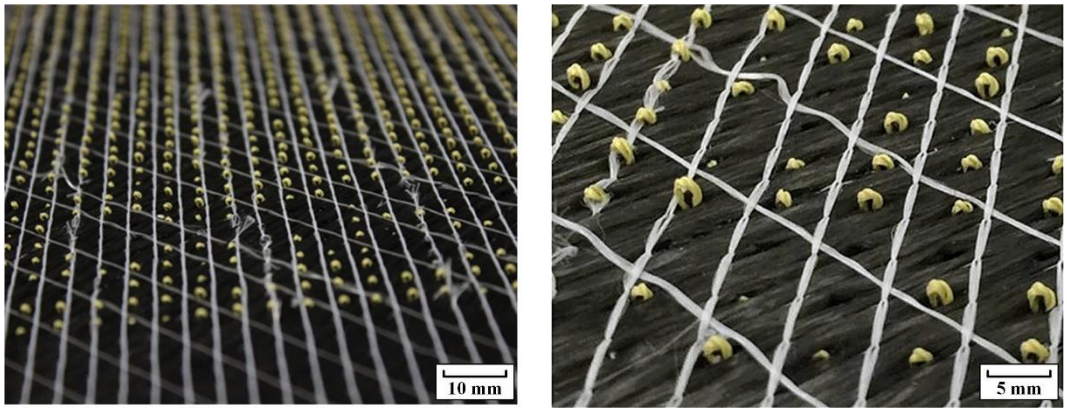

Figure 4-1: Varying loop formation across the surface of a sandwich preform. Left: Overview. Right: Close View.

Even after tufting is complete, there is still a threat that subsequent removal and handling of the preform can lead to slipping of the plies and reinforcing yarns and thus pull-out of the tufts. Between tuft insertion up until the point the part is fully cured there are numerous opportunities for the tufts to be disturbed, leading to the final observed variations as shown in Figure 4-2.

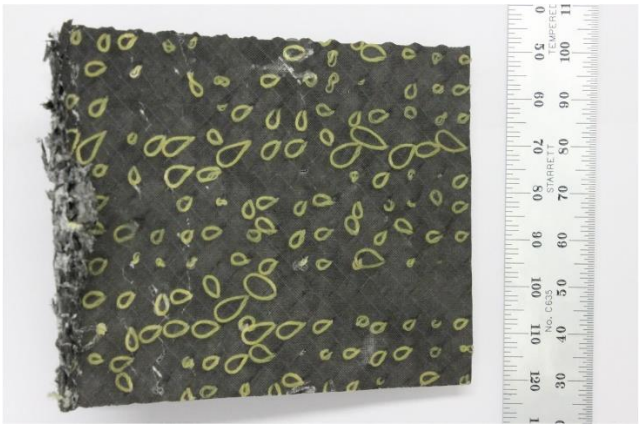

Figure 4-2: An example of loop variation visible on the surface of a cured sandwich panel.

Aside from the definition of the loop, another key variable is the type of thread used for reinforcement. Whilst the performance of different threads has been explored in the past in monolithic parts [141], no such documented investigation has been carried out in sandwich assemblies. The relatively high density and abrasiveness of the foam core, along with the additional thickness mean that a suitably resilient material must be used that can withstand the insertion process without breaking. In addition, the diameter of the thread is also a consideration, as the thread needs to fit through the eye of the needle whilst it must also be able to freely slide through as the needle is retracted. In the previous works that this study seeks to address [42,45], a tkt-20 kevlar thread with an approximate diameter of 0.37 mm was selected to meet these criteria, as outlined in Chapter 3. The output of these studies demonstrated successful tuft formation across several preforms using this thread type.

4.2 Test Coupon Design

In general, crashworthiness testing and the crushing behaviour of composite materials is not standardised meaning that methods in the literature can vary significantly [45,73,78,84,142]. Furthermore, in this case it was decided that to isolate the variables of interest, and eliminate variability across the coupon, that testing should focus on individual tufts. Whilst isolated testing of through-thickness reinforcements has been carried out in the past [143,144], a crushing load-case has not been explored in this manner. To overcome the lack of standard test methods and the novelty of isolating single reinforcements it was therefore necessary to develop a novel test method and coupon design.

4.2.1 Coupon Design

To develop the test method, initially experience was taken from previous investigations involving sandwich crush testing, but also from the ASTM standard C364 (Edgewise Compression of Sandwich Structures) [145]. In this test, a compressive load is applied parallel to the facesheets of a sandwich coupon, using rigid platens. The load is transferred to the coupon with fixed end conditions, either by clamping or bonding the edges of the coupon. The major difference between this method and that desired is the principal failure mechanism. The ASTM test method is designed to ensure failure of the coupon occurs through buckling, either by facesheet wrinkling or global column buckling of the sandwich but taking place away from the fixed ends within the gauge section of the test coupon. In the case of crashworthiness, the desired failure mechanism is progressive crushing from one end of the test coupon. To make this failure mechanism possible, as well as the necessary scaling required to suit an individual tuft meant that a redesigned coupon geometry was required.

Initial trial tests were carried out on small rectangular sections of tufted sandwich panels to explore the feasibility of reducing the scale of a test component. Using rectangular samples of dimensions approximately 30 x 20 mm (load applied parallel to the long edges), and testing with one of the shorter edges both clamped and unclamped, it was observed that a successful stable splaying and crushing mechanism could be achieved, at loading rates of 0.5-1 mm/min. It was noted that a crucial part of this success was that the loading surfaces (the short edges of the coupon) must be parallel, otherwise an unstable failure mechanism would occur. Furthermore, clamping at the base of the coupon helped to ensure that crushing failure would occur at the free end every time, as opposed to the unclamped tests where the end at which crushing initiated could not be controlled. Following these trials, a coupon geometry was designed to accommodate testing of a single tuft, with the resulting coupon geometry shown in Figure 4-3.

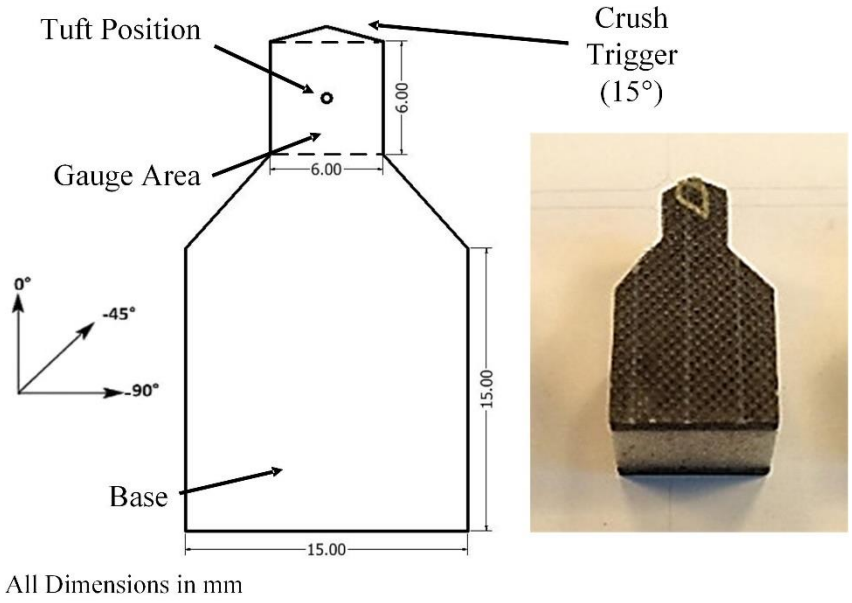

Figure 4-3: Test coupon design and dimensions (left), with a representative coupon (right).

The driving factor around the chosen geometry was to produce a gauge section that was representative of a unit cell of a tuft, based upon the tufting spacing used in prior works. The gauge section of the coupon as highlighted in Figure 4-3 is a 6 mm x 6 mm square region, with the tuft located at the centre, which represents the unit cell of a 6 mm square tuft spacing configuration. To enable stable crushing through the gauge section of the coupon, a ‘tulip’-type crush trigger was included within the design. The trigger acted as a stress concentration to promote failure, as introduced in section 2.2.2.1. A trigger angle of 15° was chosen for this design as this is above the reported threshold value for stable crushing to be exhibited in sandwich structures [146]. The base section consisted of a 15

mm x 15 mm square, large enough to clamp the coupon into an end support, as determined in preliminary trials, and suggested in the ASTM standard for edgewise compression testing. The chosen test fixture was composed of two screw-tightened steel bars of 10 mm thickness to clamp the base of the coupon (Figure 4-4). The fixture provided two roles during testing, not only did it hold the coupon upright and keep it from slipping during, but also provided some constraint on the facesheets to avoid immediate separation of the entire facesheet. Some rotation was allowed at the base of the coupon to help it sit flat against the fixture and align with the loading direction. A gradual tapered section between the base and the gauge sections was included to allow the progressive crushing failure to continue without a sharp change in geometry. The length of this section was 5 mm providing a taper angle of 26°.

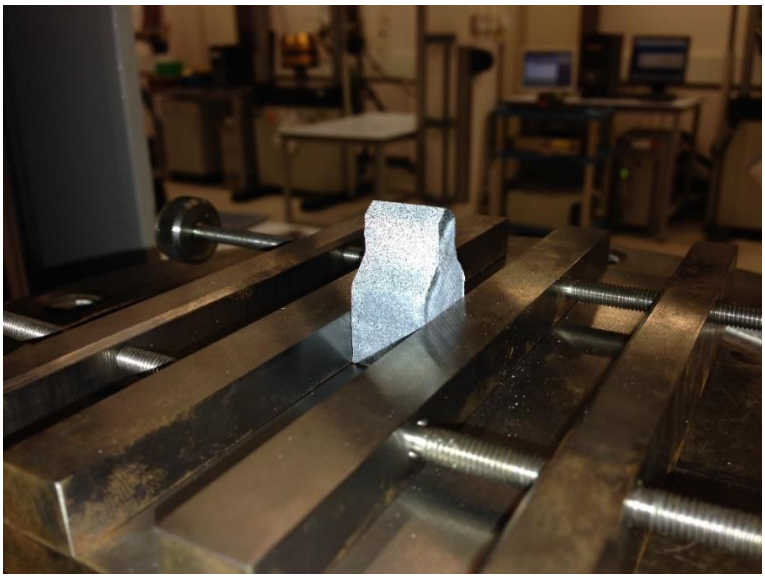

Figure 4-4: Close-up view of the sandwich test fixture used for testing, with a representative test coupon clamped in position.

4.3 Methodology

The sandwich panel used for testing was manufactured using the materials and process outline in Chapter 3.

4.3.1 Tufting Parameters

As discussed in the introduction to this chapter, the chosen variables for the tufted coupons were the tuft length and thread density. During the tufting process, the needle and presser foot starting positions and the insertion rate of the tufting head (900 mm/min) were kept constant for every data series. The stitch length between tufts was also kept constant at 15 mm to enable space for machining of the coupons between the individual tufts.

The remaining input parameters of material thickness and insertion depth were then chosen to provide single tufts with a range of loop sizes, defined as the length from the tip of the loop to the preform surface. Manufacturing parameters were held constant across an entire seam of tufts, before trimming the thread and beginning a new seam with different insertion parameters to produce a preform as shown in Figure 4-5.

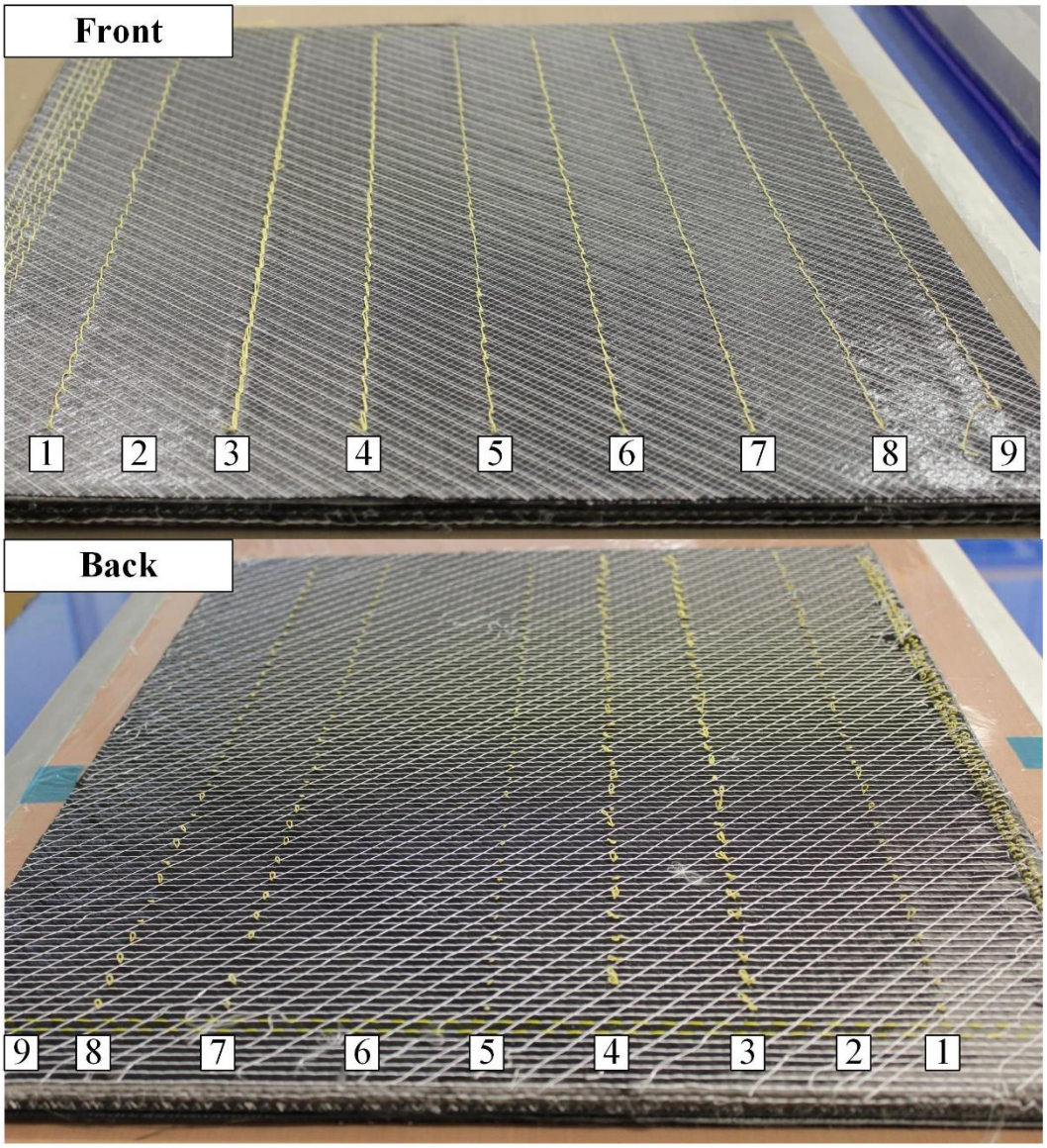

Figure 4-5: Tufted panel prior to infusion, illustrating individual tuft seams with different insertion parameters.

In addition to varying the loop lengths across seams, two other variations were also tested. In seam #6, the needle insertion depth was reduced significantly so that it did not fully penetrate through the foam core. This resulted in a partial tuft that terminated within the core. This is potentially advantageous as removing the loop entirely can avoid the potential for a resin-rich layer to form on the surface as a result of the additional thickness of the tuft

loops that sit proud from the panel surface, which has been linked to improve performance [147]. In seam #9, the thread was inserted using nominal parameters before being removed from the preform after tufting. This action left a void within the panel that would completely fill with resin, but with no TTR in place.

To achieve a variation in the localised density of the tuft and represent varying thread types, double (seam #4) and triple (seam #3) tuft configurations were created by making multiple needle insertions at the same location. This process was chosen over increasing the thread thickness as this was not possible due to the limitation of the needle eyelet and thread feed system. Several untufted baseline samples were also created by cutting from an untufted region of the panel. Example images of the tuft geometry are shown in Figure 4-7, with a summary of the tufting parameters used for each sample series shown in Table 4-1. It was observed that making multiple tuft insertions led to significant variation in the loop size that formed, as exhibited in Figure 4-6. The figure shows a triple tuft, with one noticeably larger loop. It is believed that upon each subsequent tuft insertion, the friction of the needle during retraction would pull-out the existing thread leading to the form shown.

Figure 4-6: Variation in loop formation of multi-tufted seams.

After curing, the average loop size was measured by sampling 10 tufts within each seam, the results are shown in Table 4-1, with the individual datasets named by tuft configuration or average loop size. As expected, reducing the needle penetration depth reduced the loop sizes formed; however, the loop formation was inconsistent, with significant variation of the loop sizes along each seam. This variation increases significantly with the insertion of multiple tufts, due to interaction between tuft threads, as series 3 and 4 show the greatest standard deviation.

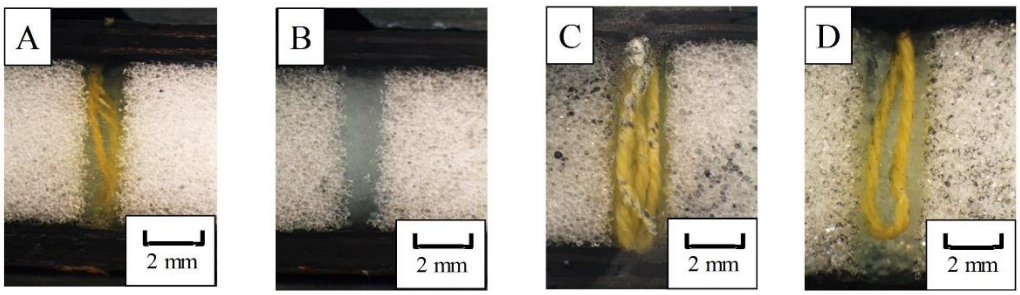

Figure 4-7: Internal micrographs of selected test coupons highlighting the tuft configuration. A) Single tuft coupon of nominal length. B) Coupon with tuft removed prior to infusion. C) Triple tuft configuration. D) Single partial tuft insertion.

Table 4-1: Tufting Insertion Parameters

Seam	Mat. Depth	Loop Depth	No. Tufts	Needle Posn.	Foot Posn.	Average Loop Length	SD	CV
	mm	*mm*	-	*mm*	*mm*	*mm*	-	*%*
1 – Baseline	-	-	-	-	-	-	-	-
2 – 4.5 mm	12	16	1	12	9	4.5	0.90	20.0
3 – 3 Tufts	12	16	3	12	9	5.45	2.26	41.4
4 – 2 Tufts	12	16	2	12	9	4.72	1.25	26.5
5 – 3.2 mm	12	12	1	12	9	3.24	0.57	17.5
6 – Partial Tuft	12	6	1	12	9	0*	-	-
7 – 3.1 mm	10	14	1	12	9	3.14	0.50	16.0
8 – 4 mm	14	14	1	12	9	3.98	0.53	13.2
9 – Resin Column	14	14	1	12	9	0*	-	-

**No loop formation on panel surface*

The cured panel was machined into individual test coupons using a diamond plate saw, with a measured variation in dimensions of ±0.5 mm. The average measured coupon thickness was 14.8 mm, which is slightly higher than predicted based upon foam core and preform thickness due to a resin rich layer forming on the surface of the panel. The average coupon dimensions and variation are shown in Table 4-2, with a breakdown of thickness variation between coupon groups presented in Table 4-3. As expected, an increase in thickness is observed with the addition of tufts when compared to the baseline. It is possible that variation between groups is limited somewhat due to the entire set of coupons being manufactured from a single panel.

Table 4-2: Measured Test Coupon Dimensions

	Base Width	Base Height	Cell Width	Cell Height	Thickness	Trigger Length	Trigger Angle
	mm	*mm*	*mm*	*mm*	*mm*	*mm*	*Degs.*
Average	15.42	15.27	6.51	5.68	14.78	1.16	18.42
SD	0.33	0.73	0.36	0.59	0.10	0.32	6.92
CV (%)	2.11	4.78	5.47	10.43	0.67	27.79	37.60

Table 4-3: Coupon Thickness Comparison

	Average	SD	CV
	mm	-	*%*
Baseline	14.70	0.07	0.46
Resin Column Only	14.76	0.05	0.34
Partial Tuft	14.83	0.07	0.45
3.1 mm Loop	14.86	0.05	0.37
3.2 mm Loop	14.82	0.14	0.93
4 mm Loop	14.87	0.07	0.49
4.5 mm Loop	14.78	0.05	0.37
2 Tufts	14.82	0.02	0.14
3 Tufts	14.83	0.06	0.42

4.3.2 Static Testing

Static testing of the coupons was carried out using a Zwick 1466 electromechanical test machine. Coupons were clamped into the metallic end support and positioned at the centre of the circular loading plates of the test machine. To help align the coupon in the loading direction, the upper crush plate was mounted to a spherical bearing and could rotate as loading occurred. A displacement control program was used to provide a constant quasi-static crushing rate of 2 mm/min; chosen to reduce the total testing time following preliminary trials at 1 mm/min. Figure 4-8 shows the positioning of the coupon within the test machine. Testing was terminated after 8 mm of displacement as this ensured the entire tufted gauge area had been crushed. A total of five samples were tested for each tuft configuration.

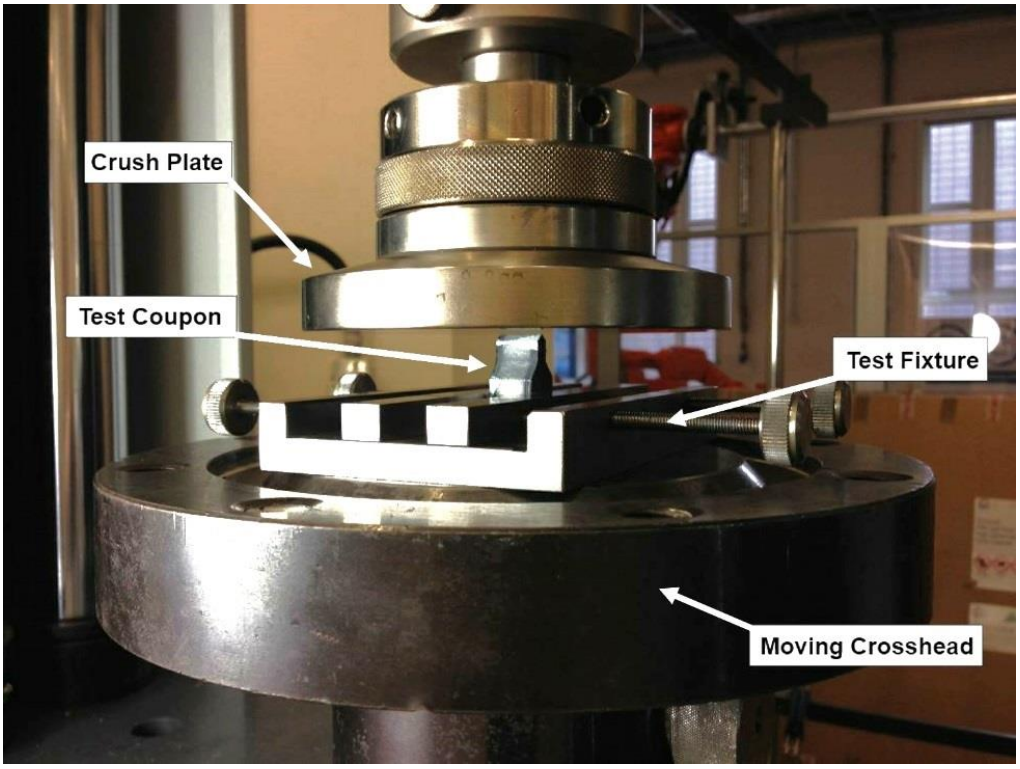

Figure 4-8: Static load case test setup illustrating clamped test coupon located within test machine.

4.3.3 Dynamic Testing

To extend testing to conditions more representative of a crash event, dynamic testing was also carried out. Dynamic loading conditions were achieved using an Instron Dynatup 9250HV drop-tower. To maintain parity with the quasi-static testing, coupons were mounted within the same support as for the static tests and impacted from above by a circular impact plate in a similar setup, as shown in Figure 4-9. The selected impact energy was chosen following an iterative process of increasing impact energies on sacrificial test coupons to determine what energy level would progressively crush the entire gauge section. The chosen impact energy was 20 Joules, which is comparable to the crushing energy exhibited by the quasi-static tests. To achieve this, the necessary impactor mass was 6.45 kg and the velocity at impact was 2.5 m/s. Due to coupon availability following iterative testing of impact energies, only two coupons could be tested per tuft configuration.

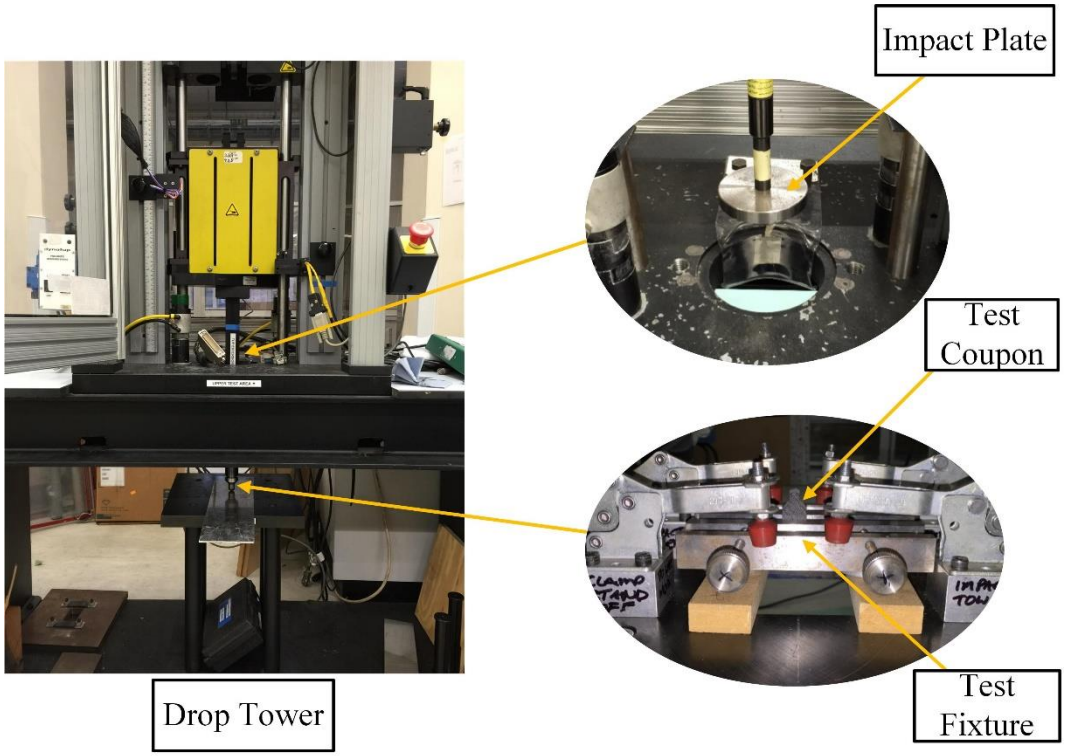

Figure 4-9: Dynamic load case test setup, illustrating coupon clamping method and circular impactor.

4.4 Results and Discussion

4.4.1 Static Crushing

Figure 4-10 outlines the stages of the progressive crushing mechanism exhibited by the test coupons. Image A shows the initial fracture of the facesheets at the crush trigger, followed by initiation of delamination in the facesheets in image B. In image C, the delamination in the right-hand facesheet has progressed noticeably, whilst crushing of the foam core has taken place as demonstrated by the shrinking of the uppermost gauge section of the foam. Finally, in image D facesheet separation has developed, as shown by the formation of a crack between the left-hand facesheet and the foam core. Delamination is now visible on both facesheets whilst the uppermost section of the foam core is no longer visible.

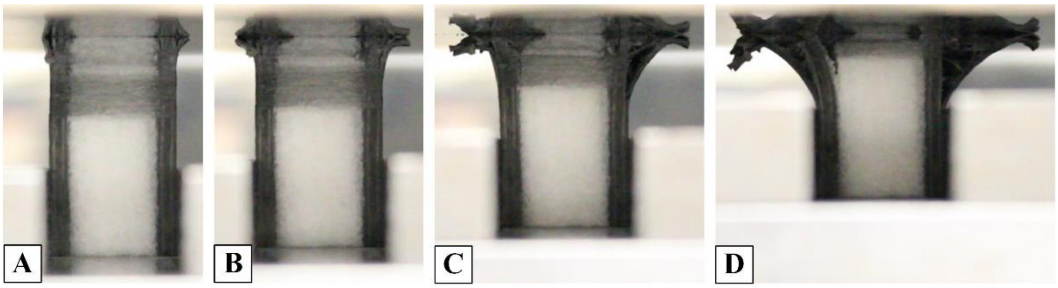

Figure 4-10: Representative stages of the progressive crushing mechanism exhibited by static test coupons. A) Initial fracture, B) Delamination formation, C) Propagation of delamination and facesheet separation and core crushing, D) Further propagation of combined failure mechanisms.

Figure 4-11 shows a single tuft coupon after testing, with the core crushing, facesheet separation and delamination failure mechanisms observed during testing all present. The failure behaviour of the tuft itself (highlighted in the figure) is not immediately apparent, as from the top view, only traces of the Kevlar thread are visible at the surface.

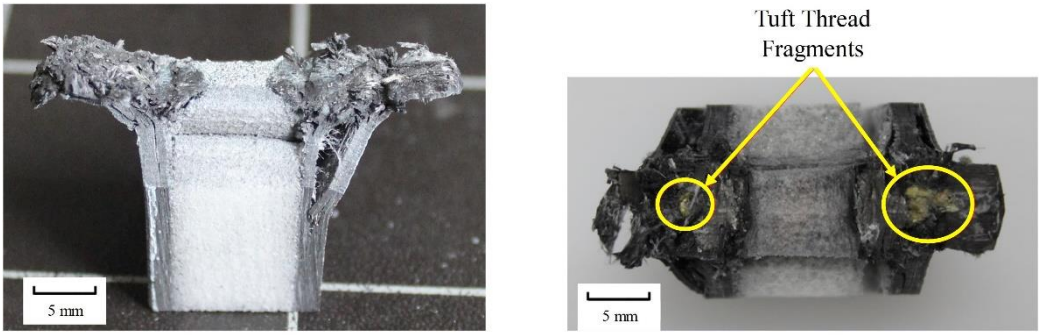

Figure 4-11: Side and top views of a representative tufted coupon following static testing. Tuft fragment colour emnhanced for clarity.

Representative load-displacement traces for several of the test configurations are presented in Figure 4-12. The chosen curves have been selected for clarity, to illustrate the differences between key data series. From the graph, each of the curves follows a distinctly similar trend that can be divided into four phases. In phase A, each of the curves show an approximately linear increase in load as the sandwich coupon resisted the applied crushing load. At its peak, the tapered trigger began to fracture and there was a noticeable drop in load. In phase B, crushing occurred within the gauge section of the coupon, with folding of the skins alongside compression of the foam core. It was at this point that, where present, the tuft begins to restrain the skins to the core, shown by an increase in the load applied to the coupon. In the selected curves shown in Figure 4-12, there is a clear load recovery within the tufted coupons when compared to the untufted baseline and the sample with only

a resin column. There is also some suggestion of a performance hierarchy, with the baseline and resin column samples showing the lowest performance, followed by an increasing load recovery observed in the partial tuft, standard single tuft, and then triple tufted samples. The lack of a reinforcing thread within the resin column appears to significantly reduce performance, resulting in a comparable or potentially weaker structure than the baseline sandwich coupon. Surprisingly, the partially tufted coupon behaved similarly to the full insertion, single tuft coupon. In phase C, the load can be attributed to continual crushing of the remaining part of the gauge section after the tuft. In phase D, an increased crushing load of the baseline coupon was observed. This was due to densification of the foam core, but also because at this point the coupon geometry begins to widen. However, this was not observed in the other tufted coupons, which remained constant through this region. In several of the tufted samples, cracks between the skin and core propagated through to the base of the coupon, which appeared to delay core densification, and this could be the cause of the relative load reduction compared to the baseline. Tests were stopped at a crosshead displacement of 8 mm, to ensure the tuft effect in region B had been captured. Beyond this point there was inadequate clearance between the crush plate and the test fixture to continue testing.

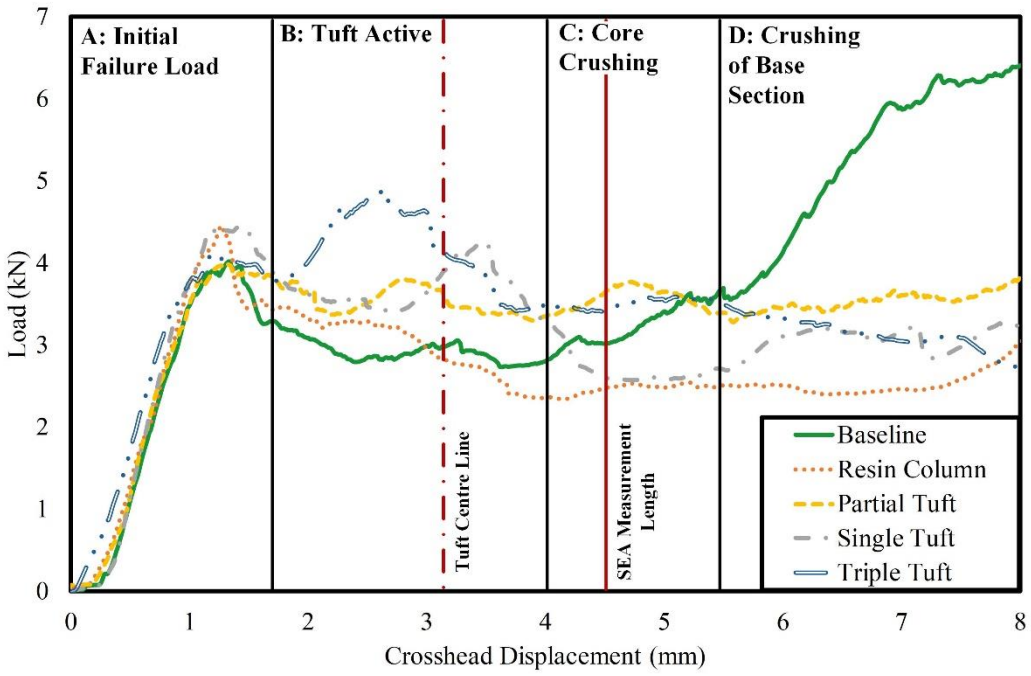

Figure 4-12: Representative static load-displacement traces for the primary tuft configurations tested.

The results presented in Figure 4-12 show that the test method can capture the positive effect of adding a tuft on the crushing performance of composite sandwich structures, whilst the strong correlation between initial peak load and the location of the 'tuft peak'

show good consistency in the method. The load recovery exhibited within the tufted coupons shows the desired reinforcement mechanism that counters the disbonding between the skins and core, but the additional load recovery shown by the baseline samples is not observed within any of the tufted samples. This suggests a further mechanism taking place after the failure of the tuft, which potentially destabilises the test coupon after its peak load.

Figure 4-13 shows several samples of interest after the core was removed. The samples represent four of the major tuft configurations; untufted, partially tufted, single tufted and triple tufted. Each of the columns shows a small portion of the facesheet remaining attached at each end. The degree of attached material appeared to vary between each sample, where the untufted interface has the least amount of material and the triple tuft interface has the most. This implies that the dominant failure mode of the tuft changes depending on how the thread is inserted or how many threads are used. Where no thread is present at the interface a clean break between skin and core was observed, but when the thread is present a fracturing of the surrounding skin takes place. Each of the tufted columns feature Kevlar tassels protruding from the skin, but currently the mode of failure of the tuft thread is not clear.

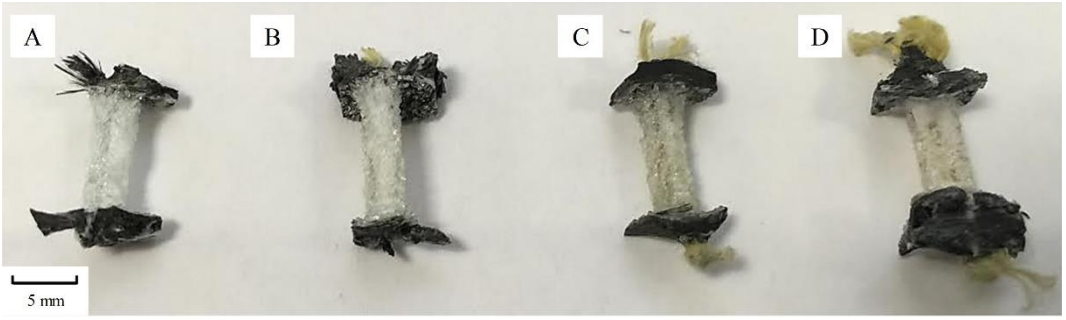

Figure 4-13: Sample tufts and surrounding resin columns removed from coupons following static testing. A) Tuft removed. B) Partial Tuft. C) Single Tuft. D) Triple Tuft.

This is an important observation, as the column remaining intact will allow it to displace through the core as crushing progresses. This mechanism could have a significant effect on the global failure of a tufted sandwich structure, as friction within the core could lead to additional energy absorption. However, it could also have a negative effect as the movement of the column could force the skins away from the core and contribute to disbonding of the sandwich. This could explain why the baseline coupons show a second load recovery in section D, whilst the tufted ones do not.

4.4.2 Dynamic Crushing

Figure 4-14 shows the representative stages of a typical coupon response under dynamic loading. As with the static coupons the failure behaviour is very similar, with initial fracture (A), and delamination formation and propagation, facesheet separation and core crushing (B, C). The notable difference in the dynamic load case is the more elastic response of the facesheets after the load is released, with the facesheets 'springing back' slightly towards their original orientation.

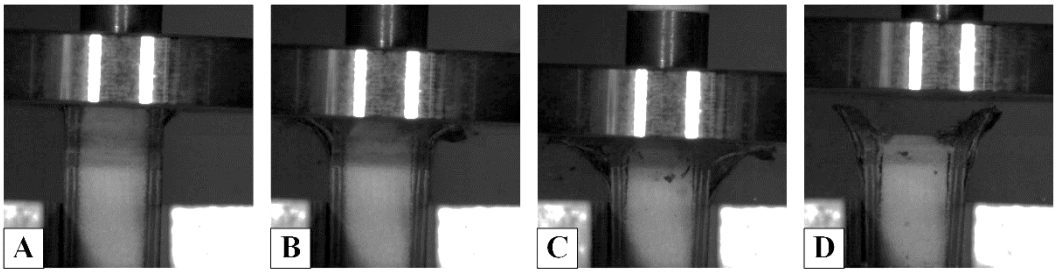

Figure 4-14: Representative stages of the progressive crushing mechanism exhibited by dynamic test coupons. A) Initial fracture, B) Delamination formation, C) Propagation of delamination and facesheet separation and core crushing, D) Elastic response of facesheets after load release.

Figure 4-15 shows representative load-displacement curves for the dynamic tests divided into the same four phases as the static tests (Figure 4-12). Similarly, to the static tests, an initial loading phase up to crush initiation was observed, followed by a load recovery due to the tuft, and finally a progressive crushing phase. Within phase B there is a clear distinction between those samples that are tufted and those that are not, with the triple tufted sample again sustaining the highest crushing load. It is noteworthy that within this section the single and partial tufted samples are more clearly separated from the untufted samples than during the static testing. After phase B, the samples all converge to a similar level, except the baseline which undergoes a second load recovery as the sample geometry widens, as was observed in the static tests. Another observable trend is the termination point of the crushing failure (marked as a solid circle), despite each sample being impacted with the same amount of energy. The triple tufted sample appears the most efficient as it stopped the impact in the shortest distance. This is followed by the single tufted sample, the baseline and then the partial tuft and resin column samples, which stopped at a similar point.

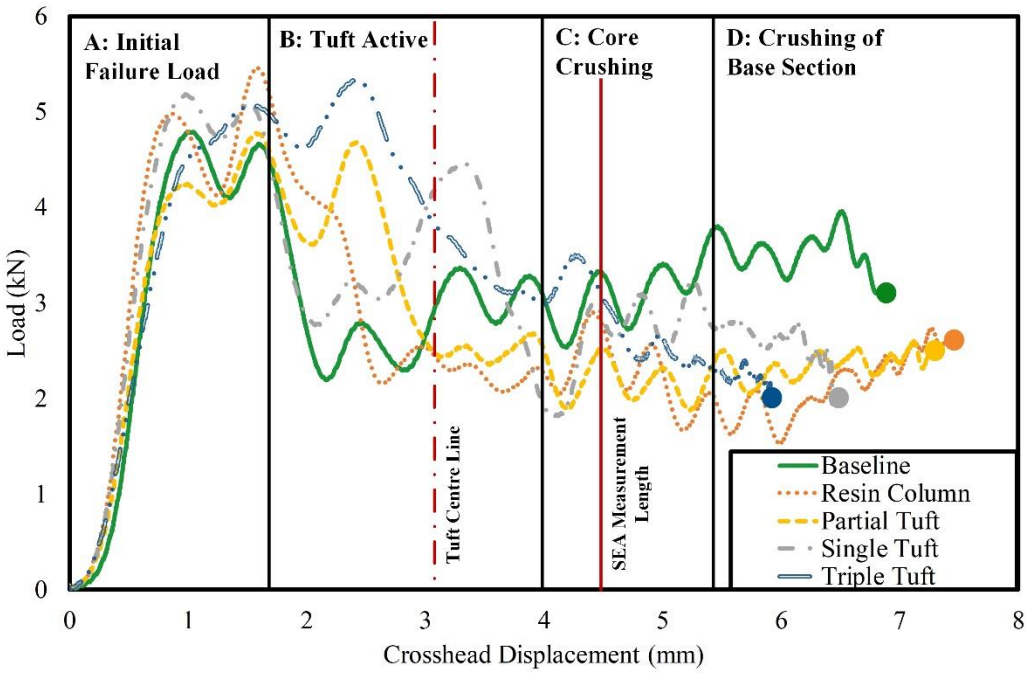

Figure 4-15: Representative dynamic load-displacement traces for the primary tufted configurations. Solid circles represent point of test termination.

4.4.3 Energy Absorption

The specific energy was approximated for each test by integrating the area under the averaged load-displacement curve using the trapezium rule and then dividing by the crushed mass of the coupon, as in Equation 2 in section 2.1.2. To estimate the mass of the crushed material, an average sandwich areal density was approximated by using the surface area of the test coupons, using the dimensions shown in Figure 4-3, and dividing by the coupon mass to give an approximate areal density of the coupon. A parameterisation of the surface area of the coupon with respect to the total crushed distance was then created, as shown in Figure 4-16 and equations 3, 4, 5, and 6, which when combined with the areal density allowed for an estimation of the crushed mass.

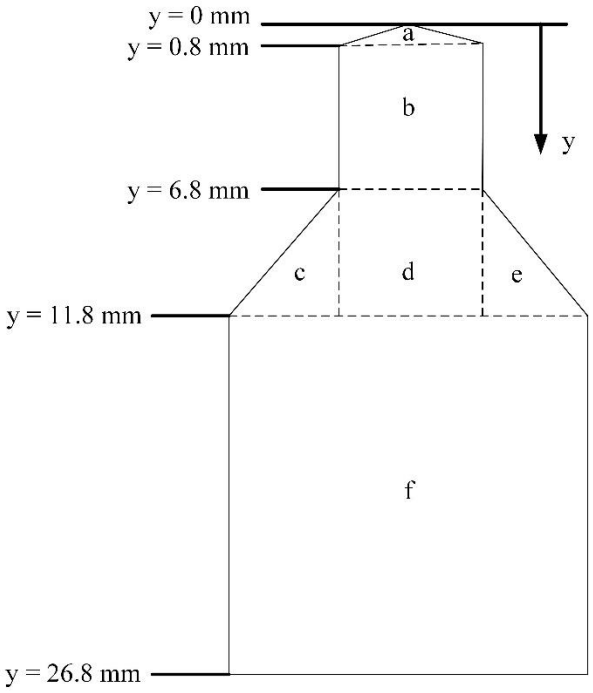

Figure 4-16: Surface area parameterisation breakdown used to estimate crushed material mass.

$$For\ y\ \leq 0.8, \qquad Area = 0.5y^2 \times \left(\frac{6}{0.8}\right) \tag{3}$$

$$For\ 0.8 \leq\ y\ \leq 6.8, \qquad Area = a + [6 \times (y - 0.8)] \tag{4}$$

$$For\ 6.8 \leq\ y\ \leq 11.8, \qquad Area = a + b + [(y - 6.8) \times 10.5] \tag{5}$$

$$For\ 11.8 \leq\ y\ \leq 26.8, \qquad Area = a + b + c + d + e + [(y - 6.8) \times 15] \tag{6}$$

To be able to isolate the region in which the tuft is active, and thus directly compare each configuration, the summation of the energy absorption and subsequent crushed mass was only carried out over the first 4.5 mm of crosshead displacement, as indicated in Figure 4-12 and Figure 4-15. Both load-displacement plots indicate that crushing force is relatively stable at this distance, and thus makes it an ideal location to terminate the test. The alternative method to this would be to use the entire dataset, up to the point that the test was terminated. This was not desirable as the variations between untufted and tufted tests in phase D would have masked the differences in behaviour between tuft failures in phase B. The calculated energy absorption values for both static and dynamic tests are shown in Table 4-4 and Table 4-5 respectively, and presented graphically in Figure 4-17.

Table 4-4: Static SEA Test Results

Group	Count	Average SEA	SD	CV
-	-	*kJ/kg*	-	*%*
Baseline	5	61.45	3.49	5.68
Resin Column Only	5	60.68	1.23	2.02
Partial Tuft	5	66.42	1.61	2.42
3.1mm Loop	5	71.78	7.72	10.76
3.2mm Loop	5	67.23	2.52	3.75
4mm Loop	5	69.91	3.40	5.71
4.5mm Loop	5	65.00	2.05	3.15
2 Tufts	5	73.90	2.77	3.83
3 Tufts	5	72.20	4.43	6.00

Table 4-5: Dynamic SEA Test Results

Group	Count	Average SEA	SD	CV
-	-	*kJ/kg*	-	*%*
Baseline	2	65.91	1.08	1.65
Resin Column Only	2	67.52	0.51	0.76
Partial Tuft	2	70.59	0.35	0.50
3.1mm Loop	2	74.09	2.70	3.65
3.2mm Loop	2	76.38	8.47	11.09
4mm Loop	2	74.96	0.72	0.97
4.5mm Loop	2	74.00	4.67	6.32
2 Tufts	2	81.88	0.07	0.09
3 Tufts	2	81.46	1.49	1.83

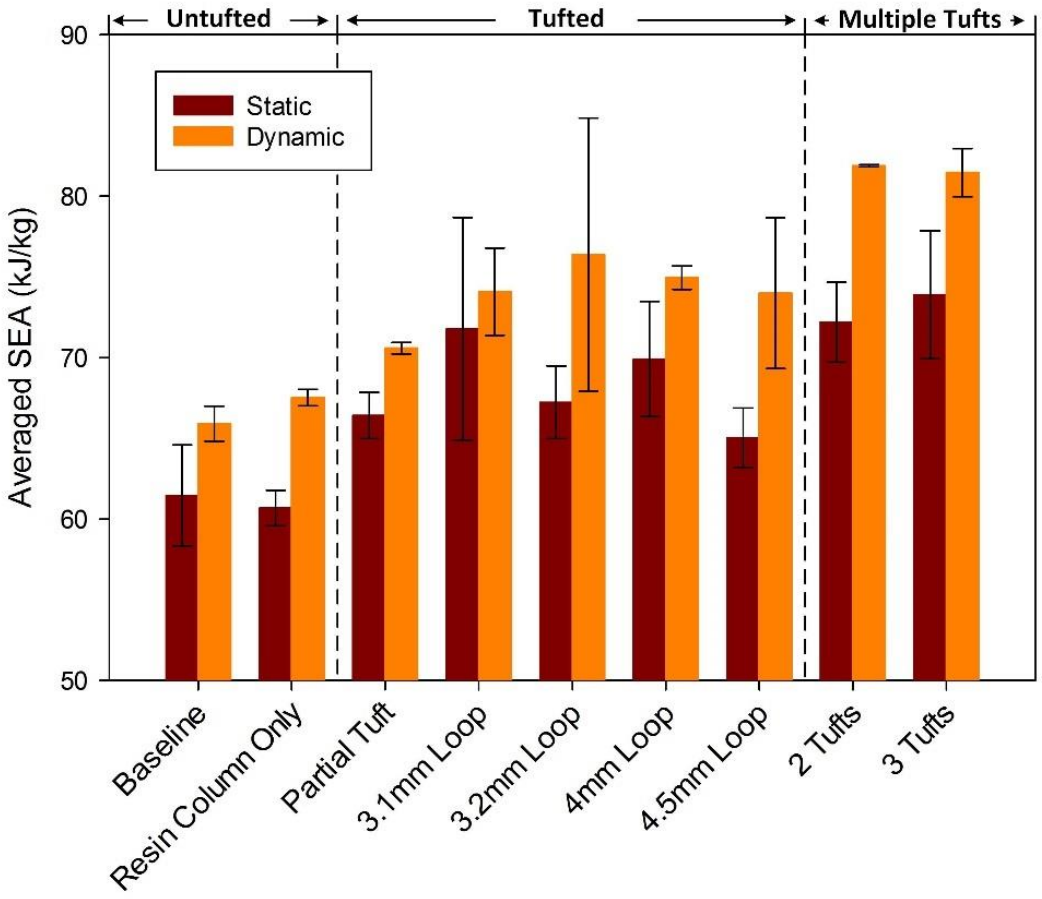

Figure 4-17: Averaged specific energy absorption for 4.5mm of crush displacement under both static and dynamic testing conditions for each tuft configuration.

Although the absolute values of energy absorption may be artificially inflated by the scale of the test coupon used, the results of the energy absorption analysis further support the variation in behaviour of the different tufting configurations. For both test types, these can be collected into three distinct groups. The lowest performing coupons were the baseline and resin column samples. The second group contains the single tufted samples of varying loop lengths, including the partially tufted coupons. There is an increase over the baseline tests, however there is no clear trend within this group between the loop size and the resulting energy absorption. The final group contains the multiple thread tufted coupons, which show a clear jump over the baseline and single tufted coupons. In all cases the SEA under dynamic loading was higher than quasi-static loading.

Analysing the energy absorbed during crushing shows that it is difficult to quantify the effect of loop length. Each series shows an increase over the baseline, but between these series a trend is not clear. It should be noted that the loop lengths with the highest performance also had the most significant variation. This is potentially an effect of the loop

direction at the surface of the coupon. Due to the limited size of the gauge area, a coupon not aligned correctly may be cut short during machining and have its performance affected. It is also still not clear how the thread itself is behaving, as was shown in Figure 4-11, where thread pull-through is not clear. The highest performing were the multiple tuft samples, which is unsurprising as Figure 4-13 appears to show a greater amount of surrounding material around the tuft fractures during failure. It is likely for this reason that loop length does not have as significant an influence on performance.

Despite the lack of a clear trend between loop length and performance, several other potentially important observations were made. The comparative performance of both the partial and fully inserted tuft coupons is a promising sign for creating a potentially lighter (through shorter resin column) structure, with a cleaner surface finish. The use of multiple tuft insertions was shown to improve energy absorption and could lead to a high performing structure. Finally, the observation of the column failure mechanism and the subsequent displacement could have a significant effect on the global failure of a tufted structure and needs to be investigated further to understand what influence it has.

Whilst the results shown here reflect only the first 4.5 mm of crush length of the test coupons, an initial assessment of the performance when using the whole dataset shows significant variations between the two methods. Whilst the results presented in Figure 4-17 show a clear increase between tufted and untufted tests, when more data is included the later load recovery in the untufted samples begins to elevate the SEA performance of these over the tufted coupons. This raises questions around the most suitable method to use to compare results and will be explored in more detail in later chapters.

Whilst a relatively high level of variation could be expected for these small-scale coupons both due to the size and complexity of machining, it is noteworthy that there is a particularly large level of variation within the baseline and 3.1 mm datasets under static loading. It is not immediately apparent at this stage why these levels of variation are significantly higher than other datasets, especially as all the coupons have been manufactured from the same test panel. However, the main outliers for these two datasets both correlate to the biggest differences in crush trigger angle, so this is the expected source of the significant variation.

4.4.4 Statistical Analysis

As a supporting measure, to identify if a statistically significant difference could be observed in the test data, a one-way analysis of variance (ANOVA) was carried out using

the built-in analysis tool in the software SigmaPlot®. Assuming a normal distribution of data, an ANOVA analysis compares the variance of results within datasets as well as between them to determine if they can fairly be treated separately. If the P value for the comparison between any two groups is less than 0.05, there is less than a 5% chance of groups not being statistically different. If it is greater than 0.05, it cannot be confidently concluded that there is a difference.

As normality of data is an important assumption for carrying out ANOVA, a Shapiro-Wilk test for normality was carried out on the datasets. It should be highlighted at this stage that due to low number of coupons tested, the dynamic results do not show a normal distribution and so was not used for this analysis. In addition, for the static data it was shown that the data also does not follow a normal distribution but did offer some useful comparisons between datasets. It is therefore necessary to emphasise that the following results are presented for information only.

The tables below present the ANOVA analysis carried out for the entire dataset (Table 4-6), comparing the untufted, tufted and multiple tuft groups (Table 4-7), and comparisons within each of those groups (Table 4-8, Table 4-9 and Table 4-10 respectively). The P-value is highlighted green for those datasets that passed the comparison test, and red for those that failed.

Table 4-6: Overall Dataset ANOVA

Source of Variation	SS	df	MS	F	P-value	F crit
Between Groups	886.82	8	110.85	7.69	5.94E-06	2.21
Within Groups	518.91	36	14.41			
Total	1405.73	44				

Table 4-7: Untufted, Tufted and Multiple Tuft Groups ANOVA

Source of Variation	SS	df	MS	F	P-value	F crit
Between Groups	729.61	2	364.80	22.66	2.11E-07	3.22
Within Groups	676.13	42	16.10			
Total	1405.73	44				

Table 4-8: Untufted Group ANOVA

Source of Variation	SS	df	MS	F	P-value	F crit
Between Groups	1.50	1	1.50	0.22	0.65	5.32
Within Groups	54.70	8	6.84			
Total	56.20	9				

Table 4-9: Tufted Group ANOVA

Source of Variation	SS	df	MS	F	P-value	F crit
Between Groups	148.52	4	37.13	2.09	0.12	2.87
Within Groups	355.04	20	17.75			
Total	503.56	24				

Table 4-10: Multiple Tuft Group ANOVA

Source of Variation	SS	df	MS	F	P-value	F crit
Between Groups	7.19	1	7.19	0.53	0.49	5.32
Within Groups	109.17	8	13.65			
Total	116.37	9				

The comparison tables presented above further support the groupings of the three sets of data, showing significant variation between the groups but less between the datasets.

4.4.4.1 Pairwise Comparison

Whilst an ANOVA analysis is useful for assessing variation within a dataset, to identify direct comparisons between variables an additional level of pairwise testing was required. The analysis was carried out using the Holm-Sidak method and a significance level test of 0.05. The list of dataset comparisons with a P less than 20% are shown in Table 4-11, with those that did not meet the test level of 0.05 highlighted in red.

Table 4-11: Summary of Groupwise Comparison Tests from ANOVA Analysis. Those highlighted in red did not meet the pass criteria.

Comparison	Diff of Means	T-statistic	P
3 Tufts vs. Resin Column Only	13.22	5.51	<0.001
3 Tufts vs. Baseline	12.44	5.18	<0.001
2 Tufts vs. Resin Column Only	11.52	4.80	<0.001
3.1mm Loop vs. Resin Column	11.10	4.62	0.002
2 Tufts vs. Baseline	10.75	4.48	0.002
3.1mm Loop vs. Baseline	10.32	4.30	0.004
4mm Loop vs. Resin Column Only	9.23	3.84	0.014
3 Tufts vs. 4.5mm Loop	8.86	3.69	0.021
4mm Loop vs. Baseline	8.45	3.52	0.033
3 Tufts vs. Partial Tuft	7.48	3.11	0.093
2 Tufts vs. 4.5mm Loop	7.16	2.98	0.125
3.1mm Loop vs. 4.5mm Loop	6.74	2.81	0.183
3 Tufts vs. 3.2mm Loop	6.66	2.78	0.189

Upon initial reflection it is noteworthy that of the 36 possible dataset comparisons only 9 of them passed the probability test to show a significant difference. A further 4 comparisons were with a 20% confidence level.

Of the comparison tests that did pass, the majority relate to comparisons between untufted and tufted coupons, with only one dataset a direct comparison between two tufted coupons. Furthermore, of the tufted coupons that showed statistical significance, most of them were multi-tufted coupons, further supporting the fact that multiple tufted coupons performed better overall.

4.5 Conclusions

Inconsistent tuft formation is an inherent problem of the tufting process, particularly for complex preforms such as sandwich assemblies. To explore and understand the influence of these variations, a series of single tuft test coupons were produced and tested under edgewise crush loading, for both static and dynamic test conditions. A consistent stable crushing mechanism was observed across the tests under both static and dynamic conditions, validating the method of testing.

The chosen test variables were the length of the tuft and the density of thread used, achieved by making multiple tuft insertions at a single location. Of the two variables considered it was observed that whilst both gave an increase in load recovery and specific energy absorption as the tuft failed, it was the greater tuft density which had a more significant influence on the overall performance of the coupon. Variation between tuft lengths and loop sizes was small indicating that this feature does not play a significant role in the failure mechanism under this specific type of load case.

By comparing static and dynamic loading conditions it was observed that the failure modes were very similar for both, with the notable exception of a more elastic response in the facesheets under dynamic loading leading them to spring back when the crush plate was removed. However, there was a noticeable increase in SEA under dynamic loading, which was observed across every dataset.

Post-failure analysis of the test coupons exhibited a separation of the tuft and surrounding resin column. Whilst at this stage the result of this separation is unknown, there was a noteworthy difference in post-tuft-failure behaviour observed in the load trace, with the untufted baseline showing a load recovery, whilst the tufted results were significantly lower. This could indicate some influence in the separated tuft on the progression of failure of the coupon and is an area to be more explored in more detail.

Chapter 5 Post-Failure Behaviour of Tufts

5.1 Introduction

As introduced in Chapter 1, the complex nature of the load case being considered coupled with the fact that the tufted reinforcement is contained within the structure means it is very difficult to understand all the failure mechanisms that are taking place during crushing failure.

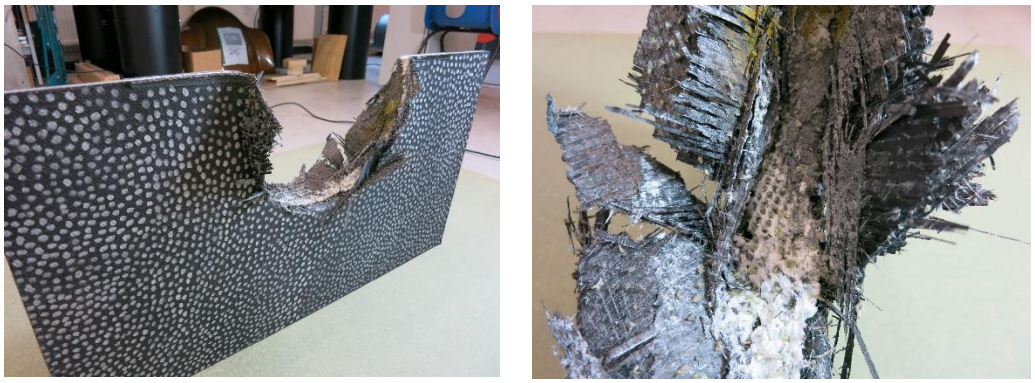

Figure 5-1: Failed tufted test panel highlighting the complexity of the failure site and the lack of clarity in how the tufts fail.

Following the work carried out in Chapter 4, it was revealed that individual tufts separate from the facesheets during failure and thus can behave independently of the rest of the structure. The load trace obtained during testing indicated a significant variation in post-tuft-failure response between tufted and untufted coupons, with the possibility that this is influenced by the displacement of the now unattached tuft within the core. To address this point, as well as to capture the failure mechanisms that take place in-situ, this chapter introduces an experimental test method capable of achieving this and the observations made during testing. This work has been published previously [148], and also forms the basis of a final year research project [149].

5.2 Resin Columns

A common phenomenon relating to the use of through-thickness reinforcement is the presence of resin rich zones due to fibre distortions around the added reinforcement. In sandwich structures this takes on even greater significance, as the brittle core cannot close-up around the reinforcement after insertion leaving a relatively large void within. When using rigid reinforcement this effect is minimised as the reinforcement is typically driven

through the core and thus only creates a channel the size of the reinforcement inserted, however with dry reinforcement, as is the case with tufting, a carrier needle is used to pull the reinforcement through. Due to the disparity in size between this needle and the reinforcing thread, a significant void is created within the core which is filled with resin during subsequent infusion thus creating a rigid column. The presence of resin columns within the core is not a new observation [150], however they are only typically characterised by their effect on the component weight and are not so directly involved in the load case as they would be under a crushing scenario as explored here.

Figure 5-2: Differing reinforcement conditions within a foam core. Left: close fit between rigid pins and foam [84]**, Right: Substantial resin columns surrounding tufts.**

5.3 Methodology

As discussed in Chapter 4, the lack of standardised testing for crashworthiness means there is no clear methodology to follow. As a result, a similar test methodology to that presented in Chapter 4 was adopted, with test coupons specified to meets the objectives of the study.

The coupon design was required to show a stable crushing failure as before, but this time with tufts visible at one edge to allow for visual assessment of the failure mechanisms to take place as the test progresses. Previous testing had revealed that a fixed boundary condition at one end of the test coupon was required to ensure stability. The opposite end of the test coupon was not constrained in any way to allow crushing to begin from this point. Through additional preliminary testing it was also found that a crush trigger was not necessary for the chosen test setup.

To define the size of the test coupon, a compromise was required, between maintaining a short enough length to avoid buckling of the coupon but ensuring an adequate number of tufts were present in the gauge section to provide an acceptable set of data. Test coupons

were cut into three different lengths to vary the number of tufts present. The shortest coupons (40 mm length) had seven tufts along the length, the medium coupons (50 mm) had 8 complete tufts, and the longest (70 mm) had 10 tufts. Whilst a datum cutting point was defined for the side of the coupons, there was none defined at each end. This meant that the lengthwise position of the tufts varied between each coupon, changing the gap between the uppermost tuft and the crush plate, and the location of the tufts that were within the clamped region at the base of the coupon. Due to the coupon dimensions, a total of 4 tufts were captured across the width of each test coupon. However, ensuring that tufts were aligned to one edge of the coupon, by machining along the outside edge of the yarn at the surface, did mean that there was a very slight offset of the tufts at the other edge of the coupon. It is important to note however, that trial tests did not indicate any instability because of this.

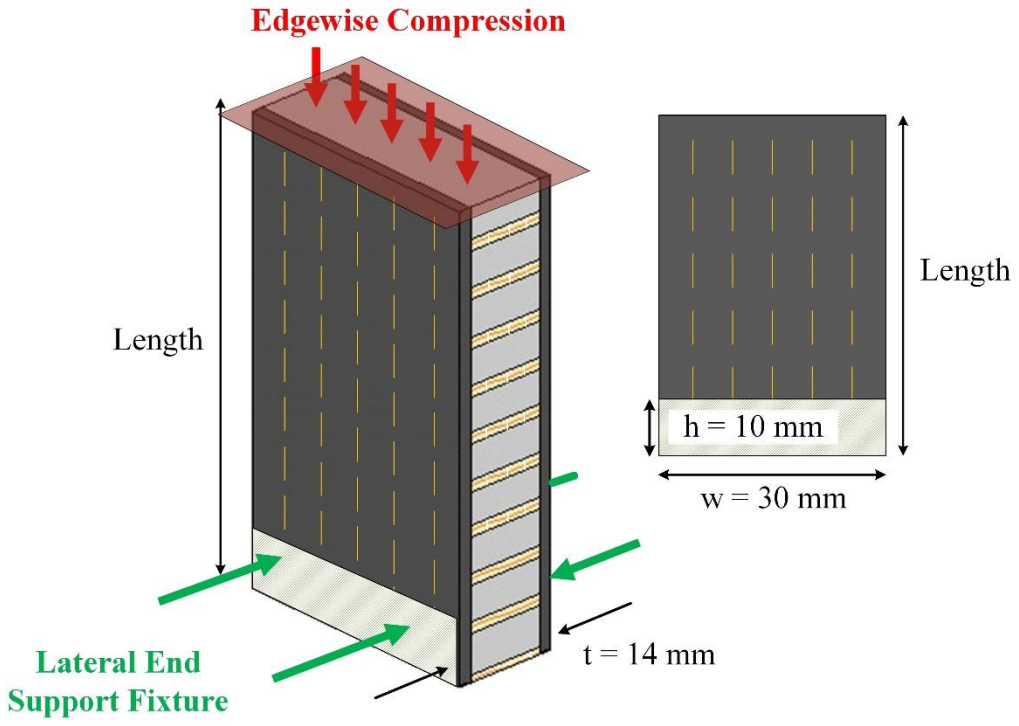

Figure 5-3: Configuration and dimensions of the sandwich test coupons.

The cured panel was cut into test coupons using a diamond blade, taking care to ensure that for the tufted panel a line of tufts was located, and thus visible, along one edge of the coupon. Polishing of the tufted edge was carried out using a Buehler MetaServ 250 Grinder-Polisher with CarbiMet Grit 320 (P400) SiC abrasive paper at 350 rpm and a constant water flow to clear excess particles and avoid scratching the coupon surface. This was done to provide clarity of the tuft thread within the resin column as well as to aid

tracking of the tufts. The coupons were then allowed to dry naturally at room temperature for a period of several hours. The coupon geometry was rectangular as shown in Figure 5-3, with the coupon length chosen as a test variable as shown in Table 5-1. The mass of the coupons was recorded to allow for normalisation of the energy absorbed, and the dimensions of each coupon were also measured using a digital Vernier calliper to check for accuracy and consistency. This data is summarised in Table 5-1.

Table 5-1: Measured Test Coupon Properties

Group	Coupon ID	Length	CV	Average Mass	CV
-	-	*mm*	*%*	*g*	*%*
A	1, 2, 3	40	0.18	12	3.4
B	4, 5, 6	50	0.03	16	2.6
C	7, 8, 9	60	0.17	19	2.1

Following the observations of Chapter 4 showing that failure modes under static and dynamic loading were very similar it was decided to proceed with static testing only, to simplify data capture. Testing was carried out using a Zwick 1466 test machine under displacement control, with a quasi-static loading rate of 2 mm/min. As before, coupons were lightly clamped at the base using a steel end fixture, ensuring no sliding of the coupon was allowed, and positioned at the centre of the test machine. Due to the unsymmetrical surfaces of the coupon (loop and thread sides), each was aligned in the same direction, with the loop surface on the right-hand side. Load was applied to the coupon from the top by a circular steel crush plate. Some rotation of the coupon was allowed within the fixture to ensure that the coupon sat flat when it contacted the crush plate. Tracking of the tufts was carried out using an Imetrum Video Gauge, with a 50 mm lens. Each of the visible tufts at the edge of the coupon were marked with a white pen at 3 points along their length to allow recognition by the video gauge (applied at the centre and each end of every tuft to give a redundancy in case of tracking losses). Load-displacement data was tracked and output by the test machine to allow for further analysis. The test setup with the positioning of the test coupon within the test machine and the camera for tracking is shown in Figure 5-4.

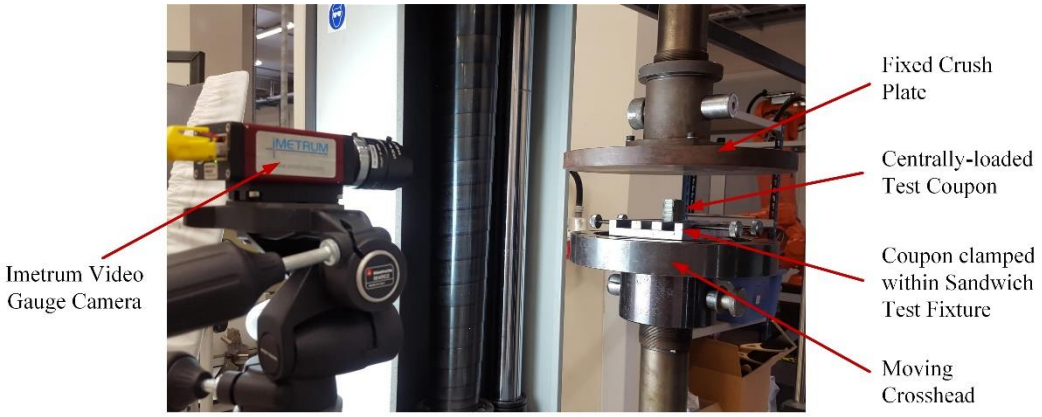

Figure 5-4: Test setup showing coupon loaded into test machine and video gauge camera positioning.

5.4 Results and Discussion

As anticipated, the main observed failure mode in the test coupons was a progressive stable crushing mechanism, however several coupons did fail in an unstable manner. Representative load-displacement traces for each group of coupons is shown in Figure 5-5, with a full set of results, including the calculated SEA for each coupon shown in Table 5-2. Those that failed in an unstable manner are highlighted in grey. No clear trends with respect to coupon lengths other than termination point were observed, so coupons will be discussed generally from here onwards.

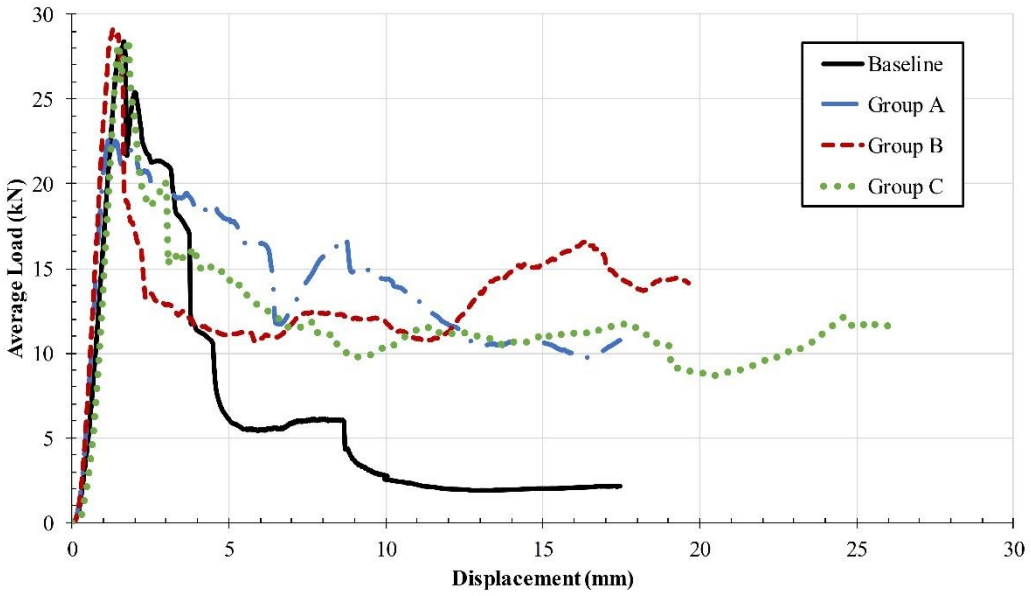

Figure 5-5: Representative load-displacement traces for each coupon type tested, compared to an untufted baseline coupon.

Table 5-2: Summary of Key Results

Coupon Length	Coupon	Crush Distance	Peak Load	Average Crush Load	Total Energy Absorbed	SEA
mm	-	*mm*	*kN*	*kN*	*kJ*	*kJ/kg*
40	A1	20.2	20.3	14.8	0.31	48.4
	A2	14.6	25.4	12.3	0.22	42.5
	A3	20.7	29.4	16.1	0.36	53.9
50	B4	17.1	37.8	11.8	0.24	41.0
	B5	24.5	35.1	17.0	0.45	53.4
	B6	23.3	23.2	11.3	0.30	36.3
70	C7	23.8	31.9	12.9	0.34	41.1
	C8	28.4	36.2	4.28	0.17	17.3
	C9	33.6	35.8	17.6	0.62	54.8

A representative progressive crushing load-displacement trace obtained from the test machine for one of the coupons is shown in Figure 5-6.

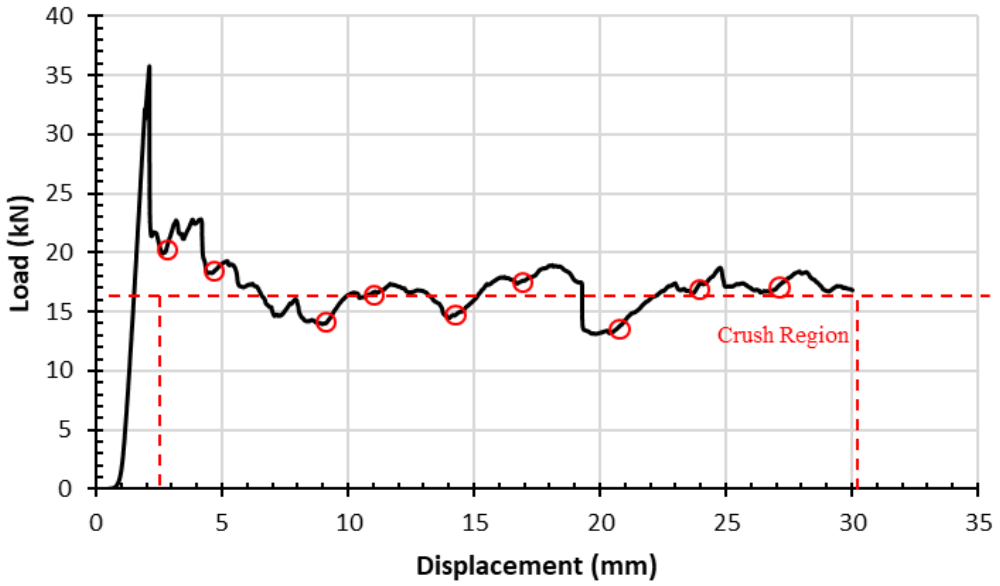

Figure 5-6: Typical Load-Displacement behaviour (shown for coupon C8).

The load trace begins by increasing linearly up to a sharp peak load where failure in the form of skin delamination begins to initiate. This peak is noticeably sharper than that observed in the results of Chapter 4, as the result of the lack of a crush trigger. Whilst the cross section of the test coupons remained constant, inconsistencies in the initial peak crush load between tufted coupons were observed (Table 5-2), which could be attributed to

several discrepancies between coupons, such as the location of the first line of tufts. After the initial peak, there is a significant drop in load, followed by a sustained loading as crushing of the coupon down its length begins to occur. The observed drop in load between the peak initial fracture load and the sustained crushing load averaged 55%, however this value varied significantly between coupons, due to the inconsistent peak and average loads observed. It is possible that these inconsistencies in failure mechanism between tufted coupons could be improved with a chamfered or triangular trigger mechanism at the tip of the coupon, to encourage a more consistent crushing failure between coupons. The points represented by the red markers in Figure 5-6, show where the progressive crushing has reached a tuft. At this point the tufting threads are restraining the separation of the face sheets until breaking of the yarn at the interface. The ensuing small increments in load by approximately 1-2 kN are due to an increase in force required to push the columns downwards, while the aramid threads are attempting to hold the tufts in place, minimising bending and splaying of the face sheets. This represents a small 7% increase in load before the threads fail and the load subsequently drops.

The tuft points, shown by the red markers, are not evenly distributed on the load-displacement curve, even though the compression rate and tuft spacing is constant. This uneven distribution likely occurs due to z-displacement of the tufts (Figure 5-7), where the foam and tufts can be forced out from between the skins when crushed.

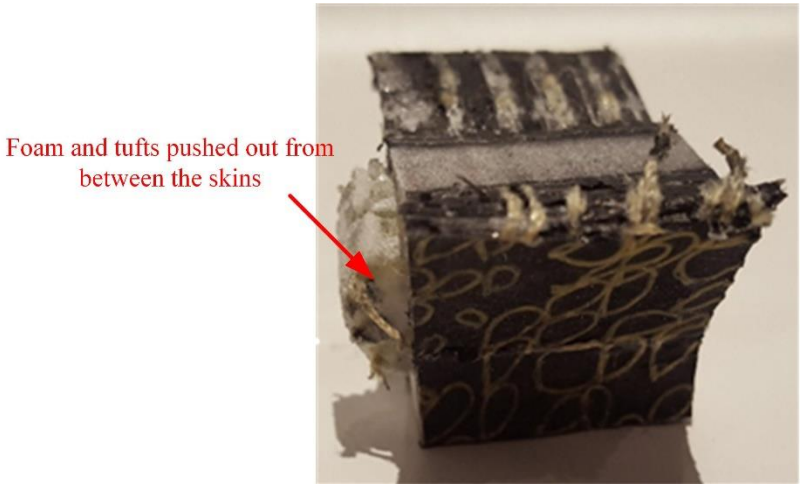

Figure 5-7: Foam crushed out of sandwich panel in z-direction (Coupon A2).

5.4.1 Column Drift

Significantly, during testing it was observed that the tufts and surrounding resin columns do in fact separate, translate and interact with each other during crushing. As the facesheets give way, the uppermost face of the core becomes exposed to the crush plate and crushing

of the foam begins to take place. As the foam is compressed its density increases significantly until it reaches a point where it effectively becomes rigid. At this stage the uppermost tuft within the coupon, which is in contact with this foam, can no longer move upwards with the motion of the crosshead as it is being held against a rigid surface. The subsequent motion of the rest of the test coupon moving upwards relative to the now fixed tuft creates a shear stress at the interface between resin column and facesheet, as well as through the tufting thread. The thread initially has a restraining effect on the shearing motion of the coupon, however once the shear strength of the tufting thread is reached, the thread breaks, and the motion continues. As the upwards motion of the test coupon continues this crushing behaviour repeats itself, with the gap between the first failed tuft and the next in line closing as the separating foam is crushed. Once the gap between these two tufts is closed, they now both become locked up against the crush plate and can no longer move (Figure 5-8B). This mechanism continues until each of the tufts within the coupon 'stack' on top of each other and can no longer move. Once this stage has been reached there is almost no foam visible between the tufts, as the foam has been compressed significantly (Figure 5-8C).

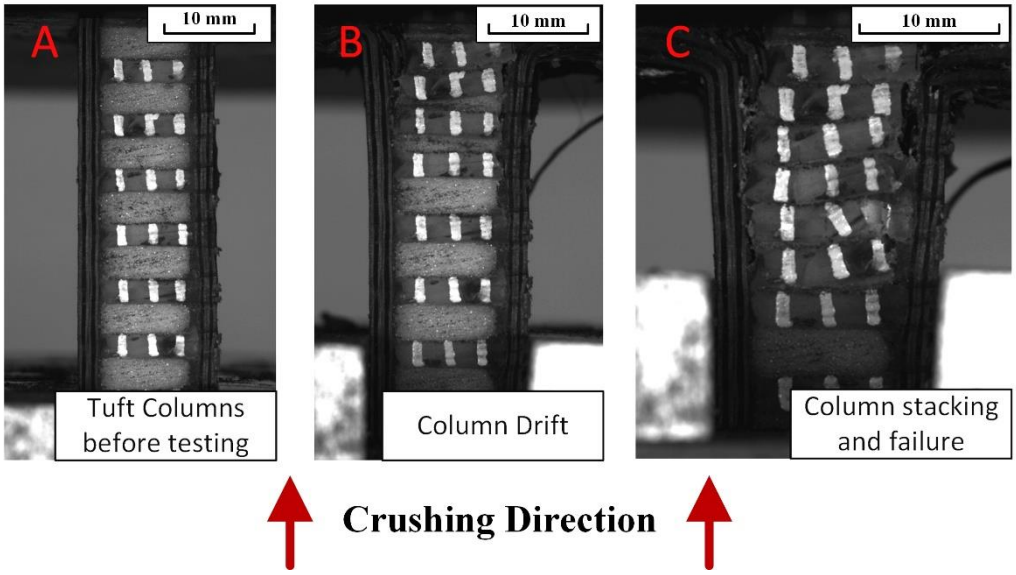

Figure 5-8: Progressive crushing mechanism observed in tufted sandwich structures (Coupon B6). A) Tuft positioning before testing. B) Separation and subsequent 'drifting' of tufts. C) Stacking and failure of tuft resin columns.

An example of the tracking results recorded by the video gauge system is shown in Figure 5-9. Each of the curves within the figure represents the position, relative to the fixed crush plate, of the centre point of each tuft within the coupon. The sequential motion of the tufts

discussed previously is clearly indicated in this diagram. As the coupon is loaded, the material at the top begins to crush and the uppermost tuft begins to move. After a short distance, this tuft strikes the impact plate and can no longer travel any further. This is shown by the flattening of the curve in the figure. Each subsequent tuft then sequentially moves towards the crush plate until they strike the preceding tuft and the curve flattens. The initial gradient of the curves is approximately 2 mm/min which shows that the column movement is dependent on the loading rate of the test machine, which indicates an element of control of the failure mechanism assuming the tufts remain within the line of the coupon, unlike the observation in Figure 5-7. Not only is it dependent on the applied loading rate, but also the defined spacing between the tufts.

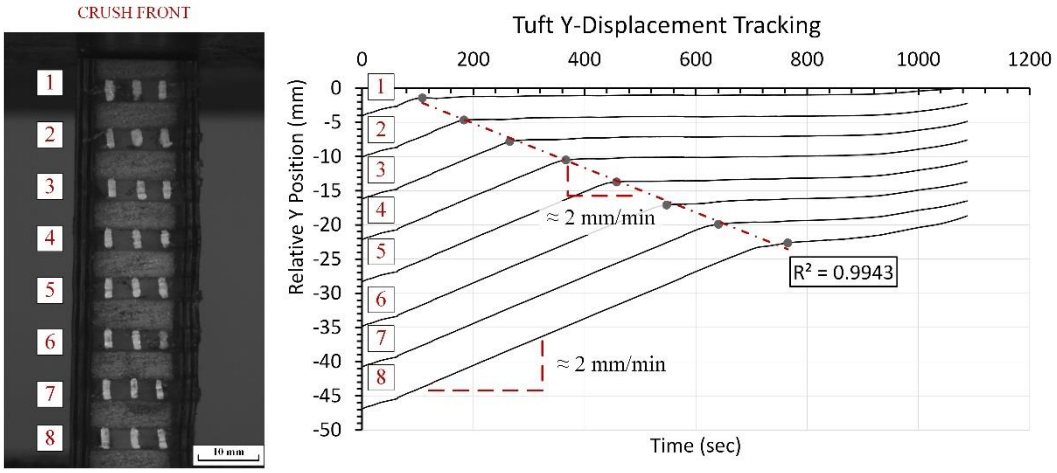

Figure 5-9: Coupon C8 y-displacement tracking for individual tufts demonstrating controlled collapse.

5.4.2 Detailed Failure Behaviour

Whilst the most noticeable observation made during testing was of the drifting mechanism of the tufts, a review of the captured test videos revealed several other consistent failure mechanisms that occurred as crushing progressed. Still images are captured from videos to identify these critical regions of failure. The most representative cases (coupons A3, B4, and C8) were selected for analysis. Regions of interest can be traced back to the supporting load-displacement plots and are circled at the relevant locations.

5.4.2.1 Coupon C8: Damage Initiation and Local Facesheet Buckling

Region 1 highlighted in Figure 5-10 indicates the damage initiation phase of sandwich coupon C8. This trend is observed across all test coupons, where a sharp increase in load occurs up to the initial failure load of the coupon. At this point, the outermost ply tends to delaminate, and the sandwich begins to destabilise, which is represented by a sudden drop in load.

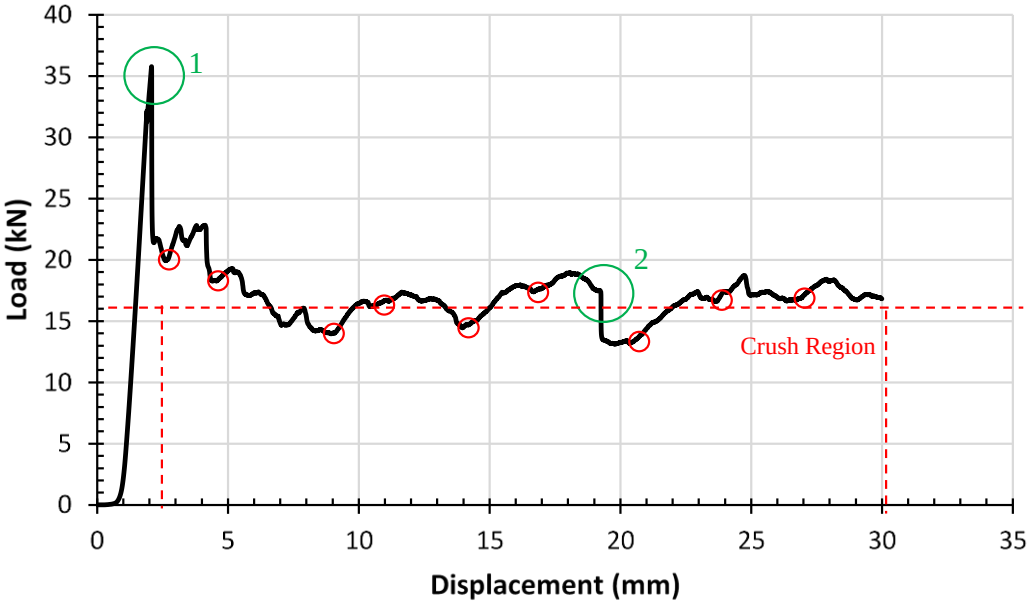

Figure 5-10: Load-Displacement graph for Coupon C8.

Figure 5-11 shows the instant when the damage forms as an initial opening of the skin. Across the different test coupons this initial failure would take two slightly different forms, a peeling delamination of the outer plies, or a diagonal shear crack at the tip of the coupon, leading to a small section of the skin breaking off from the rest of the coupon. For most of the coupons tested both failure mechanisms occurred, but in separate facesheets.

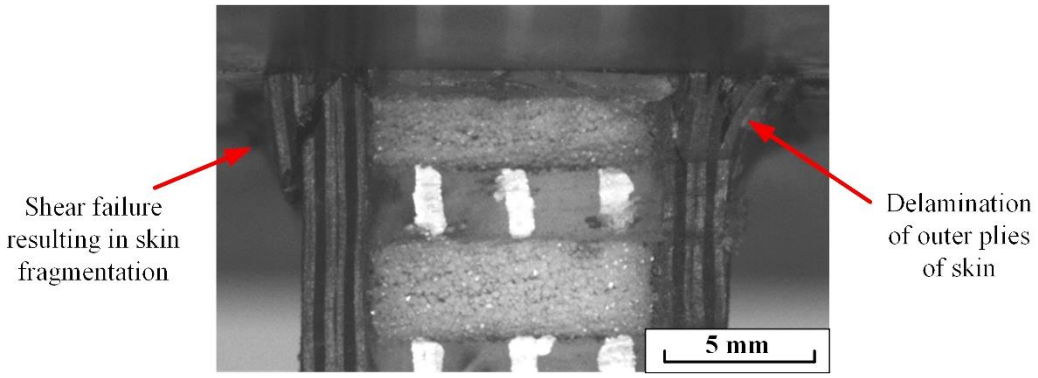

Figure 5-11: Initial failure of facesheets at uppermost edge of the test coupon (Coupon C8).

Region 2 highlighted in Figure 5-10 indicates a second sudden drop in load at a crush length of approximately 19 mm. Reviewing the test video for this coupons indicates that this drop is due to damage propagation caused by the localised buckling of the sandwich coupon after a shear dislocation in one of the facesheets. Figure 5-12 shows the localised fracture formation in the facesheet, alongside a clear disbond of the core, represented by the dark regions adjacent to the facesheet. The separation of the core from the facesheet means that

lateral stability is lost and localised buckling failure of the facesheet can occur. Although the fracture mechanism causes a sudden drop in strength of the sandwich coupon, it is short-term, and the load recovers back to the 16 kN average load level because of the added stability of the remaining connected tufts within the coupon.

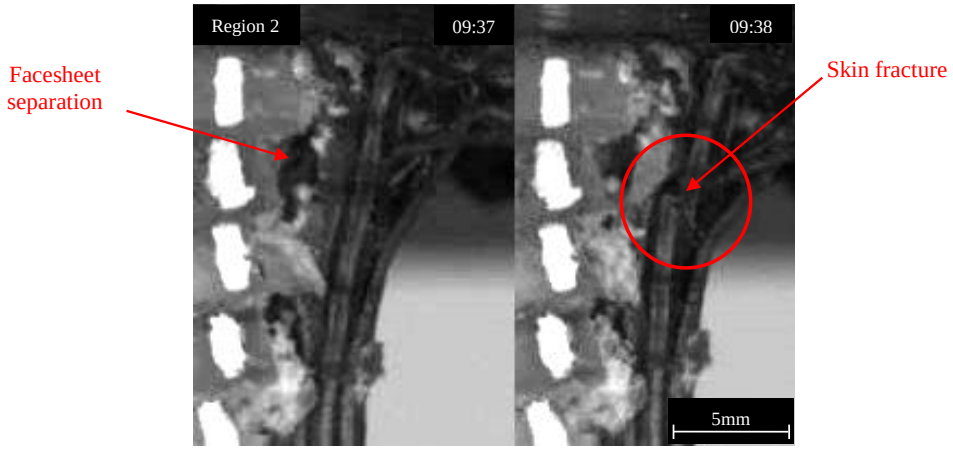

Figure 5-12: Facesheet separation and fracture at 19mm crush displacement (Coupon C8).

5.4.2.2 Coupon A3: Local Facesheet Buckling, Tuft Pull-Out and Column Sliding

Region 3 in Figure 5-13 displays a sharp drop in load, which similarly to the failure highlighted in Region 2 previously, is due to a localised facesheet buckling failure. Unlike the previous example, this failure occurs prior to any noticeable failure in the core or tufts adjacent to the facesheet, resulting in a relatively premature failure mechanism after only 2.8 mm of crush displacement.

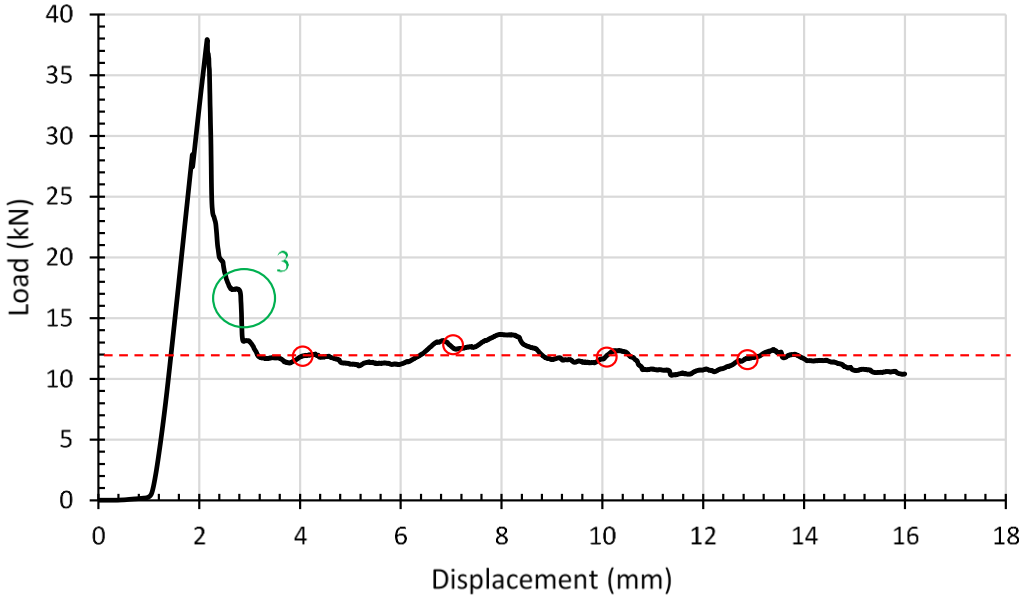

Figure 5-13: Load-Displacement graph for Coupon A3.

This failure appears to be a result of inherent flaws that form at the site of tuft insertions, including fibre misalignment and resin rich zones. When compressive load is applied to the facesheet these flaws can lead to the formation of kink bands, because of the reduced stability of the laminate. Figure 5-14 shows the before and after appearance of the fracture.

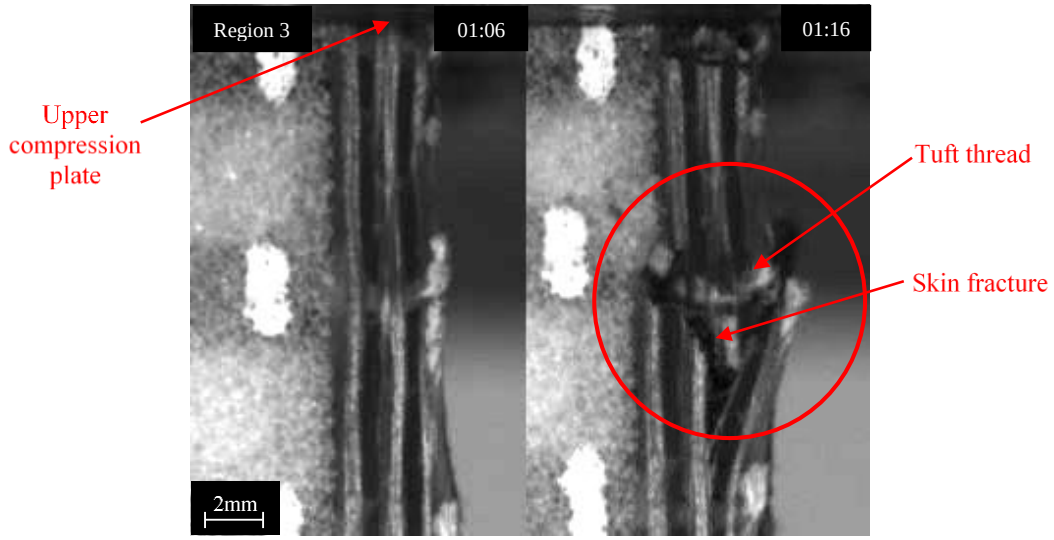

Figure 5-14: Failure due to facesheet instability at 2.8 mm crush displacement (Coupon A3).

The result of this fracture mechanism was the formation of a diagonal shear crack transversely across the core. This caused the uppermost tuft column to displace laterally, shifting in the direction towards the fracture initiation site on the right hand facesheet. After

a short period of time as crushing progresses the column begins to realign back to a central position, with the still-attached lower portion of the two facesheets effectively acting as guides to align the column perpendicularly to the crush front. The gradual recovery over time to its original 'neutral position' is shown in Figure 5-15.

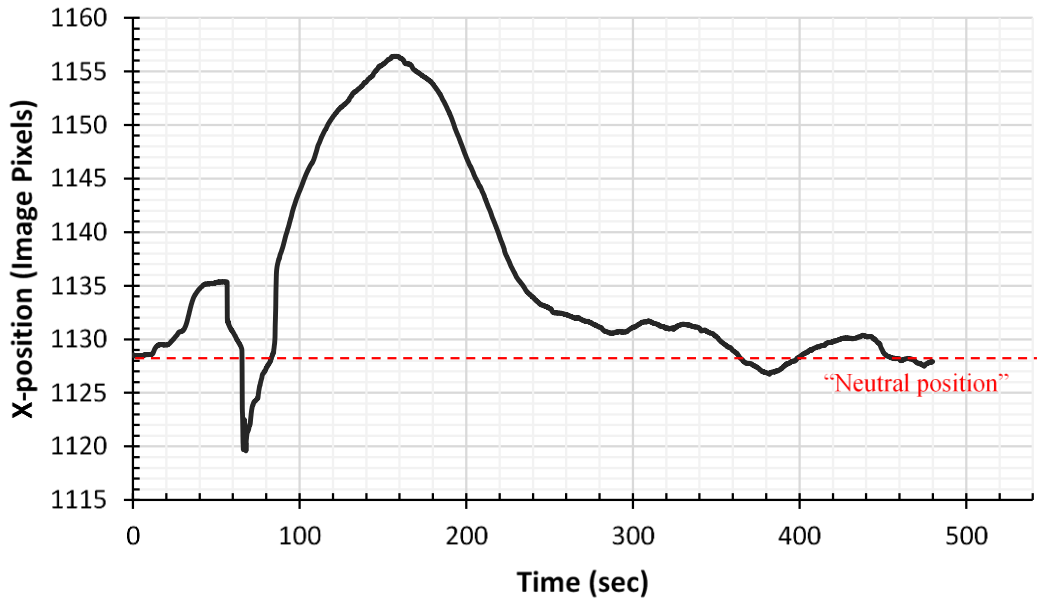

Figure 5-15: Horizontal displacement tracking of the first tuft in Coupon A3.

A close-up view of Coupon A3 revealed a rare example of pull-out of the tufting thread, as shown in Figure 5-16. This indicates that adhesive failure had occurred within the resin column, prior to the tufting thread breaking at the skin-core interface. However, it is not yet clear why the thread was pulled-out in this case while most other coupons show that the threads break. One possibility is due to the alignment of the thread in the column where the straightness of the thread can indicate how much extension the thread can undertake before it fails. Furthermore, the amount of twist the thread is experiencing and overall condition of the yarn when locked in the resin during cure can affect its fragility to the loads experienced during edgewise crushing. Another possibility is that it can be affected by the variables chosen at the panel tufting process, such as loop size and the thickness of the yarn, although the indication from the work presented in Chapter 4 suggests this is not the case. No noticeable features are visible on the load trace to indicate this failure mode, and whilst the crush region is markedly smoother than other coupons tested it is very difficult to correlate the two at this stage.

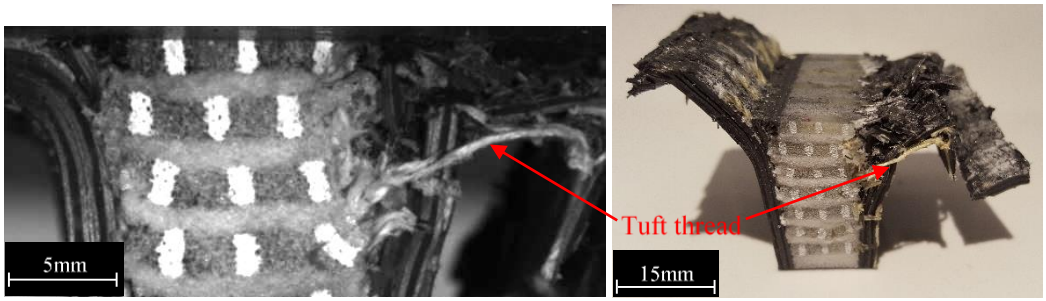

Figure 5-16: Tuft thread retracted from resin column (Coupon A3).

5.4.2.3 Coupon B4: Local Facesheet Buckling, Column Rupture and Column Sliding

Similar to coupon A3, Region 4 in Figure 5-17 shows an early facesheet fracture after the first tuft through the formation of a diagonal shear band, as shown in Figure 5-18, causing an instantaneous loss in compressive strength. The coupon recovers from this instability when the tufts began to support the structure, indicating that the initial dominant feature of the sandwich structure is the facesheet.

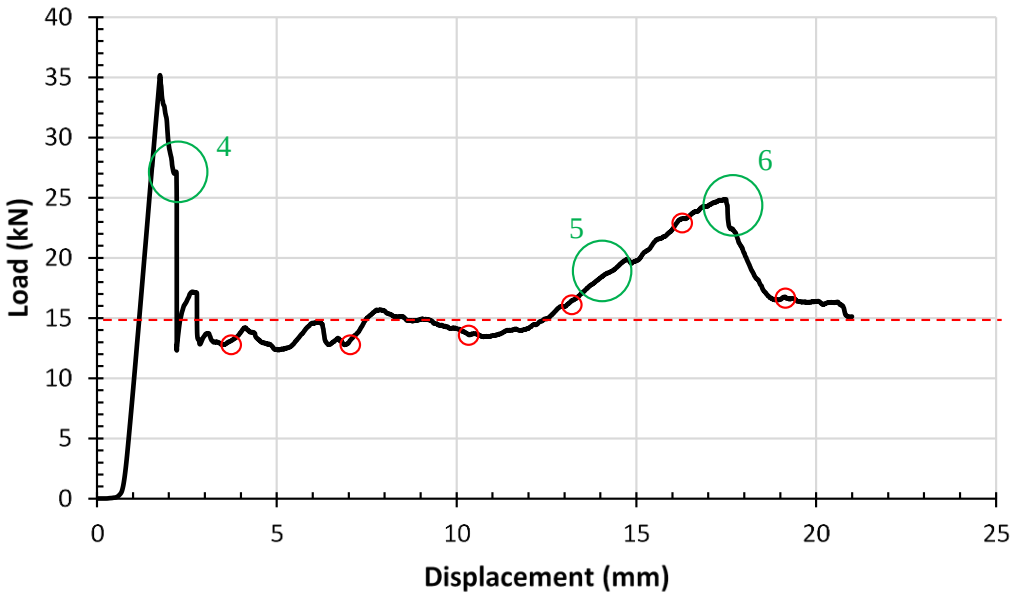

Figure 5-17: Load-Displacement graph for Coupon B4.

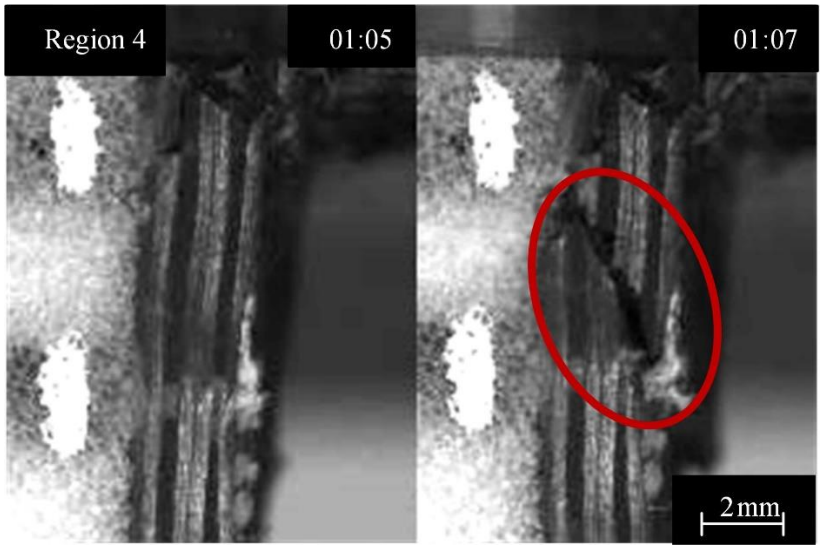

Figure 5-18: Shear band (highlighted in red) formation at 2.2 mm crush displacement (Coupon B4).

In addition to the stacking of the tuft columns, it was found that rupture failure of the columns would also occur. Column rupture would take place in the lower portion of the coupon when the applied crushing force on the column was reacted by the still attached tuft threads at each end of the tuft. The resultant applied bending load would lead to flexural failure of the column as shown in Figure 5-19.

The reaction of the resin columns under bending appears to coincide with an increase in load of the sandwich coupon, as highlighted in region 5 of the load-displacement trace. Ultimately this leads to localised buckling in the facesheet at region 6, which results in a sharp drop in load back to the baseline level.

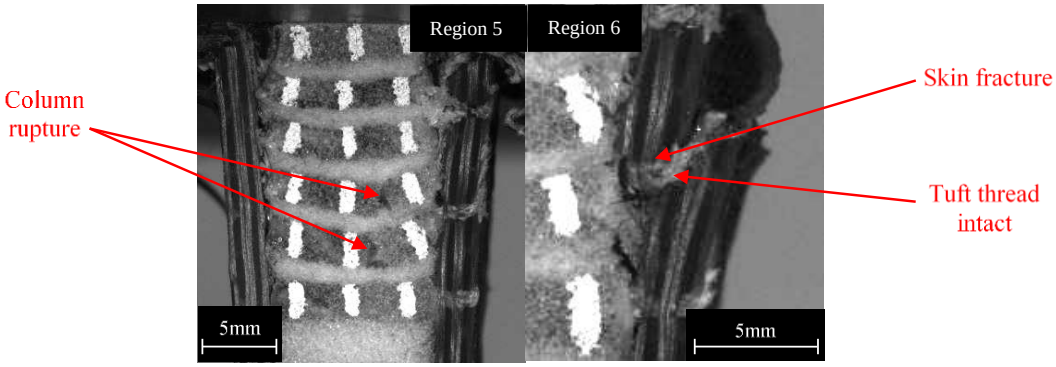

Figure 5-19: Resin column rupture (left) & skin fracture (right) at 16 mm & 18 mm crush displacement (Coupon B4).

As was observed in Coupon A3, the x-displacement tracking plot shown in Figure 5-20 demonstrates that the first tuft displaces laterally during crushing, before recovering back

to its ‘neutral position’. Reviewing the test video indicates that this recovery occurs as soon as the non-fractured face sheet separates from the core as crushing progresses. It was also observed that the point of recovery in Figure 5-20 is also the point at which the load is highest after the initial peak, prior to delamination and when the skin fractures in Region 6. This is a possible indication that a fully aligned stacking of the columns will result in a higher load, while partial stacking will take less load.

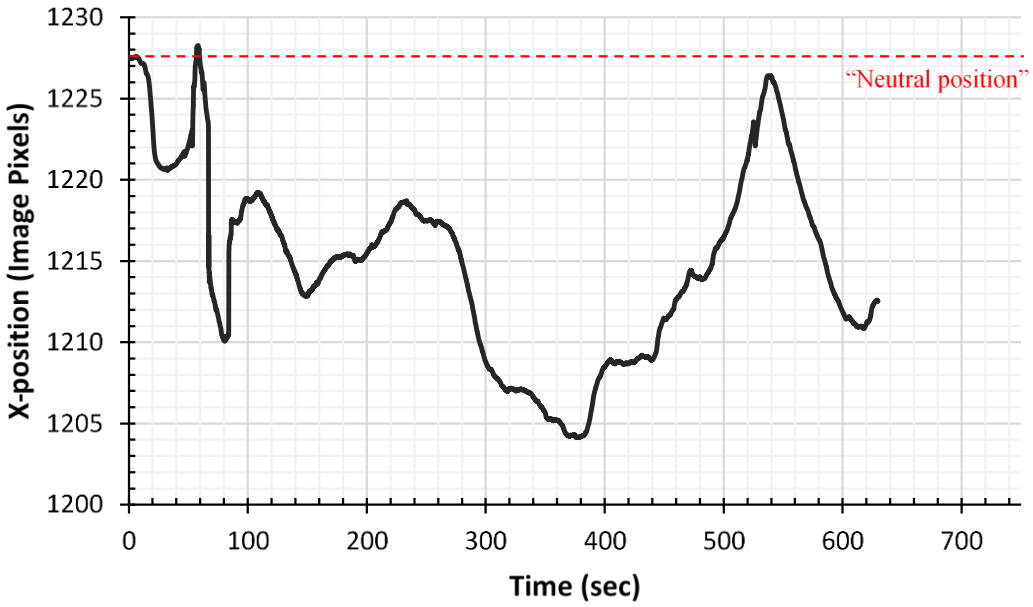

Figure 5-20: Coupon B4 1st Tuft x-displacement tracking over time, showing recovery back to a neutral position.

5.4.3 Unstable Failure in Tufted Sandwich Coupons

Whilst most of the tufted coupons failed by a stable progressive crushing mechanism, several of the coupons did demonstrate signs of instability during failure, due to inherent weaknesses in the structure. These uncontrollable failure mechanisms will be covered in detail in this section.

In A1 for example, a diagonal shear crack within the facesheet, like the type shown in Figure 5-18, occurred much lower down in the coupon, close to the clamping point, as shown in Figure 5-21. The crack formed diagonally within the spacing between the two tufts, beginning at the skin-core interface and terminating at the outer surface of the skin. The location of failure suggests a weakness caused by the resin rich region around the tuft, as well as a possible interaction with the test fixture. The formation of the crack led to a localised buckling of the facesheet at the failure site and continued crushing of the facesheet

laminate around this point. The coupon ultimately began to bend under the pressure applied by the crush plate on one side, causing the fractured skin to disbond. The skins remained predominantly intact which meant that a significant proportion of the energy absorbed was done so by the reaction of the test fixture itself rather than the coupon.

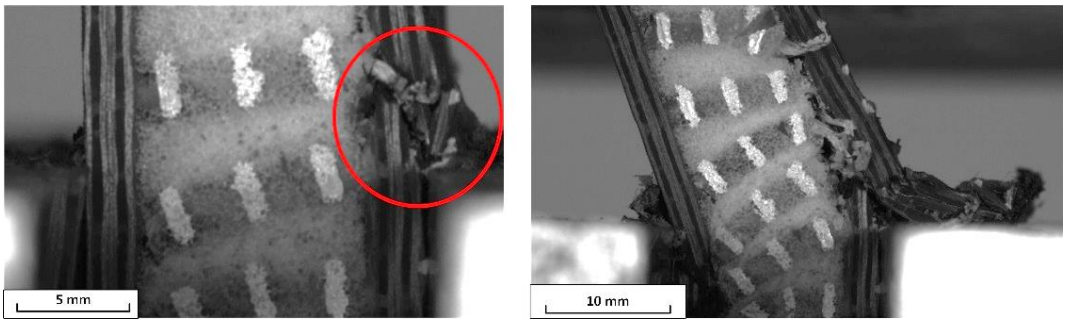

Figure 5-21: Left, Skin fracture and localised buckling at test fixture (highlighted). Right, Resulting bending failure of test coupon due to skin collapse. (Coupon A1).

During testing of coupon B5, a diagonal shear crack formed through the right-hand skin, level with the third tuft. This fracture led to separation of the skin, with the upper part remaining attached to the core but the lower section beginning to disbond from the core. An unbalanced loading of the coupon began to occur as the weaker right-hand side began to collapse, causing the tufts to rotate (Figure 5-22), and leading to cracks appearing within the foam core and the tufts. As failure progressed, the lower section of the skin began to slide past the upper section, whilst the other skin remained mainly intact. Despite this behaviour, column drift occurred as with the more stable coupon failures, resulting in a gradual failure of the test coupon and comparable energy absorption to other tufted coupons.

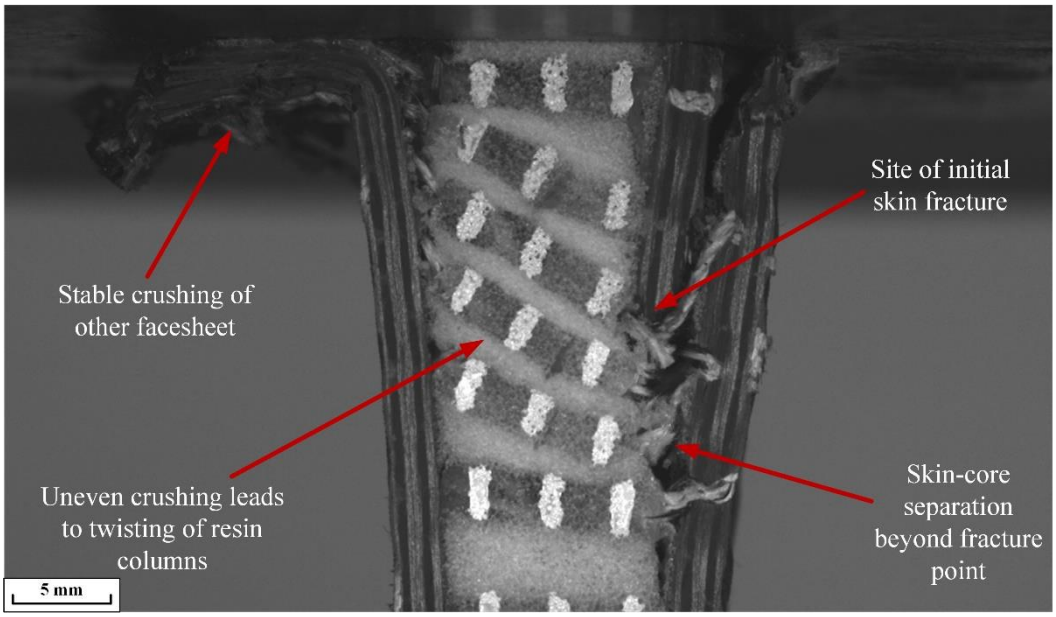

Figure 5-22: Failure mechanism after skin fracture in Coupon B5.

In another coupon (C7), noticeable curvature was observed due to bending. After a short time, a crack formed within the skin on the compression side (right) (Figure 5-23). As with before (B5), this formed in line with a tuft location, suggesting an inherent weakness here due to the resin pocket formed within the skin and core. Disbonding also began to propagate from this point downwards. As observed before, the coupon effectively split into two, with the upper portion remaining intact, whilst the lower section began to slide past it. Noticeable bending of the tufts occurred below the fracture point, resulting in rupturing of several of the resin columns. Due to the unbalanced load on the coupon, buckling occurred in the opposite skin, causing the coupon to pivot further. Testing finished with the coupon effectively folded on top of itself, and through-thickness crushing beginning to occur.

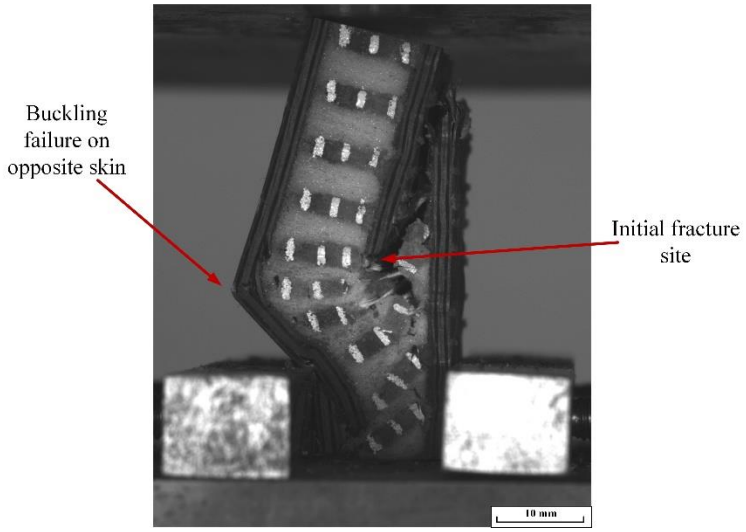

Figure 5-23: Local skin fracture and global buckling of Coupon C7.

Whilst these failure mechanisms demonstrate similar levels of energy absorption to the idealised progressive crushing mechanism observed in most of the tufted coupons, they are not ideal due to their unpredictability. The common factor in each of these instabilities was a fracture located within the skin well ahead of the crush front, as compared to the relatively early fracture mechanisms detailed previously. This weakened the structure and generally led to an unstable collapse of the coupon. It is apparent from the figures that this initial fracture site occurs at a tuft insertion point, where a resin rich region is formed due to the void created by the needle passing through the fabric. Whilst overall tufting can improve the failure mechanism it is important to note that it can contribute to flaws within the structure which can lead to inherent weaknesses being formed.

5.5 Conclusions

Tufted sandwich coupons have been tested under edgewise compression to capture the mechanical behaviour during crushing failure. Test coupons were designed to ensure that tufts were visible along one edge and thus could be tracked as failure occurred. Failure of the tufted coupons was observed to initiate through delamination and fracture of the skins at the crush front, rapidly followed by a sequential drifting and stacking of the resin columns as well as bending and crushing of the facesheets in parallel to this. Moving forward it is useful to understand the role that column drift plays in the overall energy absorption of the structure.

The tufted coupons generally failed in a consistent manner, in direct correlation to the applied loading rate and tuft spacing. The upside of this is the indication that the progressive failure could be controllable through a defined tuft pattern. In addition, the ability of the initial tufts to ‘realign’ during failure, coupled with the noticeable change in failure mode from interfacial failure to bending failure of the tufts along the length of the coupon indicates that tufts are more effective located close to the initial failure site. With these factors in mind, weight efficient structures could be created by optimising the tuft pattern within the component.

Whilst most of the tufted coupons failed in the desired stable manner, several exhibited unstable collapse failures due to cracks forming at flaws within the facesheets, which appeared to be related to the tuft insertion process. Future work would need to investigate this in more detail to understand how these flaws form, and whether the defined tuft pattern could be rearranged to reduce this by ensuring potential flaws are spaced far enough apart.

Chapter 6 Understanding the Significance of Column Drift

One of the key observations made during the testing outlined in Chapter 5 was that of the drifting of the tufts post-failure, and subsequent stacking as the crushing progressed. This is a mechanism that occurred consistently across test coupons, however what is currently not clear from these observations is the role that this mechanism plays in the overall mechanical performance of the structure for this load case. Understanding this is important for improving design, as currently the presence of resin columns in the structure results in a significant increase in weight. If the interactions between tufts could be shown to provide added benefit in energy absorption, then the structure could be redesigned to try to encourage this behaviour and improve the structural efficiency. Alternatively, if this mechanism was shown to have a negligible effect then a potential design improvement could be to remove the resin column completely. This work has been previously published in [151,152] and forms the basis of a final year research project [153].

6.1 Methodology

To understand the column drift mechanism, it was necessary to focus on only two elements of the sandwich structure, the foam core and the rigid resin columns. As with previous experimental tests, several test approaches were first evaluated to choose the most suitable method of representing the drifting of tufts within the core. An initial trial was carried out by testing a section of the foam in edgewise compression which with tufts inserted would be the closest possible representation of previously tested sandwich coupons. However, the relatively low thickness and stiffness of the foam sheet was such that it was too unstable under load and would fail by buckling (Figure 6-1) and not crushing as desired.

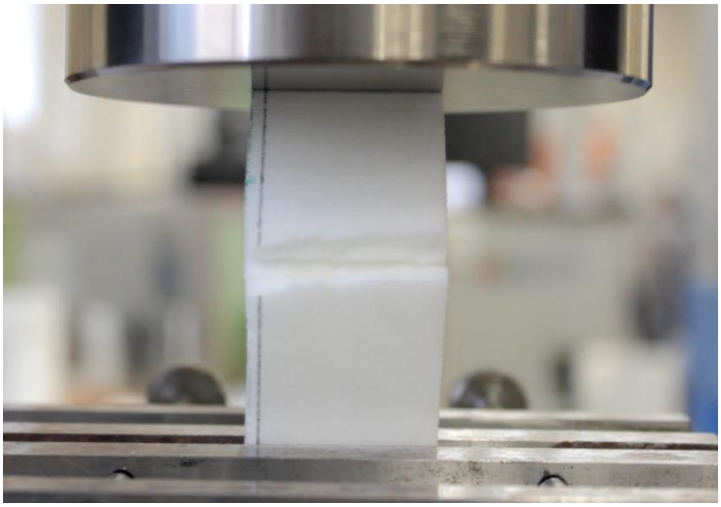

Figure 6-1: Buckling of foam sheet under direct edgewise compression loading.

A second trial was carried out, loading the foam in a flatwise direction, to increase its crushing stability. Short pins were cut to 10 mm from lengths of steel rod (Figure 6-4) and placed on the foam to simulate the presence of the resin columns. Whilst movement of the rod through the foam was observed, the relatively low thickness resulted in a very short termination time for the test, and the inability to use multiple tufts in one coupon. The large load required to crush the foam also meant that it was very difficult to observe the changes affected by the insertion of the pins.

For the final chosen test configuration, it was decided to pull the pins through the core in a tensile manner, instead of relying on compressing the foam core. To achieve this, a test fixture was designed and produced, capable of supporting and applying load to pins embedded within the foam core. The design of the test fixture is shown in Figure 6-2. The design of the fixture allows for the insertion of multiple pins, to simulate different tufting configurations. The spacing between each hole was 6 mm, to match the minimum spacing used in previous testing [45,140]. The fixture was laser cut from transparent Perspex sheets of 10 mm thick, to allow visual tracking of the pins as they moved through the foam.

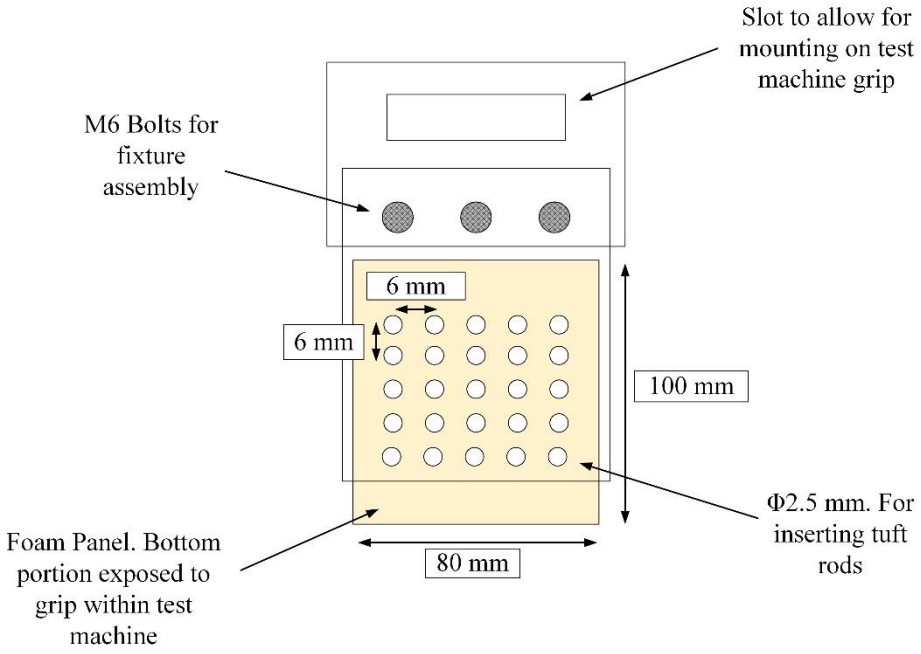

Figure 6-2: Schematic of test fixture used.

Load was applied to the sample using a Shimadzu desktop electromechanical test machine, with a 1 kN load cell. The upper part of the fixture featured an opening for the upper stage grip of the test machine to slot into, whilst at the bottom a section of the foam was left exposed and was mounted in the lower test grip, as shown in Figure 6-3. Initial trials revealed that the foam would slip within the test grips, so sandpaper (P60 grit) was used to increase the friction between sample and loading grip and avoid slipping. The loading rate applied was 4 mm/min. An Imetrum® video gauge system was used for visual tracking of the test. This camera system was able to track the movement of individual pixels within an image, thus following the movement of the pins as they moved through the foam. The system also allowed video playback of the test, allowing failure behaviour to be viewed and identified.

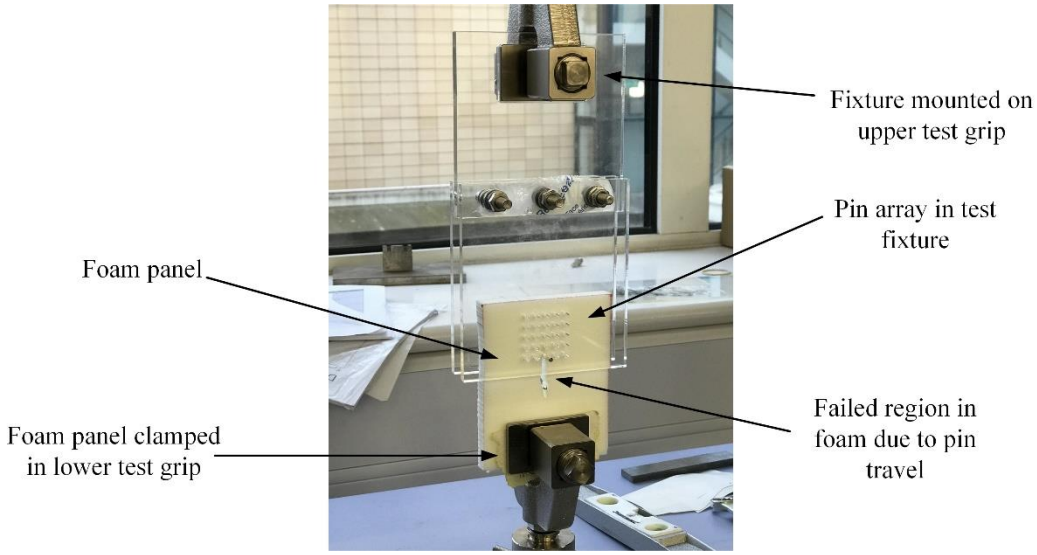

Figure 6-3: Setup of test fixture on Shimadzu test machine.

For the materials selection, the same Rohacell® 110 IG-F closed-cell foam by Evonik (110 kg/m^3) used in previous experimental work was chosen for the core. As a preliminary feasibility test, a rigid steel rod of 2.3 mm diameter was chosen to simulate the tufts (Figure 6-4). This choice was primarily made to provide an "off-the-shelf" solution for initial trials; however, it was also believed that avoiding any deformation or fracture of the pins during testing would help to encourage the desired stacking behaviour. Due to the differences in stiffness between the metal pin and the resin column it can be expected that the forces measured in the trial are not directly representative of a typical resin column but allow an initial proof-of-concept and comparisons to a baseline case to be made. Future work should look to address this by selecting a material with comparable properties to the resin system used for the tufted panels across the rest of the works presented.

As can be seen from the image, there are slight differences in geometry and dimensions of the two columns. Whilst the tufting needle is smooth, and the dimensions are fixed, the resin infusion process through the foam core leaves a rough outer surface. The rigid steel rod used is therefore an idealised geometry.

Figure 6-4: A comparison of a tufted resin column (left) and the steel pin used (right).

To insert the pins, a small pin hammer was used to gently knock the pins into the foam. To apply loading directly to the pins, those that were required to be loaded were left deliberately longer than the through thickness dimension of the foam and test fixture, to allow the test fixture to pull the pin as it moved. To simulate collisions between the loaded pins and the passive unloaded pins it was necessary to cut these slightly shorter than the foam thickness, so they could move freely through the material, and not scrape against the test fixture as it passed. A total of nine configurations were tested, with varying locations and numbers of pins inserted to simulate different tuft configurations. Initially a baseline set of data was created, using a single, centrally positioned pin. Further configurations were then created to explore the effects of multiple pins, either loaded in parallel or in line with each other, as well as more complex two-dimensional pin arrays. A summary of the test configurations and their naming conventions is given in Figure 6-5. Those pins that are loaded and those that are not are highlighted in the figure.

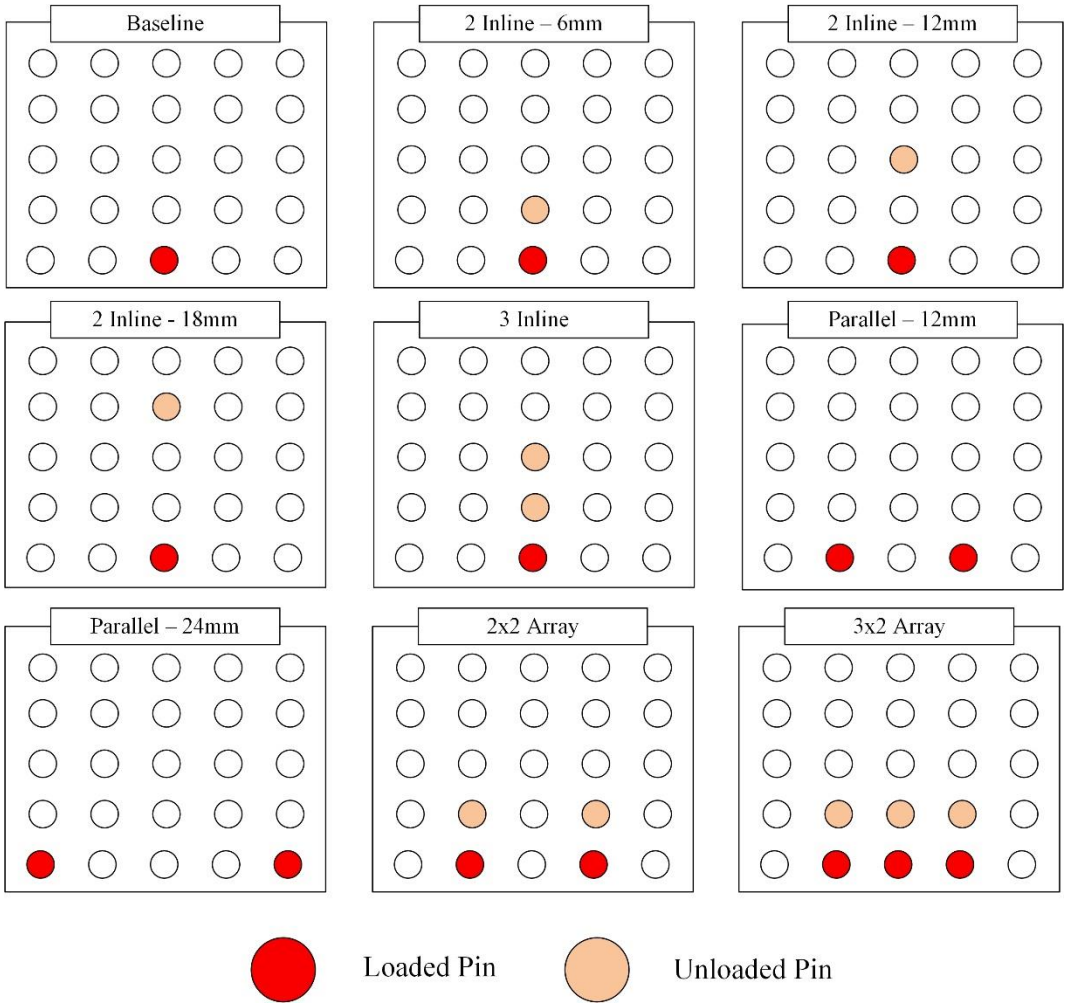

Figure 6-5: Positioning of loaded and unloaded for each test configuration considered.

6.2 Results and discussion

6.2.1 Baseline Testing - Single Pin

The results of the baseline tests, featuring a single central pin are shown in Figure 6-6. The load trace shows an initial sharp increase in load up to the point of failure initiation in the foam. Beyond this point the rod begins to slide through the foam sheet (Figure 6-8A). As the rod slides, it compresses material in its path, resulting in a gradual increase in load as the test progressed. Of the four samples tested, each showed a very similar trend in loading, although some variation between the peak loads were observed. This is potentially due to the insertion method of the rod, as tapping the pin against the foam could have led to cracks and potential weak spots in the material. This would be inconsistent between samples and thus result in slight variations in load.

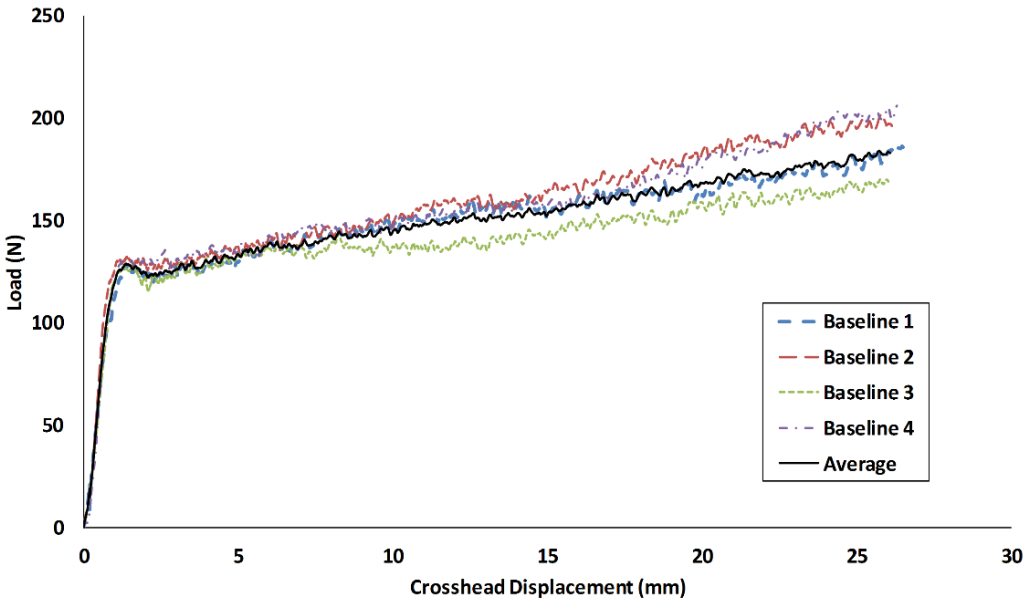

Figure 6-6: Load-displacement results for baseline tests.

6.2.2 Multiple Pins

Following on from the single pin baseline tests, configurations featuring multiple tufts were tested to explore the interactions between the tufts. Two placement strategies were explored, firstly by loading the pins in parallel, followed by lining the pins up in the same vertical plane. These were finally combined to give a two-dimensional array of pins.

6.2.2.1 Parallel

The results of the parallel tests are shown in Figure 6-7. Due to the consistency between results only two test samples were used, with a varied gap size between them. It can be seen from the results that the load is approximately double the baseline because of loading two pins in parallel, due to the requirement to crush the foam in two different locations. Doubling the gap between the pins had no effect on the load. Another noticeable difference when compared to the baseline was the smooth transition from the initial rapid load increase phase to the rod moving stage. This may be due to the increased number of pins stopping rotation of the sample, and thus eliminating any sudden changes in load.

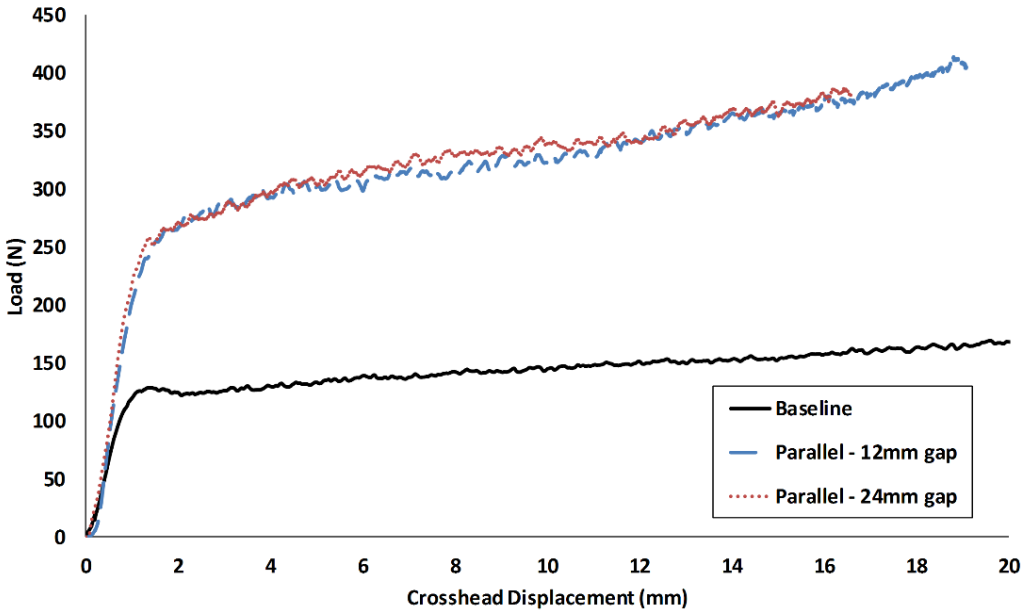

Figure 6-7: Load-displacement results for parallel pin configuration tests.

6.2.2.2 Inline

For the inline tests, the pins were placed in a straight line along the centre of the foam panel. Following the load trace in Figure 6-9, the load in each case increased sharply at the same rate as the baseline until the foam around the pin began to fail. From this point onwards, the load of each test configuration generally increased, although with significant fluctuations in the load. For the 2 pin configurations, there is a secondary increase in load as the loaded and unloaded pins begin to collide with each other, and the unloaded pin is driven through the foam (Figure 6-8B). From this point onwards the load remains steady, above the baseline load curve, but tends to return to the baseline level as the test progressed. The secondary rise in load changed with pin spacing, with the 6 mm occurring earliest, followed by the 18 mm and then the 12 mm. The 3 pin configurations showed a similar trend, but with two noticeable load increases corresponding to the two pin interactions taking place. It was observed during testing that in a number of cases the loaded pins would slide around the unloaded pins, as seen in Figure 6-8C. Similar behaviour has been observed in metallic structures, where compressive residual stress around pins can cause redirection of fatigue cracks [154]. However, it is not clear at this stage if this behaviour is occurring here. It was apparent that this occurred more often with larger pin spacing, which implies that the larger the gap, the harder it is to control the pin movement and collisions. Because of this, the shortest gap (6 mm) resulted in the largest consistent increase in load, as the unloaded pin was pushed for a much longer distance.

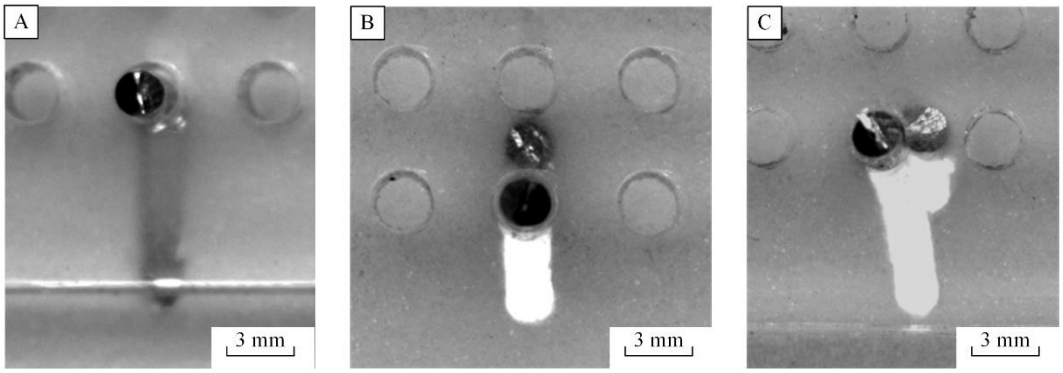

Figure 6-8: Sliding mechanism of pins through foam. A) Single pin baseline. B) Two pins inline moving together. C) Two pins inline, loaded pin realigning to avoid unloaded pin ahead.

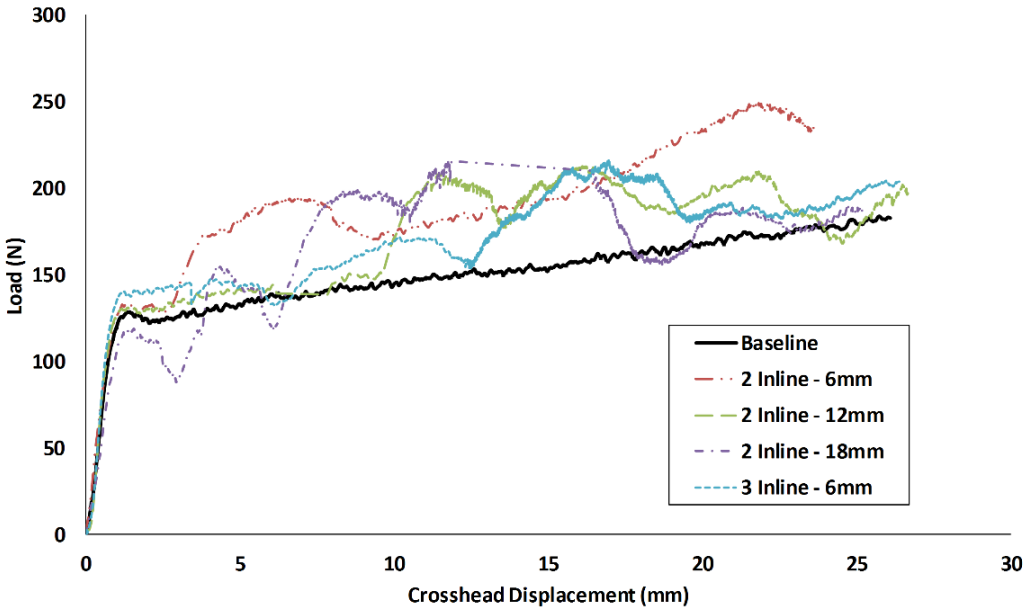

Figure 6-9: Load-displacement results for inline pin placement tests.

6.2.2.3 Array

By increasing the number of pins in both directions the load trace is observed to increase concurrently. As with each of the test configurations discussed previously, the initial loading phase follows a sharp increase in load before levelling off. The 2 x 2 array showed a slight drop in load after this point, followed by a load recovery at around 4 mm of displacement. The sustained load from this point is approximately 20% higher than the 2-pin parallel configuration. There is a slight increase and peak of the load at 17 mm of displacement, because of the loaded pins moving past the unloaded pins. The 3 x 2 array showed a much greater increase in load, because of the 3 loaded pins. As with the 2 x 2 array, there is a slight drop in load after the initial rise, followed by a steady increase. After a short test displacement of 7 mm, cracks began to appear around the loaded pins which

grew rapidly and fractured the foam. At this point the test was aborted and was not continued due to the foam being unable to handle the excessive loading conditions.

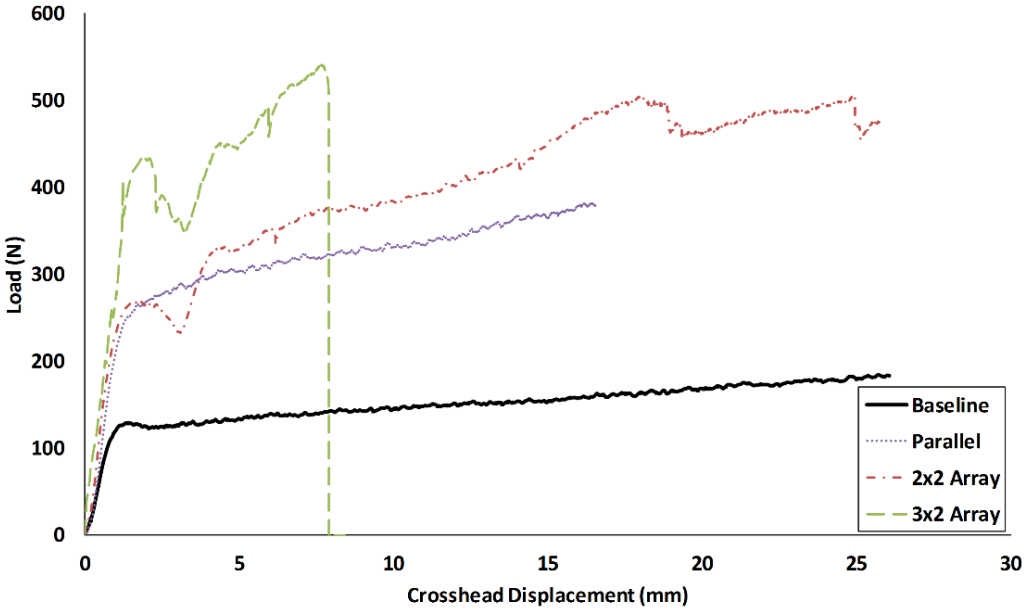

Figure 6-10: Load-displacement results for array pin placement results.

6.2.3 Energy Absorption

The specific energy absorbed during the tests was calculated for each sample by accounting for the mass of foam crushed in the path of the loaded pins. As can be seen from the results in Table 6-1, the efficiency of energy absorption generally increased with increasing numbers of pins in the loading direction. The additional work required by the loaded pin to compress the foam surrounding the next pin and then the work required to move that pin meant that energy absorption was generally higher for each configuration. Another point to note is that magnitude of the energy increase and the consistency between results. The variation between results also increased as the gap space increased, which suggests there is greater margin for error for the loaded pin to move out of alignment as it travels through the foam.

Compared to the values shown in Chapter 5, the absolute energy absorbed during these tests was relatively small, roughly two orders of magnitude lower than the full sandwich coupons tested previously [148]. Whilst the higher energy demonstrated in the sandwich coupon tests features an increased number of tufts, this suggests that for the tuft drifting mechanism to be of any benefit to the overall crushing performance then the tuft density within the sandwich panel should be high. However, testing has shown that collisions between tufts on a small scale can still add significant improvements to the energy

absorption of a single tuft. If these collisions could be controlled, by forcing the path of the tuft during failure, a substantial increase to the energy absorbing efficiency of the structure could be made.

Table 6-1: Averaged energy absorption results for each pin configuration tested.

Type	Work done per unit length	% Change	CV
	J/mm	*%*	*%*
Baseline	0.15	-	4.50
2 pins inline – 6 mm	0.19	28	5.04
2 pins inline – 12 mm	0.17	14	22.3
2 pins inline – 18 mm	0.16	6	9.24
3 pins inline – 6 mm	0.2	32	20.0
2 pins parallel	0.32	109	0.78
2 x 2 array	0.18	22	16.0
3 x 2 array	0.13	-16	0

6.3 Future Test Development

Whilst the test method outline in this work has successfully captured data from the tuft drift and collision mechanism during crushing, there are still aspects to the test that could be improved. The first of these is to select a material for the pin that is more representative of the resin column that the rigid steel pin used here. The high stiffness of the pin is likely to transfer more load thus inflating the contribution of the pin to energy absorption over a more flexible resin column. As such an alternative material with a flexural stiffness close to that of the epoxy resin system would be a better choice. Another change is to ensure a clean insertion method for placing the pin within the foam panel prior to testing. The current method using a small hammer gives rise to the possibility of damage forming within the foam, as well as the potential for the pin to not enter the foam at the correct angle. An improved method would see the use of a linear actuator with an actual tufting needle fitted to ensure a clean hole through which to insert the pin. The second step required would be to ensure no rotation of the foam panel, or transverse motion of the pin is allowed, to ensure clean contact and continued stacking between the loaded and unloaded pins. A more advanced level of investigation would consider geometry differences of the tuft as well, as noted in previous chapters the tufts have a tendency to drag some of the skin with them (Figure 4-13).

6.4 Conclusions

A novel test method has been developed and demonstrated to represent the behaviour of tufts within a sandwich structure during crushing. A metallic pin was used to represent a tuft and inserted into a foam panel. The pin was loaded in tension to force it to slide through the foam. Consistent loading results were observed for a single pin before the test was expanded to consider multiple pins in different configurations.

It was observed that the load required to drive the pin was directly proportional to the number of parallel pins being loaded. Pins placed in line with each other also showed an increase in load, particularly when the pins successfully stacked and moved together. This stacking behaviour was inconsistent and was hard to achieve the greater the distance between pins, or the larger the number of pins used. The results of this chapter have indicated that there is some positive benefit towards energy absorption because of column drift, particularly when using a high-density of tufts. However, comparing the energy required to drive a pin through the core against the energy absorbed by sandwich crushing in Chapter 5 suggests that the added benefit is minimal. When considering the significant weight increase because of column formation, it could be more beneficial to remove this resin ingress completely to improve structural efficiency.

Future developments to this test would need to focus on ensuring the pins travel in one fixed direction without realigning, as well as an improved insertion technique to ensure flaws are not present within the foam before testing. It would also be useful to carry out testing on the other contributing failure mechanisms in this manner, to understand the relative contributions of energy absorption that these add to a tufted sandwich structure under edgewise crushing failure.

Chapter 7 Case Study - Reclaimed Material and Tufting

7.1 Introduction

As discussed in Chapter 1, one of the challenges that the automotive industry must face is ensuring that the manufacture of future vehicles is more sustainable. Whilst end-of-life recycling of composites has not yet reached the required level of technical maturity, dealing with the large amount of waste material that is produced from composite manufacturing processes is potentially an easier route to targeting the vast amounts of material that would otherwise be sent to landfill.

However, whilst the reuse of scrap material is a promising route to sustainability, the materials in question still suffer from a knock-down in mechanical properties that regular recycling processes are known for. This is firstly due to the cutting of the virgin material, which will ultimately lead to discontinuities in the assembled preform, as well as the necessary handling stages which can risk damaging the plies. These factors are difficult to quantify and therefore make scrap material too unpredictable to work with for producing load-bearing structural components. For this reason, additional reinforcement, such as through-thickness tufting, could be required to stabilise the structure. If designed correctly, this stable assembly combined with the potential for increased fractures sites using discontinuous reinforcement could help to promote highly efficient energy-absorbing failure mechanisms.

As such, a case study has been carried out to investigate the use of tufting in conjunction with reclaimed process waste. This chapter explores the use of reclaimed composite waste in energy absorbing sandwich structures under both static and dynamic loading conditions. Two different forms of reclaimed material will be considered, firstly by directly reapplying patches of off-cut waste from a layup operation, followed by using a commercially available reformed aligned non-woven mat. Tufting will then be incorporated to reinforce the structures through-thickness, helping to stabilise them and maximise the performance under this specific load case. This work has been previously published in [155] and is part of a final year research project [156].

7.2 Methodology

7.2.1 Materials

Two separate commercially available fibre products were investigated in this study. The reference virgin material was a unidirectional non-crimp fabric (NCF) supplied by SGL (Sigratex C U320-0/ST), with an areal density of 320 g/m^2, 50k fibre count and approximate cured ply thickness of 0.36 mm, as used in previous chapters. The reclaimed material was a Recatex™ type 62 nonwoven complex, with an areal weight of 200 g/m^2 and approximate cured ply thickness of 0.72 mm, also supplied by SGL. This material is formed by cutting scrap material into small pieces, realigning the fibres in a carding process, before stitching them back together. Whilst the fibre orientation of this material is not completely unidirectional, a preferential direction of almost double the strength and stiffness has been shown when aligned to the stitching direction [135]. A visual comparison of the two materials is shown in Figure 7-1, where the differences in fibre arrangement and stitch type can be clearly seen. Additional supporting information for these materials is included in Chapter 3

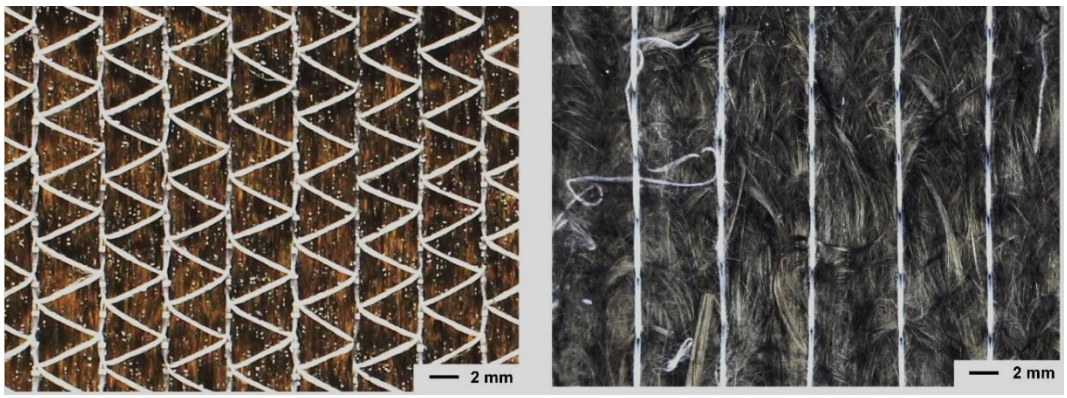

Figure 7-1: Material samples showing the difference in fabric architecture of the two types investigated (Left: UD NCF, Right: Reclaimed Mat).

7.2.2 Configuration

The two reinforcement styles were used to create four different sandwich skin configurations for this investigation:

- A continuous virgin laminate for reference, with a triaxial layup sequence of $[45/0/-45]_s$ was chosen to match the work discussed in previous chapters. The chosen layup totalled six plies per facesheet and produced a skin thickness of approximately 2 mm.
- A reclaimed offcut laminate, to simulate directly reapplying waste off-cuts from a ply cutting or layup operation. This configuration was formed by placing 50 mm wide

strips of material cut from virgin material on a CNC ply cutter, to match the layup sequence of panel 1, with the assembly configuration shown in Figure 7-2. To avoid overlapping the gaps between strips, each ply was offset by 12.5 mm as reported by [39], where a high static mechanical property retention was demonstrated with materials in this form.

- A reclaimed laminate, formed using the commercially available reprocessed fabric with the aim of matching the thickness of the first two panels. Three layers were used in each skin to provide a 2 mm skin thickness, and each layer was aligned with the stitching in the load direction to maximise the mechanical properties.
- A hybrid laminate, formed from the virgin and reclaimed fabrics, by substituting the central reclaimed ply of the previous configuration for a unidirectional virgin one. Due to the thickness difference between virgin and reclaimed material, the resulting skin thickness was approximately 1.8 mm, slightly thinner than the other three laminates.

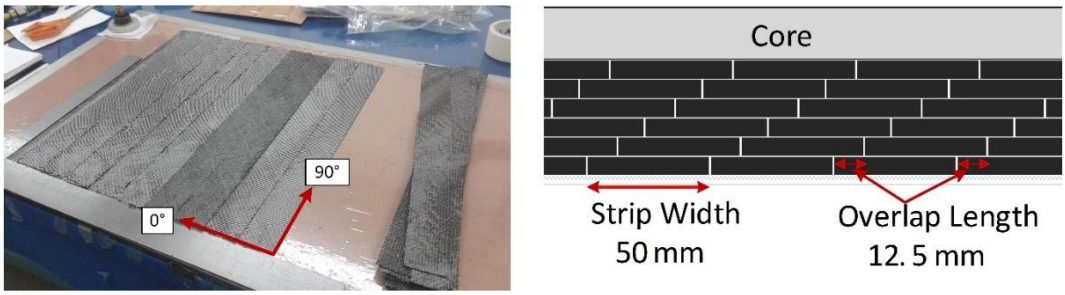

Figure 7-2: Laminate design for reclaimed off-cut configuration.

7.2.3 Coupon Manufacture

A total of four sandwich panels (500 mm x 450 mm) were assembled, tufted and infused following the procedure in Chapter 3. Whilst the reclaimed SGL material did not feature any binder in the fabric, it was put through this procedure also to replicate the compaction of the other panels. To minimise the number of panels to be manufactured, half of each panel (225 mm x 500 mm) was tufted as shown in Figure 7-3.

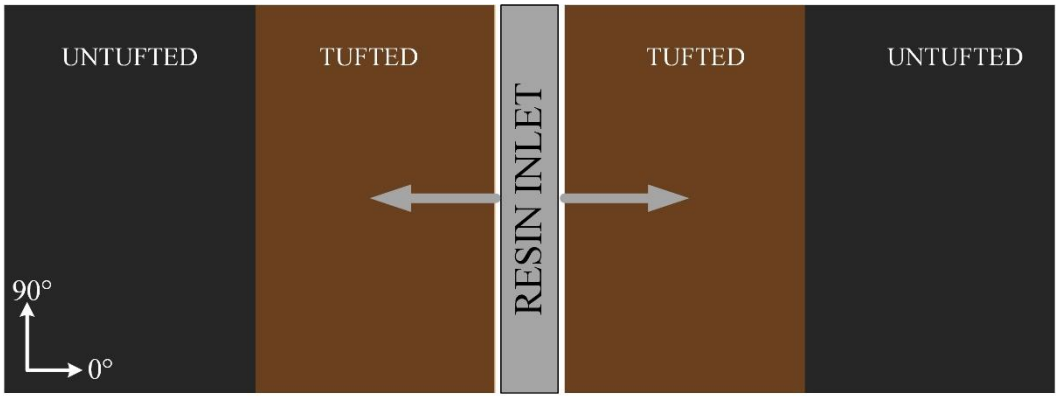

Figure 7-3: Overview of panel layout, including tuft locations, and infusion strategy used.

To further minimise manufacturing steps, two panels were infused simultaneously on a single tool plate. The two preforms were positioned as shown in Figure 7-3, with a metallic spiral tube placed between them to create a continuous flow front across the width of each. Flow media was placed on both faces of each panel to aid resin flow. As the tufted regions required more resin to fill the voids created within the core, these were infused first to ensure full wet-out before progressing onto the rest of the preform.

7.2.4 Coupon Design

A previous study by Marasco [84] demonstrated a method for successfully testing through-thickness reinforced sandwich structures. The chosen coupon geometry and dimensions is shown in Figure 7-4. The most notable feature of this design is the sharp tulip style trigger at the tip of the coupon. This trigger is necessary to promote stable crushing of the test coupon, whilst the tulip design is preferable over notched or bevelled designs to avoid exposing the tufts at the tip and to simplify manufacture. Each of the test coupons were cut from the panels using a water jet cutter, however the water jet was not able to cut through the hard resin columns in the tufted coupons, which required additional trimming using a milling machine to ensure the coupon edges were flat. Whilst the location of the tufts within each coupon was not accounted for during cutting, due to the relatively high tuft density it

was assumed that each coupon would contain a similar number of tufts. When cutting the off-cut coupons, the gaps between strips were aligned perpendicular to the loading direction.

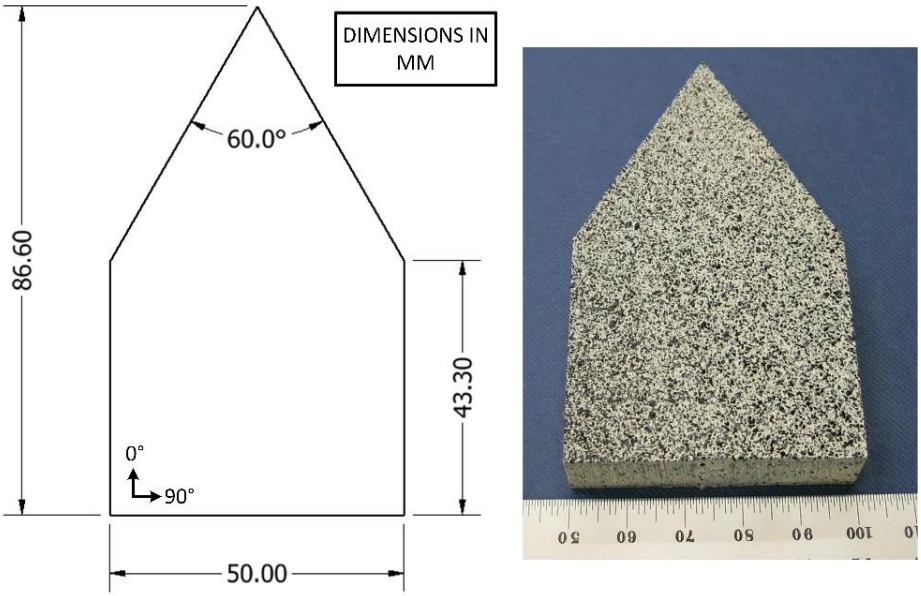

Figure 7-4: Overview of the basic dimensions (left) and test coupon geometry featuring DIC speckle pattern (right).

A summary of the coupon configurations and properties is shown in Table 7-1. The fibre volume fraction and void contents were not directly measured, but are estimated based on the use of the same materials and process in [135]. The fibre volume fraction in the reclaimed mat plies is notably low, in part because of poor fibre nesting between plies during compaction. It should also be noted that in the case of the tufted coupons these values are not representative, as tufting has been shown to locally increase fibre volume fraction and lead to an increase in localised porosity [92].

Table 7-1: Summary of Test Coupon Configurations

Facesheet Configuration	Skin Lay-up Sequence	Average Coupon Thickness		Average Coupon Mass		Fibre Volume Fraction	Void Content
		Untufted	Tufted	Untufted	Tufted		
		mm	*mm*	*g*	*g*	*%*	*%*
Virgin Continuous (V)	$[45/0/-45]_s$	14.3	14.7	24.5	32.4	54.6	1.9
Reclaimed Off-cuts (S)	$[45_{ST}/0_{ST}/-45_{ST}]_s$	14.3	14.9	24.2	32.4	54.6	1.9
Hybrid (H)	$[0_{RE}/0/0_{RE}]$	13.6	13.7	18.4	25.0	23.5	3.6
Reclaimed (Reprocessed) Mat (R)	$[0_{RE}/0_{RE}/0_{RE}]$	14.3	14.4	20.7	27.3	13.5	4.1

RE – Reclaimed layer (0 indicates principal fibre direction)

ST – Discontinuous strip

7.2.5 Test Method

Both quasi-static and dynamic testing were carried out on the test coupons. Static testing was performed using a Zwick 1466 electromechanical test machine, with a 50 kN load cell. A sandwich test fixture was used to apply a clamping pressure at the base of the coupon to stop the coupon sliding and to avoid buckling failure. The coupon was positioned at the centre of the test machine between two parallel circular loading plates as shown in Figure 7-5. A displacement control programme was used to provide a constant quasi-static crushing rate of 6 mm/min. Testing was terminated at a crush length of 50 mm before any interaction between the coupon and the lower plate could take place, with a total of five samples tested for each facesheet configuration. A Dantec digital image correlation (DIC) system was used to obtain the strain field within the coupons during crushing, with a fine speckle pattern applied as in Figure 7-5.

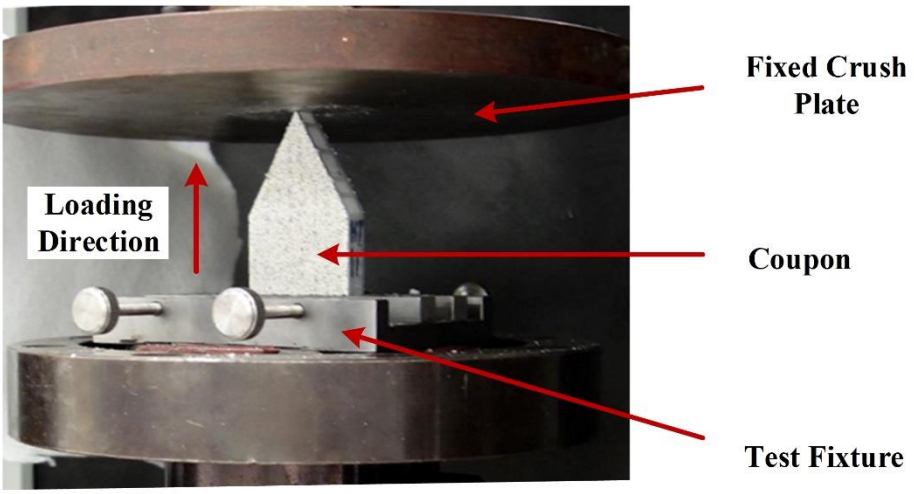

Figure 7-5: Overview of the static loading test setup showing coupon positioning and fixtures.

Dynamic testing was carried out using an Instron Dynatup 9250HV drop tower. Samples were mounted within the same sandwich fixture as for the static tests (Figure 7-5) and impacted from above by a steel disk designed to mimic the crush plate used in static testing. An iterative process to determine the impact energy to use was initially employed, to ensure as much of the gauge section was crushed as possible. The impact height was varied providing different impact energies, with the resulting damaged coupon inspected visually to determine the crush distance. Due to limitations of the drop height of the tower, a maximum attainable impact energy of 200 Joules was used. The pneumatic rebound brakes on the drop tower were removed, to ensure that they did not restrict the impactor during crushing. The total mass of the impactor (impact plate, tup, and additional ballast) was 28.8 kg, with a drop height of 0.7 m, and a resulting impact velocity of 3.7 m/s. As with the static load case, a total of five samples were tested per skin configuration.

7.3 Results

7.3.1 Static Failure Modes

The failure mechanisms under static loading for both untufted (Figure 7-6) and tufted (Figure 7-7) show noticeable differences between the types of materials tested. For the untufted case, the virgin coupon failed by disbonding and splaying of the facesheets. Delamination occurred in the skins and the foam core was progressively crushed to the point where the impact plate terminated. In complete contrast, the reclaimed mat samples failed with multiple fracture planes though-thickness of the facesheets occurring perpendicular to the loading direction, leading to local buckling within the facesheet as the crush plate displaced through the sample. The foam core was compressed to the final crush

length, but skin fracture propagated past this point. There were no obvious signs of delamination within the skins, although only a limited number of ply interfaces were present in each facesheet. In the hybrid coupons, fracture was the dominant failure mechanism with local buckling failures occurring as crushing progressed in a similar manner to the reclaimed mat, although ply delamination was now also present. The interfacial cracks did not propagate beyond the core as they did in the reclaimed mat coupons. The off-cut coupons failed in a very similar manner to the virgin coupons, with splaying and delamination of the facesheets occurring. However, unlike the virgin coupons, skin-core disbonding extended a short distance beyond the final crush point on one side of the coupon.

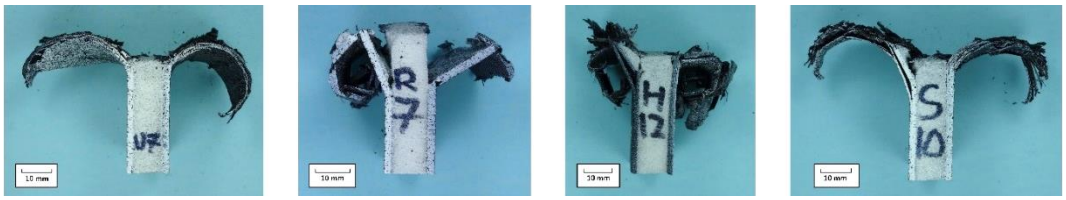

Figure 7-6: Representative failed untufted coupons after static testing. From left to right: Virgin Continuous, Reclaimed Mat, Hybrid, Reclaimed off-cuts.

In the case of the tufted samples, the failure mechanisms observed were like those of the untufted coupons. The curvature of the failed skins was noticeably higher in each case compared to the untufted coupons, because of fewer fracture planes forming in the facesheets. This is particularly clear in the hybrid coupons, which appeared to roll rather than fold.

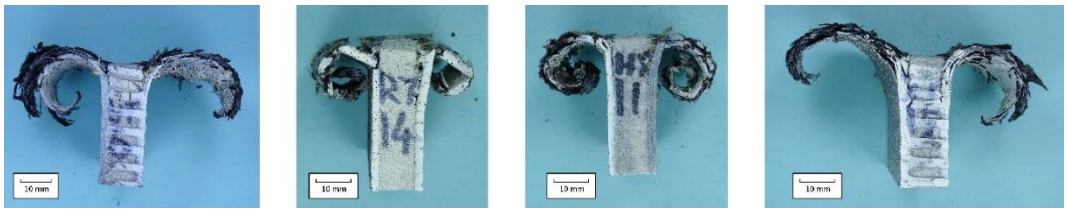

Figure 7-7: Representative failed tufted coupons after static testing. From left to right: Virgin Continuous, Reclaimed Mat, Hybrid, Reclaimed off-cuts.

7.3.2 Dynamic Failure Modes

The failure mechanisms captured during dynamic testing for the untufted coupons show significant variation between the different facesheet configurations. The primary mechanism for the virgin material (Figure 7-8A) was delamination and bending of the facesheets, as before under static loading conditions. The failure was noticeably more elastic than the static load case, with the facesheets partially returning to their original shape

after the load was removed, indicating less fibre failure because of the reduced crushing distance, a possible explanation for the reduced load and SEA in the dynamic coupons compared to the static ones. Skin-core disbonding was localised to the region of crushed material. The foam core within this region was compressed down to the final crush distance.

During testing of the reclaimed mat material coupons (Figure 7-8B), skin-core disbonding occurred almost immediately after the impact plate contacted the test coupon. This disbond occurred over the entire exposed surface, with the skin fracturing at the edge of the test fixture. Due to the early separation of the facesheets, only a small amount of material at the tip of the coupon was crushed, with the foam core experiencing most of the impact force, and thus it was crushed substantially and fractured into several pieces.

The hybrid test coupons (Figure 7-8C) initially failed by fragmentation and delamination at the tip of the test coupon. Skin-core disbonding began to occur and in one skin this propagated down to the test fixture. After separation of one of the skins, the applied load was unbalanced resulting in a shearing of the foam core. Due to the collapse of the core, the impact plate slid across the coupon, leaving the remaining skin relatively intact.

Failure of the reclaimed off-cut material (Figure 7-8D) was similar in nature to the virgin configuration. Failure initiated through delamination at the tip of the coupon. Disbonding then began to occur resulting in splaying of the face sheets. More fragmentation of the skins occurred compared to the virgin material. After testing the skins did spring-back slightly, but not as much as the virgin test coupons.

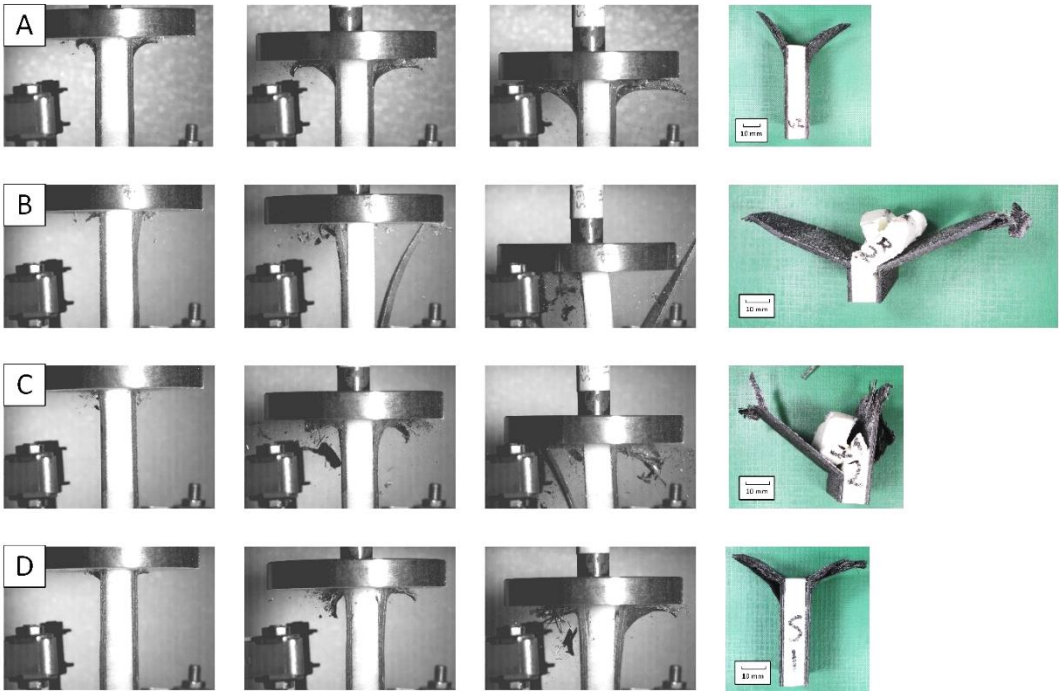

Figure 7-8: Representative dynamic failure mechanisms of untufted coupons. A: Virgin Continuous, B: Reclaimed Mat, C: Hybrid, D: Reclaimed off-cuts.

In general, failure of the tufted test configurations showed significantly less variation between materials than their untufted versions. Coupon failure was also very consistent within each configuration. In all cases, failure initiated through delamination and fragmentation of the skins. Progressive crushing of the coupons then commenced, with noticeably more fragmentation occurring compared to the splaying and delamination mechanisms observed in the untufted tests. Shear failure occurred at the interface between facesheet and core, accompanied by failure of the tufts at the same interface. Following this, the failed tuft and surrounding resin column were driven down through the core. This phenomenon has been observed previously [148], however its role in failure is unclear. The only major noticeable difference between skin configurations is the geometry of the skin after failure. The virgin (Figure 7-9A) and off-cut (Figure 7-9D) coupons have mainly undergone splaying. This differs to the reclaimed mat (Figure 7-9B) and hybrid (Figure 7-9C) laminates which have multiple fracture planes and have resulted in the skins folding in upon themselves as was seen in the static tests, albeit over greater crush distances.

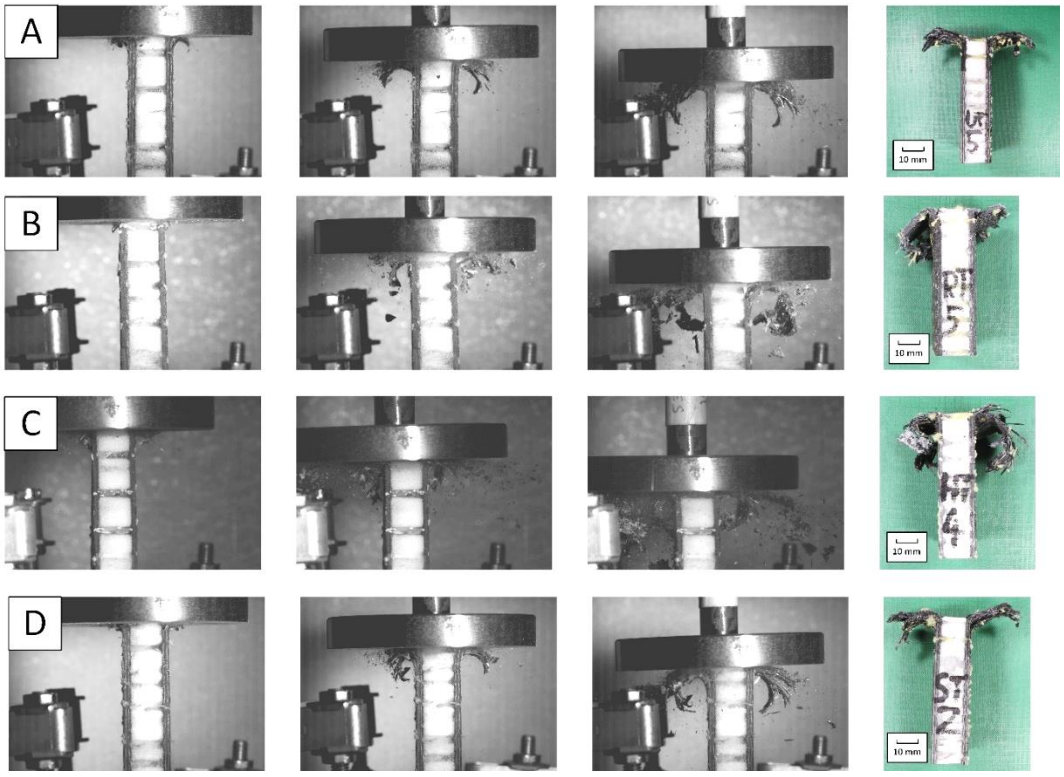

Figure 7-9: Dynamic failure mechanisms of tufted coupons. A: Virgin Continuous, B: Reclaimed Mat, C: Hybrid, D: Reclaimed off-cuts.

7.3.3 Load-Displacement

Representative load-displacement plots for both static (Figure 7-10) and dynamic (Figure 7-11) cases show a trend of increasing load as crushing progresses and the coupon widens. In all cases (static/dynamic, tufted/untufted), the virgin continuous fibre test coupons sustained the highest loads, followed by the reclaimed off-cut material, the hybrid configuration, and finally the reclaimed mat material. In the static load case, the force required to crush the coupons increased for each skin configuration once they were tufted. The reclaimed off-cut material load trace also now closely matched the virgin continuous. For the dynamic case, the loads for the virgin and off-cut material did not increase significantly after tufting, however there was a noticeable increase for the reclaimed mat and hybrid test coupons. The greatest difference was noticed in the maximum crush displacement of the test, which was reduced for all material types by as much as 40% because of the maximum impact energy limitation. Other notable differences in the load traces was the saw-tooth effect seen across all but the virgin coupons, changed upon dynamic testing indicating a greater instability during dynamic loading. Another notable feature was a greater defined initial peak load across all configurations when testing in dynamic conditions compared to static.

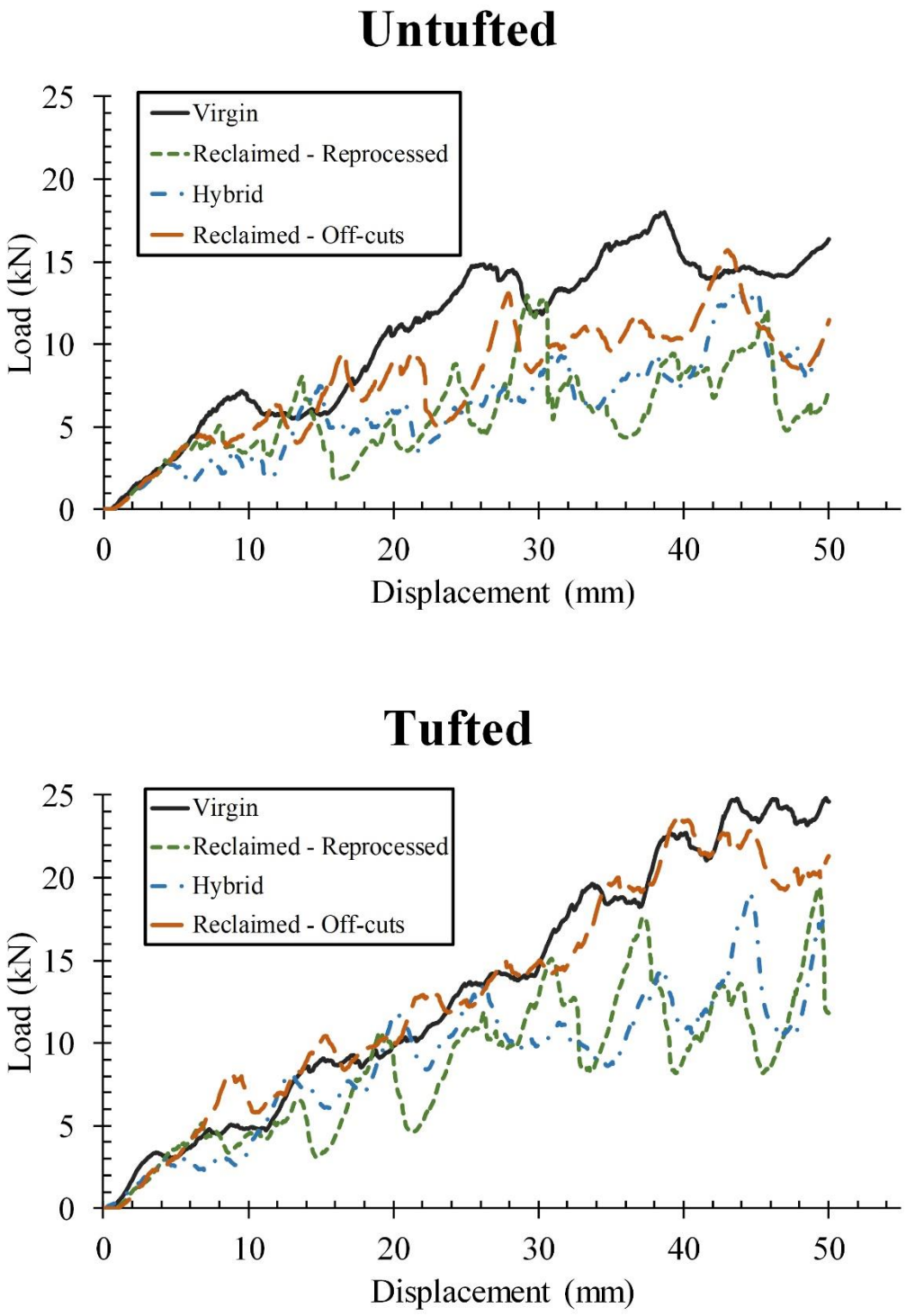

Figure 7-10: Representative quasi-static load-displacement results.

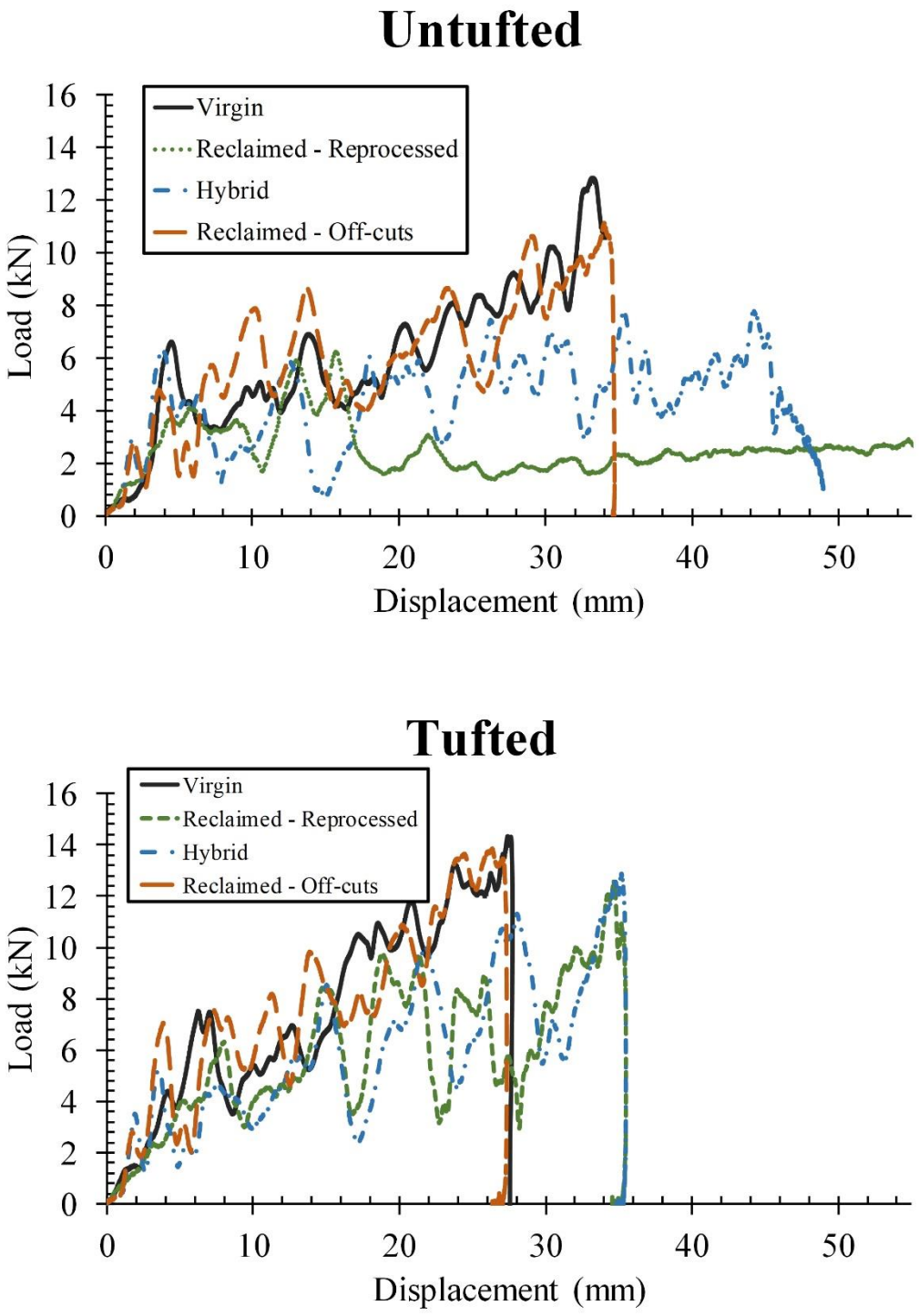

Figure 7-11: Representative dynamic load-displacement results.

7.3.4 Specific Energy Absorption (SEA)

An approximation for the SEA was given by integrating the area under the load-displacement curve using the trapezium rule, and dividing by the crushed mass of the

coupon, as outlined in equation 2. The average SEA of all test configurations is shown in Figure 7-12.

Whilst the crushing distance for static testing could be controlled and was held constant, the distance travelled, and behaviours observed during dynamic testing varied significantly between test configurations. Thus, for the purposes of calculating the energy absorbed, it was decided that each coupon's independent crush length would be considered, rather than normalising to a standard length (as performed in Chapter 4). This decision was made to fully account for each of the varying failure mechanisms across the test coupons, some of which occurred later than others. Whilst this risked capturing significant variation in data points, this was the best way to capture the variation in physical behaviour across the different configurations.

In a similar manner to the method shown in Chapter 4, to approximate the mass of the crushed material, an average sandwich areal density for each configuration was calculated by using the surface area of the test coupons with the dimensions shown in Figure 7-4 and dividing by the as-measured coupon mass. From a known surface area of the coupon over the chosen crushing distance, the areal density could then be used to find the crushed material mass.

It was observed that across all configurations the SEA was increased by the presence of tufting. The magnitude of this increase varied across each configuration, with the most significant difference observed in the dynamic reclaimed mat results because of the notable change in failure behaviour. The SEA generally decreased slightly across the configurations under dynamic loading. Of all the configurations tested, the virgin continuous material had the highest SEA as would be expected. This was followed by the reclaimed off-cut material, the hybrid laminate and finally the reclaimed mat material. It was also noteworthy that the deviation of results was smaller in the tufted coupons than for the untufted, for both static and dynamic loading. This was reflected in the consistent failure modes observed across all the tufted coupons, which is an important observation for discontinuous materials as variation is typically much higher than in continuous fibre materials.

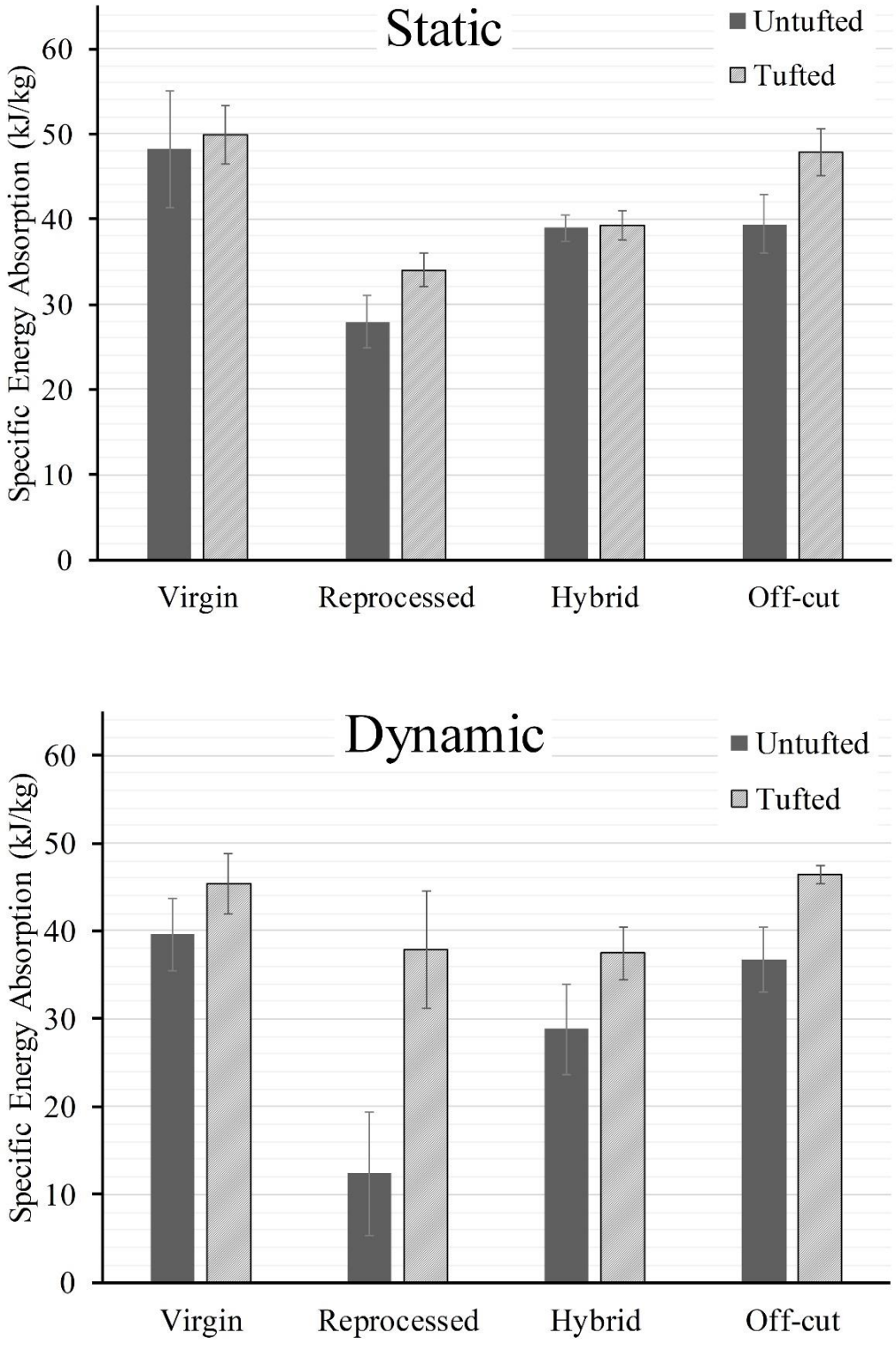

Figure 7-12: Averaged SEA results for static and dynamic tests.

7.3.5 Digital Image Correlation (DIC)

DIC imaging of the static testing is show in Figure 7-13. It shows the tangential engineering strain in the loading direction across the different coupon configuration.

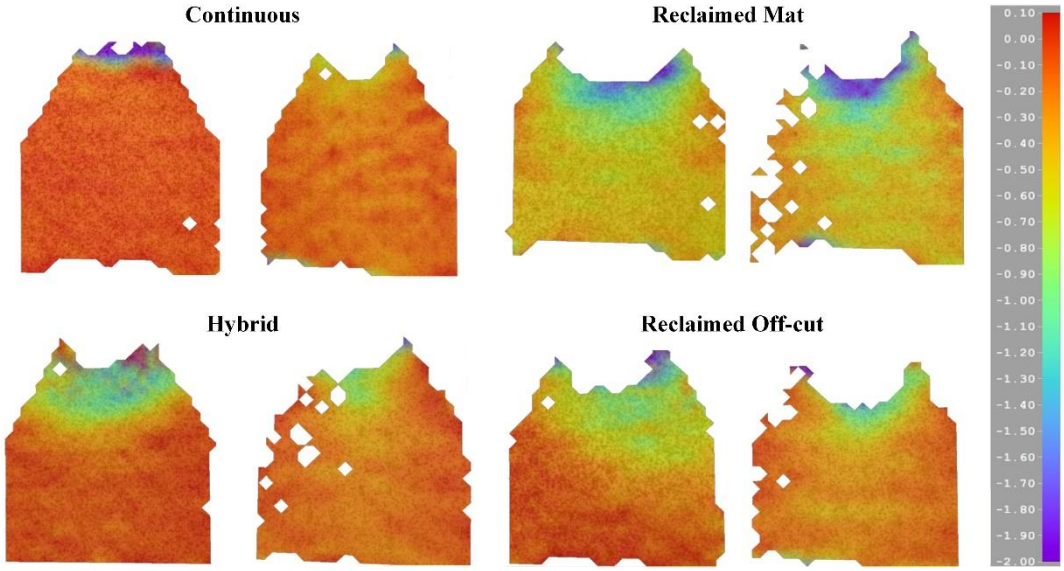

Figure 7-13: Representative DIC imaging showing engineering tangential strain (%) distribution for the untufted (left) and tufted (right) samples.

These results show that the strain distribution over the coupon surface can be significantly affected by the choice of facesheet material and configuration. The continuous material creates a highly localised region of high strain at the crush front. In the reclaimed mat material, the strain is relatively high across the entire coupon, with a localised band of high strain at the crush front. The hybrid coupons show similarities to both the continuous and reclaimed mat materials, with low strain across most of the coupon, but with a large band of high strain surrounding the crush front. The off-cut coupons also display a similar strain pattern.

Overall, the act of tufting caused the strain to be distributed over a wider area of the test coupon. This is most obvious in the continuous coupons. Notably the reclaimed coupons are relatively unchanged after tufting, as the strain distribution across the coupon was already high. This suggests that the failure mechanism is dominated more by than the strength of the interface, rather than the stiffness of the individual facesheets.

7.4 Discussion

7.4.1 Untufted

Testing revealed that the choice of skin reinforcement had a significant influence on the failure mechanism and performance of the sandwich coupon. The reference test coupon, featuring a laminate of virgin continuous material, failed in a typical stable crushing manner as per [73], involving disbonding, splaying, and delamination of the facesheets, and

compression of the foam core. This is reflected in the DIC strain map, where it is shown that a localised region of high strain at the crush front is present, corresponding to the gradual localised failure.

The use of the reclaimed mat greatly reduced the stability of the failure mechanism. Skin-core disbonding propagated beyond the crush front of the coupon resulting in separation and fracturing of the facesheets, as shown by the notably higher strain field across the coupon. The failure was amplified by the dynamic load case. Failure of the reclaimed mat material appears to be initiated by global buckling of the facesheets, because of the low fibre volume fraction, and thus stiffness, of the material, as well as the low ply count and minimal number of delamination sites possible. This caused failure at the interface between skin and core resulting in the premature separation of the facesheets. This was reflected in the relatively low forces sustained by the coupons and the significant decrease in SEA compared to the reference virgin coupons, despite the reduced coupon mass. Due to sudden catastrophic failure of the reclaimed mat coupons under dynamic loading, the variation in SEA was markedly higher than all other configurations tested.

In contrast to the reclaimed mat, the off-cut reclaimed coupons behaved similarly to the virgin continuous coupons. The overall failure mechanism was the same, and the resulting load trace followed a similar trend. The strain field demonstrated features of both the continuous and reclaimed mat strain distributions, with higher strain at the crush front dropping to zero towards the base of the coupon. The resulting SEA under static loading was at a similar level to the hybrid laminate. Under dynamic loading the SEA results were more comparable to the virgin laminate. The presence of discontinuities in the form of cut plies therefore appear to have had varying effects on the performance. No clear fracture planes were observed along these discontinuities, however the reduced load carried under static loading implies the discontinuities weaken the structure to some extent.

In the case of the hybrid configuration, the unstable failure observed in the reclaimed mat coupons was alleviated to some extent by substituting one of the reclaimed mat plies for a virgin continuous ply. The addition of a virgin ply changed the facesheet stiffness enough to delay the onset of buckling, as shown by the relatively low strain field, and thus stabilise the failure. The delay of buckling and facesheet disbonding allowed for more fracture planes to occur within the facesheets, which account for the additional energy absorption of those coupons. Whilst this configuration delayed facesheet disbonding, it did still occur and ultimately the coupons failed by unstable collapse. These hybrid coupons displayed combined failure mechanisms of both the reclaimed mat laminate and the virgin continuous

laminate. The resulting SEA of the hybrid coupons was subsequently halfway between the reclaimed mat and virgin configurations and shows promise for the ability to tailor the laminate properties with these materials.

7.4.2 Tufted

Tufting of the sandwich coupons had the general benefit of stabilising the failure mechanism across all configurations. Tufting changed the failure modes observed by delaying the failure of the bond between skin and core to ensure crushing failure, ultimately leading to an increase in SEA across each coupon type.

In the static load case, the difference in failure mechanisms between tufted and untufted coupons is not that significant, although the facesheets of the reclaimed mat and hybrid configurations appear to have failed in a more gradual crushing manner than the untufted coupons. The biggest noticeable increase for the static load case is that the forces of the load trace for the tufted configuration are higher for each configuration. Due to the added weight of tufting, this equated to marginal increases in SEA for the unidirectional and hybrid coupons but increases of as much as 20% in the two reclaimed configurations. The DIC strain fields for the tufted coupons all show minor differences when compared to the untufted coupons. In this case of the continuous and hybrid configurations there are regions of relatively high strain away from the crush front, indicated by the increase in yellow-coloured regions on the surface of the coupon. This is potentially an indication of a reduction in in-plane stiffness within the facesheets because of the added tufts. For the two reclaimed configurations this effect is reversed, as more low strain red-coloured regions begin to appear. This is most likely an indication of the stabilising effect of the tufts, transferring the applied load over the whole sandwich coupon, rather than just the facesheets.

Under the dynamic load case however the differences are far more noticeable. An almost uniform failure mode is observed across each of the tufted configurations, involving some delamination and fragmentation of the facesheets, and compression of the foam core. The overall crushing distance is much shorter due to the greater amount of energy absorbed by the stabilised facesheets, as well as possibly by the failure of the tufts, and this is reflected in the increased SEA compared to the untufted coupons.

Overall, the tufts delayed the onset of separation between skin and core, restricting this mechanism to the distance over which crushing of the coupon takes place. Restraining the

disbonding mechanism ultimately led to a larger proportion of the facesheets being crushed relative to the untufted coupons. This resulted in a greater overall energy absorption of the tufted coupons compared to the untufted counterparts. Despite the increase in SEA across all configurations, a similar trend was observed to the untufted coupons, with the virgin material having the highest performance and the reclaimed mat having the lowest. The most significant change noted is that the reclaimed mat showed a substantial increase in SEA under dynamic loading after tufting, when compared to the static load case.

Tufting in this application could therefore be a tool to improve the performance if a desired level of SEA was required to be reached. Optimisation of the tuft layout could also improve SEA, by reducing the tuft density to limit weight addition due to resin infiltration. Furthermore, performance could be improved by adjusting the orientation of the tufts within the core. Previous work has shown that aligning the reinforcement at 45° can be particularly effective at resisting in-plane shear loading [94,150,157].

7.4.3 Comparison of Reclaimed Materials

Of the two reclaimed configurations tested, the off-cut material generally performed higher. The off-cut material performed at a comparable level to the virgin material, particularly under dynamic loading conditions. Whilst the same material and layup was used, this suggests that the fracture planes present due to the cut plies were not large enough or not at the right location to drastically reduce the performance and stability of the facesheet. The avoidance of catastrophic failure was also aided by using the through-thickness ply overlap technique to offset the resin rich regions. The relatively poor performance of the reclaimed mat is most likely attributed to the reduced fibre volume fraction of the material. The reduced volume fraction would negatively affect the stiffness and strength of the material which led to the buckling of the untufted facesheets and low energy absorption of the crushed coupons. This performance could be improved by moving away from the vacuum infusion process used in this investigation for higher consolidation pressures as shown in [135], although in the case of a foam-cored sandwich structure these high pressures are not practical due to the risk of crushing the core. Alternatively, the improved results of the hybrid configuration over the reclaimed mat configuration suggests that tailoring the laminate may be possible. The results suggest that only a small proportion of virgin material is necessary to stabilise the failure significantly however not enough data is available at this stage to propose an optimum configuration. The relatively large thickness of the reclaimed mat plies does however limit the design flexibility, if weight and/or dimensional limits are enforced in more complex laminates.

Whilst ultimately this work suggests that off-cut material performs better for this design application, it is important to note that the usefulness is dictated by the quality of off-cuts obtained. Off-cut geometry may not be as consistent as the idealised strips used here, requiring far more pieces to assemble the laminate and resulting in an increased number of fracture surfaces that would severely limit the processability and performance of the structure. It is also important to note that the handling of the reclaimed mat was much easier than the delicate off-cuts, greatly affecting processability which is an important consideration when moving into an industrial environment.

Test results suggest that tufting is a necessary process to stabilise the failure mechanism of the sandwich coupons, particularly for the reclaimed materials. It is unlikely that the reclaimed mat would be used in this type of application without some form of reinforcement through-thickness, the off-cut material was more stable without tufts and could therefore be used without reinforcement depending on the geometry and quality of the off-cuts used.

What is apparent from this work, is that further investigation into reprocessed material is required to better understand the mechanical behaviour under a wide range of load cases. Whilst some background mechanical characterisation has been carried out [135], it is necessary to carry out further work to explore things such as compressive behaviour and interlaminar properties. An additional area of interest would be to explore the adhesive properties when assembled into a sandwich structure, particularly as the surface architecture of the fabric is very different to a standard NCF. Furthermore, whilst a consistent process may be used to produce these materials, as with the off-cut materials discussed here, they are still very much dependent on the life and handling of the material in its virgin state. As such a statistical analysis of variation within mechanical properties would be of further use to understanding the behaviour of these fabrics.

7.4.4 Specific Energy Absorption

Whilst for the analysis of these experiments it was decided to use the full crushing length to measure the specific energy absorption, calculations were also carried out to measure the specific energy absorption for a normalised length of 19.32 mm, chosen as this was the minimum crushing length achieved by all test coupons. The results of this have been overlaid on to the original dataset (appearing as light colour shaded bars) in Figure 7-14.

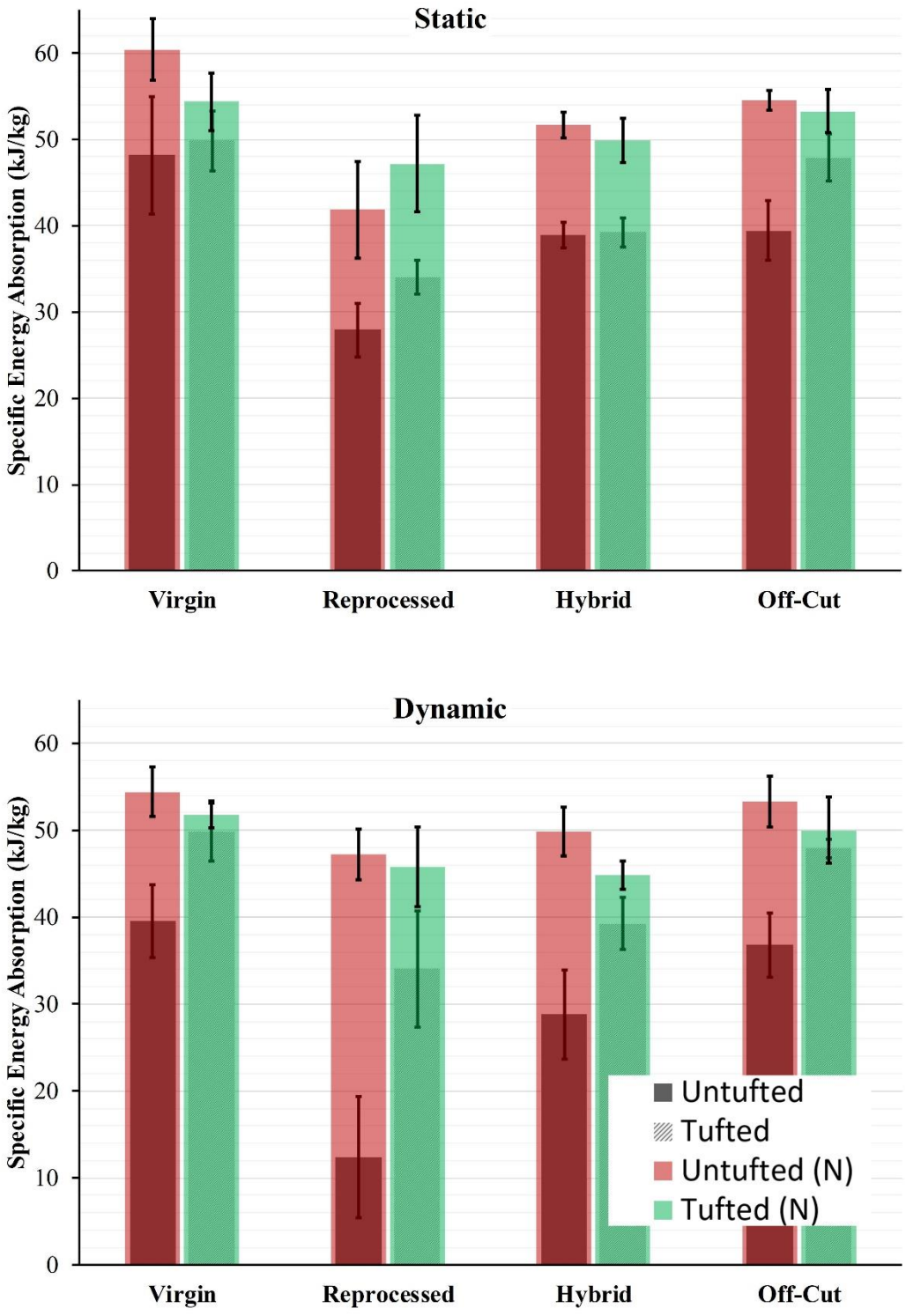

Figure 7-14: Overlaid SEA comparison graphs demonstrating the fluctuations in measured performance when considering normalised data to 19.32 mm (coloured shading) or individual datasets (dark shading).

As can be seen in the graph, there are noticeable differences in SEA when the normalised and un-normalised data are compared, with the normalised SEA higher in all cases. This is

understandable, as generally even the most unstable test configurations would demonstrate some stable crushing at the start of the test before collapse. It is also noticeable that the variation between the two datasets is reduced for the tufted configurations, because of the more consistent failure mechanism throughout the test. For the example of the reclaimed mat coupons under dynamic loading, there is a dramatic change in the failure mechanism as the test progresses, as shown in Figure 7-15. Because of this, the crushed material mass becomes difficult to estimate, as the separated facesheets are no longer active. This leads to an underestimation of the SEA, as in reality the active material is much less than predicted. However, whilst this makes for a more conservative approximation of the SEA, the coupon has in fact completely collapsed and so is not serving as an efficient energy absorbing structure. At the same time, normalising the data to a fixed reference length has the effect cancelling out the differences between many of the datasets, inaccurately reflecting the differences between each laminate configuration. This raises the question of the effectiveness of SEA as a standalone analysis metric for complex structures such as these, as the complex failure mechanisms are not easily compared between tests.

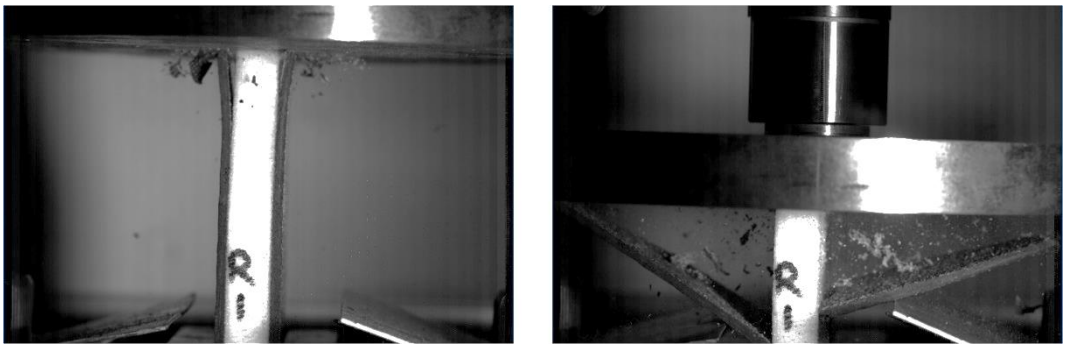

Figure 7-15: An example of the significant change in failure mechanism that occurred during crushing of a reclaimed mat test coupon.

7.5 Conclusions

In this study, reclaimed carbon fibre has been applied as the reinforcement of the facesheets of energy absorbing sandwich structures. Of the two reclaimed configurations investigated, the commercially available mat was the lowest performing, exhibiting unstable and unpredictable failure in the form of buckling and low overall energy absorption compared to the other configurations tested. The Hybrid configuration of reclaimed and virgin materials exhibited a more stable failure and thus greater energy absorption, offering the potential to tailor these laminates. In comparison, the off-cut material performed more comparably to the virgin continuous reinforcement but was more difficult to handle during assembly and could be improved with automation.

The addition of through-thickness reinforcement played a significant role in all configurations by helping to improve energy absorption, however the biggest improvement was seen in the dynamic tests on the reclaimed material, where the failure mechanism completely changed. Tufting was able to increase the absolute energy absorption across each of the test configurations, however the increased weight of tufting due to the resin rich regions surrounding the tufts meant that the increase in SEA was not as significant. Overall, the use of tufting with reclaimed material is a promising 'value-added' application that demonstrates the potential for using waste material in a wider range of applications.

Comparing the method of calculating SEA by normalising to a fixed length or using the full dataset raised the question of the suitability of SEA for complex structures with significant mass loss during crushing. Results using the two methods differed significantly making it unclear of the true comparative performance between coupon types.

Chapter 8 Discussion

8.1 Introduction

Prior to this investigation, only a limited amount of work had been carried out on the use of tufting for reinforcing composite structures through thickness, compared to more commonly used methods such as stitching or z-pinning. Within this, much of the focus has been on the processing influences as well as on the interlaminar reinforcement of monolithic laminates. Through the efforts of Lukaszewicz and Blok et al. [42,45], it was successfully demonstrated that tufting as a TTR technology is applicable in sandwich structures, and can be used successfully to supress separation of the facesheet-core interface, thus improving the energy absorption in edgewise loading conditions as desired for automotive applications. Through the current work, a series of experimental methods have been used to help generate an understanding of the collapse mechanisms of tufted sandwich structures for this load case, and the role and influence that the tufts have within this.

This chapter will discuss the use of tufting in sandwich structures in general, looking at how the learning developed through this work can better inform the design of these structures in the future. This will also look at the processing of these structures, and this could be improved to increase the feasibility of using these structures in a mass production environment.

8.2 Results Summary

Table 8-1 summarises the key numerical results crush test cases carried out in this work. SEA and peak load figures presented are averages of each dataset.

Table 8-1: Summary of Key Test Results

	Static		Dynamic	
	SEA	Peak Load	SEA	Peak Load
Type	*kJ/kg*	*kN*	*kJ/kg*	*kN*
Single Tuft Trials (Chapter 4)				
Baseline (Untufted)	61.45	3.98	65.91	4.87
Resin Column Only	60.68	4.57	67.52	5.56
Partial Tuft	66.42	4.51	70.59	5.07
Single Tuft (Average of all loop lengths)	68.49	4.37	74.86	5.23

	Static		Dynamic	
	SEA	Peak Load	SEA	Peak Load
Type	*kJ/kg*	*kN*	*kJ/kg*	*kN*
Double Tuft	72.20	4.95	81.88	5.42
Triple Tuft	73.90	5.11	81.46	5.32
Rectangular Crushing Trials (Chapter 5)				
A – Tufted 6 mm spacing (40 mm length)	48.46	25.04	-	-
B – Tufted 6 mm spacing (50 mm length)	42.69	32.02	-	-
C – Tufted 6 mm spacing (60 mm length)	37.69	34.60	-	-
Triangular Coupon Trials (Chapter 7)				
Baseline $[45/0/-45]_s$/Rohacell 110 IG-F	48.20	-	39.58	-
Baseline – Tufted 6 mm spacing	49.86	-	45.36	-
Reprocessed Reclaimed $[0_{RE}/0_{RE}/0_{RE}]$	27.90	-	12.41	-
Reprocessed – Tufted 6 mm spacing	34.05	-	37.87	-
Hybrid $[0_{RE}/0/0_{RE}]$	38.96	-	28.83	-
Hybrid – Tufted 6 mm spacing	39.27	-	37.49	-
Off-cut Reclaimed $[45_{ST}/0_{ST}/-45_{ST}]_s$	39.42	-	36.79	-
Off-cut – Tufted 6 mm spacing	47.91	-	46.43	-

To evaluate the overall set of results, the immediate comparisons that can be made are to the works by Blok et al. [45] (same test materials) and Marasco [84] (comparable coupon design). Results from these sources indicate SEA values in the range of 20 kJ/kg for an unreinforced case, up to 64 kJ/kg for a pin reinforced core. These figures are like those obtained from the presented works here, perhaps with some inflation of SEA in this work due to the smaller, more stable coupon sizes under consideration.

When comparing to other works on the SEA of sandwich structures, very high variation in results can be observed with values of SEA well below those reported above. This is because the SEA metric depends on many interacting failure mechanisms which are influenced by multiple factors such as material types, trigger mechanism, loading rate, and presence of TTR to name a few.

As would be expected, the influence of tufting led to an improvement of SEA over the baseline in each case, with a general increase in peak load as well. Also, as expected is the change in measured SEA as a result of changing loading rate. However, the trend varied

between test types, with the single tuft test coupons showing an increase in SEA with higher rate testing, while the triangular coupons considered in Chapter 7 showed the opposite.

From a design perspective, what these numbers highlight is that obtain a high SEA, the sandwich structure must feature aligned continuous fibre facesheets, a high-density tufting thread, and a suitable crush trigger mechanism. With these features in place then SEAs at the upper end of the work presented here could be obtained. However, it is believed that further work to optimise the tuft architecture and material selection could improve these numbers even further, as outlined in the following sections.

8.3 Optimising Tuft Design

One of the main objectives of this work is to improve the performance of tufted sandwich structures under edgewise loading. Ultimately to improve performance it is necessary to improve the energy absorption of the structure or reduce the structural weight required to achieve this to maximise the SEA. With an understanding of how these structures behave and the role the tufts play within this, it is possible to circle back to the design process and consider how tufted structures would be designed differently to optimise this relationship.

From the work carried out on single tuft test coupons in Chapter 4, it was apparent the results of varying loop lengths and partially formed tufts that the tuft loops do not contribute to the energy absorption performance of the structure in this load case. Instead these surface features lead to the creation of a thin resin film on the panel surface and will therefore result in an increase in both weight and thickness of the panel. Furthermore, the work presented in Chapter 5 and Chapter 6 suggests that the presence of excess resin in the form of the surrounding resin columns within the core does little to stabilise the structure or increase energy absorption when considering this load case.

Measurements from this work, as shown in Table 7-1, show an average increase in mass of 30% when comparing untufted and tufted components for the 6 mm tuft spacing used. Whilst this tufting density used is at the upper end of what is practically achievable, this number is significant as it begins to diminish the improvements in SEA. This is demonstrated in Figure 7-12 where several of the datasets show very close results for SEA for both untufted and tufted configurations. One route to improving this efficiency is to use a more optimised tufting pattern, i.e. using a lower density pattern with larger gaps between each tuft, or by strategically positioning tufts in critical locations. The other option is to reduce the weight penalty of the tuft itself. The addition of the tufting threads contributes

only a very small percentage to the weight increase (~2%) of the component which means the significant factor is the ingress of resin during infusion.

To reduce this weight penalty a method is required to seal the tuft during infusion or reduce the size of the void formed, as well as to reduce the surface profile of the tuft to stop the resin rich surface layer forming. With these considerations in mind, an ideal tuft design based upon these criteria would therefore appear closer to a rigid z-pin, existing as a discrete pin within the preform whilst not protruding outside of the surface of the facesheet. A simplified example of how this might look is shown in Figure 8-1.

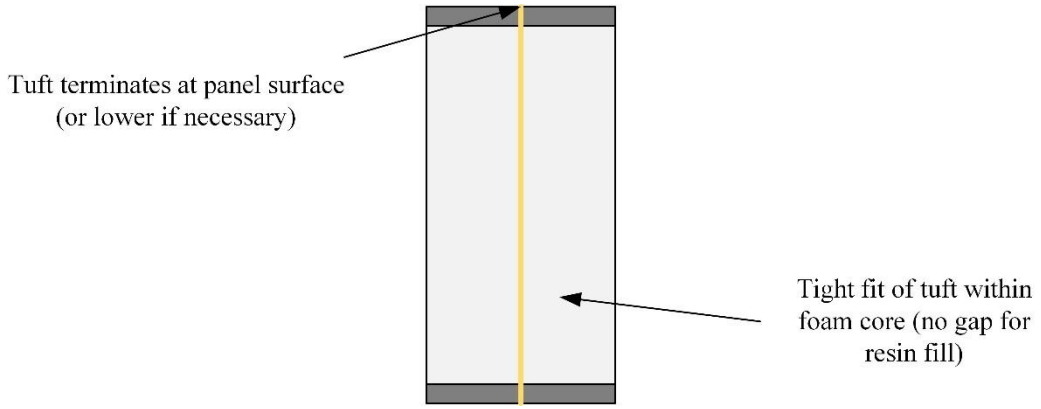

Figure 8-1: Simplfied idealised tuft geometry to reduce structural weight.

To be able to achieve a flush surface finish, tufts could either be inserted with the depth set to minimise penetration through the back surface of the preform, or by removing the surface loops after insertion. Adjusting the depth would be more appropriate in a production environment, as it doesn't require an additional step, whilst the results presented in Chapter 4 suggest that there is no significant performance knock-down from a partially inserted tuft. Removing the surface loops after tufting would not only increase processing time but also risk damaging the delicate preform, particularly risking pulling out the tufts. This was tested by Dell'Anno et al. [92], who noted that mechanically removing the loops after tufting was possible and could be achieved without disturbing the tuft itself. However, the method was deemed to be practically infeasible due to the processing time required.

To remove the excess resin surrounding the tuft it is necessary to minimise the size of the channel created by the needle as much as possible. Ensuring a tight fit between the core and tufting thread will minimise resin ingress, allowing only some resin flow along the length of the tuft via a capillary effect that would enable the tuft itself to be wet-out. Alternatively, if the surrounding column could be sealed prior to infusion then this would

also limit the amount of resin entering the column. However, what is currently not clear is the resulting mechanical performance of the component if this excess resin is removed. For the latter method of sealing the column but leaving the void in place, the flexural stiffness of the panel would most likely be reduced. The collapse mechanism in-plane may also change during crushing, due to the presence of voids within the foam that could lead to sudden drops in load as the foam core was crushed.

As part of this work, trials were carried out to test the theory of eliminating resin columns. This was carried out by blocking the flow of resin into the voids within the core using an adhesive film layer (3M adhesive film AF163-2) at the interface between facesheet and core. Lab scale trials revealed the adhesive layer would successfully "heal" over the top and bottom of the void after heating (Figure 8-2), however efforts to replicate this using the actual tufting process were not successful (Figure 8-3).

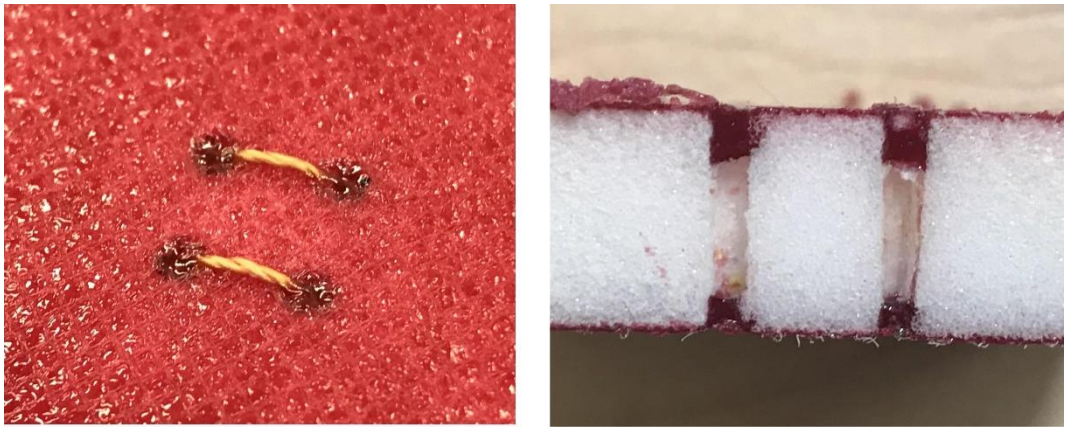

Figure 8-2: Example of lab-scale trials to 'heal' needle channel. Left, adhesive film sealing off tuft threads. Right, channel closed-off at top and bottom.

It was revealed that the tuft insertion mechanism did too much damage to the resin film, which was not allowed to flow for long enough to heal over the void. It would be useful to carry out further trials in this area, to at least gather information on the performance of panels with these resin columns removed.

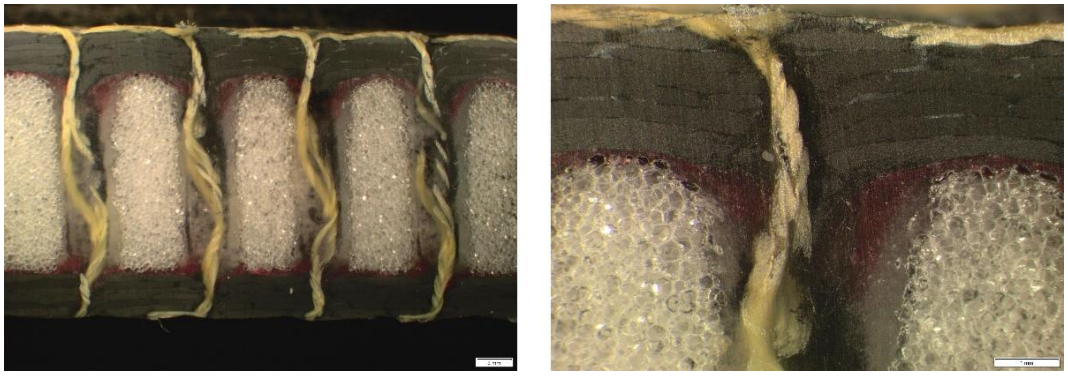

Figure 8-3: Microscope image demonstrating unsuccessful attempt to seal the core with adhesive film (red layer) after tuft insertion.

A consideration that should be made around exploiting this methodology is the effect it may have on the manufactured quality of the panel. The use of an additional adhesive layer between facesheet and core, either globally across the panel or locally at individual tufts, could interfere with the resin flow front during infusion. This has the potential to lead to trapped air pockets within the material and thus a higher degree of porosity within the cured laminates. The works carried out in Chapter 5 indicate that whilst tufted sandwich structures typically follow a repeatable failure pattern, local weaknesses at the tufts could in some cases lead to unexpected unstable failure mechanisms. It is therefore necessary to improve process control to minimise porosity within the structure or look to minimise the amount of excess resin altogether, offering the advantage of a reduction in parasitic weight.

A potential further option to improving tuft efficiency would be to completely remove most of the central portion of the tuft from within the core, leaving only a short segment across each facesheet-core interface, as illustrated in Figure 8-4.

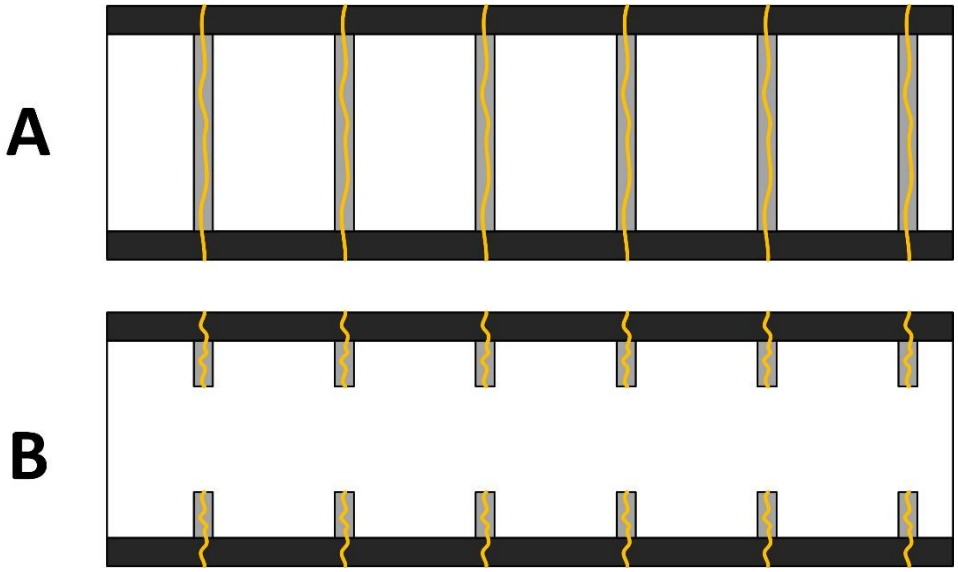

Figure 8-4: A proposed double-sided tufting method to reduce excess weight due to resin ingress. A) Traditional tufting method, B) Shortened tufts with insertion from both sides of the preform.

This could be achieved by inserting very short tufts across both interfaces; however, the downside of this method is that it would then require access to both sides of the preform. Not only would this double the processing time to tuft the preform but would also demand removing the preform from the mould to allow access to the other side, which goes against one of the advantages of the tufting process. For this method to be worthwhile, a relatively large core thickness would have to be used, otherwise the penetration depth of the needle from both sides would be deep enough to intersect and ultimately fill the core anyway.

8.4 Materials Selection

One area that has not been covered in much detail in this work in favour of focusing more specifically to the overall structural behaviour is the material selection of the components. Previous work has demonstrated some variations between core type as well as facesheet layup and thickness [45]. Ultimately the conclusions of this work suggested that these variables considered were more influential to the stability of an untufted panel rather than a tufted one. By increasing the stability of an untufted panel, through increasing panel stiffness and thus buckling stability of the components, as well as increasing the strain to failure of the foam core to improve the integrity of the facesheet-core interface, it was shown that the improvement in energy absorption by tufting was less pronounced. Furthermore, through the work carried out in Chapter 7, it was shown that after tufting, facesheet configurations, either continuous fibre laminates or reclaimed mat, had similar performances (Figure 7-12). This indicates that there is an optimum balance to be found

between the design of the laminate and the improvement in energy absorption performance that tufting provides.

What is of more interest for these components from a material selection viewpoint, is any manufacturing implications that may arise, particularly during the tufting process. For example, certain facesheet layups or materials, if too thick or dense, may be very difficult for the tufting needle to penetrate. Likewise, the tufting thread must be able to pass through the preform with a low enough friction level and without breaking, to successfully form the tuft. This significantly limits the number of available material choices for the tufting thread. The core must also be soft enough to allow needle penetration without damaging the needle, especially if a large panel is being tufted. In relation to section 8.2, one area of interest would be to investigate a more elastic foam core that may heal itself slightly after tuft insertion, closing the gap around the tuft thread and limiting the entry of resin into the core.

8.5 Specific Energy Absorption

A major question raised, particularly during work with reclaimed fibre materials, is one of the applicability of SEA as a metric for assessing the performance of composite sandwich structures. In Chapter 7, issues were discovered when trying to compare the SEA for a normalised test coupon, i.e. a fixed measurement length across the dataset to directly compare multiple coupons, to an absolute value using the entire crush distance of the coupon. It was found during this work that due to significant changes in the failure mechanism, both between different coupons and within the same coupon during a test, these two methods would result in very different magnitudes of SEA. One of the reasons for this was the significant loss in mass that was observed when failure involved complete separation of the facesheet. Because this is not directly considered when calculating SEA then the performance can tend to be underestimated. Whilst this was noticed in a few special cases when using relatively weak reclaimed material, there will always be some loss of mass when working with composite materials due to fragmentation failure. The current SEA metric does not account for these losses, nor does it account for the individual elements of the system, such as the foam core, the resin, the fibre reinforcement or the individual tufts. Even with a simple measurement of weight of the coupon before and after the experiment, it would not be immediately clear where and when the loss of mass has occurred. Ultimately the only way of tracking this may be by capturing the failure numerically, if the right level of modelling fidelity and accuracy could be achieved.

8.6 Technology Readiness

Automotive components need to be produced rapidly through a high degree of automation and very short cycle times. Whilst the test panels considered in this work are relatively simple and thus straightforward to automate, and the tufting process itself is already driven by commercially available robotic control, where the limiting factor in using these components would exist is that the steps taken so far do not lend themselves to very high production rates. The tuft insertion process on an entire floor panel using the rates considered in this work would take a time in the order of a few hours.

One way to improve tufting productivity would be to introduce multiple needle arrays to insert tufts over a larger area in a short time. A sandwich stitching method proposed by Potluri et al. [93] shows a similar design feature that could be exploited with tufting Figure 8-5, where a line of needles is used to insert a row stitches in one go, rather than inserting individually.

Figure 8-5: Needle array for stitching sandwich preforms as proposed by Potluri et al. [93]**. This system indicates a potential way of reducing process time for tufting of large sandwich structures.**

Another way to improve process rates could be to use increased insertion rates, to insert the tufts in a shorter space of time. To explore this, the test rig outlined in section 3.2.1.3 was used, with insertion rates varied from 100 mm/min to 1,000 mm/min [137]. To compare the differences between samples, an empirical ‘quality matrix’ was created to assess the observable damage and features within the needle path after insertion. It should be noted that the assessed ‘defects’ were selected based upon empirical evidence from preliminary trials and were not based upon a Design of Experiments (DoE) methodology. An example of the typical load trace observed is shown in Figure 8-6, with examples of

some of the features observed and related scoring system shown in Figure 8-7 and Table 8-2 respectively.

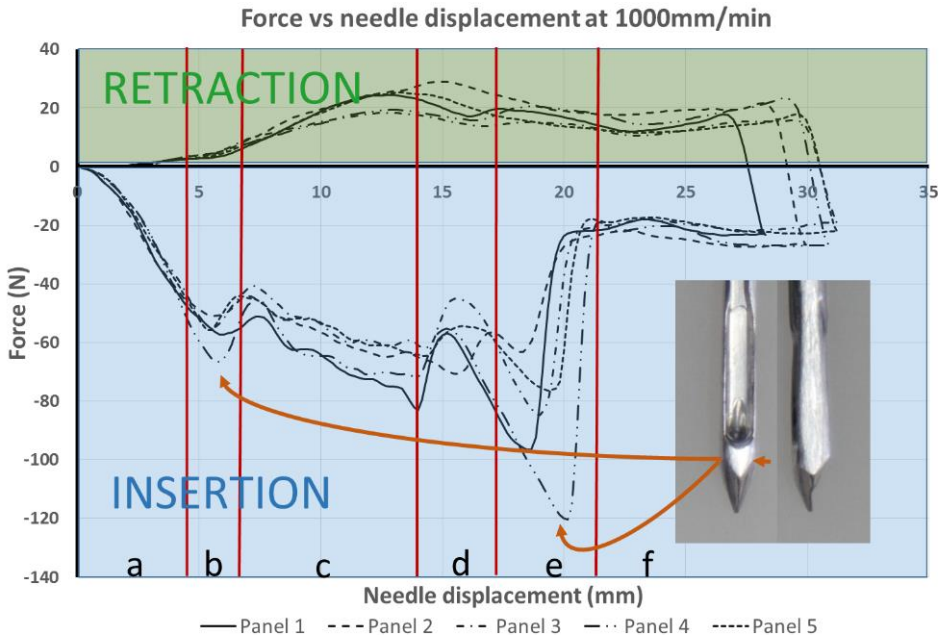

Figure 8-6: Load-displacement behaviour of a tuft insertion at 1,000 mm/min.

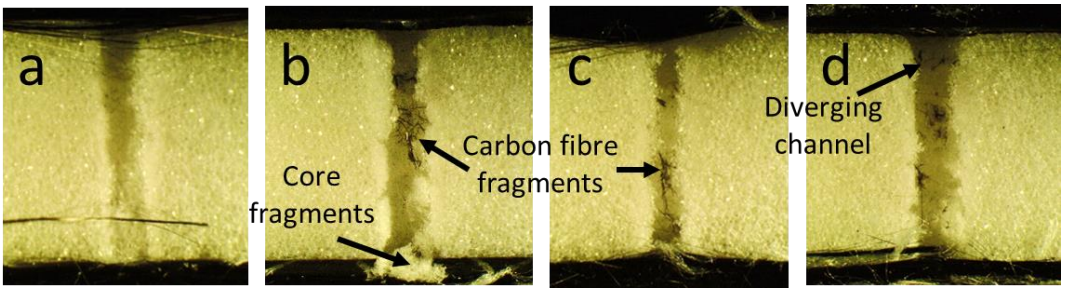

Figure 8-7: Needle insertion features; A: near ideal insertion, B: carbon fibre and core fragments, C: carbon fibre fragments, D: divergence of the needle channel.

Table 8-2: Needle Insertion Scoring Matrix

Fibre Fragments	Opening Diameter	Core Fragments	Rating
%	*mm*	*%*	-
Total Blockage	>3.8	Total Blockage	0
<90	<3.8	<90	0.1
<80	<3.6	<80	0.2
<70	<3.4	<70	0.3
<60	<3.2	<60	0.4
<50	<3.0	<50	0.5
<40	<2.8	<40	0.6
<30	<2.6	<30	0.7
<20	<2.4	<20	0.8
<10	<2.2	<10	0.9
0	2.0	0	1

By plotting the assessed 'quality' of the needle insertion against the insertion rate, as shown in Figure 8-8, there is an apparent trend in increasing quality at higher rates by creating a cleaner needle channel, which is ideal for reducing process times. However, the empirical nature of these results means that further work needs to be done in this area to understand the effect that increasing the rate may have on the structural integrity of the preform as well as understanding how the results of this lab-scale demonstrator scale up to larger components.

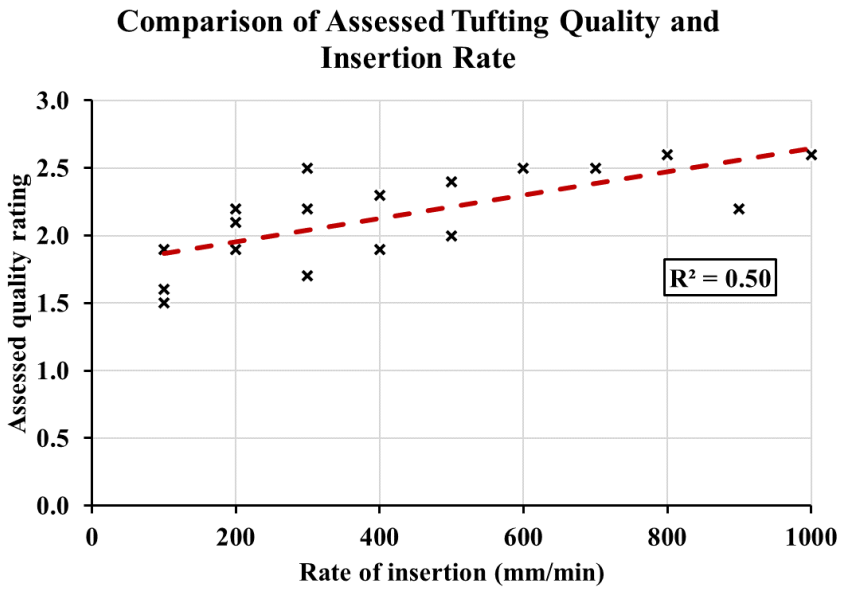

Figure 8-8: Plot of assessed 'quality' of insertion against insertion rate.

Another consideration to be made is that the VARTM method considered in this work is not a valid production method for automotive components due to the high amount of manual labour plus the slow processing time associated with it. To meet the high production rates required, these components would have to be injected under very high resin pressures within rigid tooling. Whilst monolithic components can survive this harsh environment, it is not clear what effect this would have on the preform. For example, the foam core has a limited compression strength making it susceptible to crushing in the mould, whilst the tufts are not tightly anchored within the preform and may be prone to being displaced by the high-pressure resin flow. This would be in a manner akin to fibre washout seen in high pressure injection processes. In other automotive sandwich panel examples, such as those manufactured by Bright Lite structures [29] (see Chapter 1) this challenge has been overcome with the use of polycarbonate honeycomb type cores, which are flexible enough to be formed in a press prior to injection, and then the cells fill with resin during injection to provide additional rigidity. Ultimately not enough is known yet about how these components would behave in a rapid production environment and so more work needs to be done on the manufacturing of these components to help understand this.

Chapter 9 Conclusions

A summary of the major conclusions from this work is presented here. Conclusions are broken down by work packages, with an overall summary presented at the end.

9.1 Manufacturing Process

A basic introduction of the tufting manufacturing process for sandwich preforms was carried out through the development and use of a bespoke tufting tool. The tool allowed for observations of the effect of needle insertion and the subsequent tuft formation, with attempts made to look at the effect of increasing insertion rate to reduce processing time. Indications from testing are that increased rate does lead to a 'higher quality' tuft but results at this stage are empirical and need further work to prove this.

Further observations were made through the full-scale manufacture of various test panels, as well as microscopy of cross-sections of the manufactured parts. Within this, the major observation was the presence of resin columns within the foam core due to the needle insertion. These were later shown to become active during the crushing of a tufted component.

9.2 Single Tuft Testing and Component Design Variables

Development of a new test method for characterising the crushing behaviour and performance of single tufts under edgewise compression has been carried out, with the aim of understanding the effect of tuft variables. To achieve this, a novel coupon design was created, based upon previous sandwich crushing test coupons and the ASTM standard for edgewise compression of sandwich structures, to enable failure at the desired location around the tuft. The initial focus was on validating the test method by carrying out trial testing on various coupons. Results of the testing showed good correlation between the failure mechanisms in the coupons, including splaying of the facesheets and crushing of the foam core, as well as the load trace recorded by the test machine. These mechanisms were observed under both static and dynamic loading conditions and showed a close match to the expected sandwich crushing mechanisms observed in previous works.

During testing both tufted and untufted coupons, there was a noticeable shift in the load trace, with the tufted coupons displaying an increase in load as the tuft interacted with the

crush platen. This demonstrated the method's capability of capturing the restraining effect of the tuft on the crushing failure mechanism.

The tufted coupons outperformed the baseline sandwich coupons due to increased energy absorption under both static and dynamic load conditions. They also outperformed coupons tested with the tufting yarn removed, suggesting at this point, no significant benefit of the resin column to energy absorption over a short crushing length. Varying the loop length by adjusting the insertion depth of the tuft indicated no clear correlation with energy absorption performance, however, increasing the local tuft density by inserting additional tufting yarns showed a significant jump in performance. Overall, the dynamic coupons showed higher energy absorption despite a very close match in failure behaviour.

Whilst not visible during testing, the results observed provided an indication of the type of failure that the tufts would experience under this load case. The jump in performance because of an increase in thread density implied that shear failure at the interface of the resin column and the core was taking place, as opposed to a Mode I pull-out type failure. This assumption was later validated by dissolving the foam core and observing the failed tuft. In general, dynamic loading conditions exhibited higher forces and thus energy absorption of the coupons, however there were no clear differences in the failure mechanism between the two load cases.

9.3 Failure Mechanisms and Resin Column Behaviour

Following the hypothesis of the way the tufts fail within the structure there was a clear need to capture these failure mechanisms for a better understanding of the process. A quasi-static crush test was chosen, with the decision to expose a seam of tufts along one edge of the coupon to allow visual identification and tracking of the failure mechanisms as they took place.

In general, the test was able to successfully capture the overall global failure behaviour of tufted sandwich structures. It also enabled identification of the numerous localised failure mechanisms that took place within the various components of the sandwich, including the facesheets, core and the tufts themselves. This set of testing was able to support the hypothesis of a shear mechanism being the primary failure mode of the tufts at the skin-core interface. In addition to this, it was also observed that after failure the tufts can migrate through the core in a drifting mechanism. As this happens, the surrounding core material is crushed until the point the tufts collide with each other and then begin to stack together.

This mechanism was shown to be consistently linked to the tuft pattern, indicating a degree of controllability through tufting pattern design.

Further failure mechanisms observed included fracturing of the facesheets linked to flaws surrounding tuft insertion points and rupturing of the resin columns surrounding the tufts due to bending. The first of these points suggests that tufts should be inserted selectively to ensure flaws cannot coalesce and lead to an unstable fracture mechanism. The latter indicates that tufts undergo different loading conditions depending on where they lie within the component, and thus could be tailored to respond to this. Tuft pull-out was also observed in a couple of tests. It was not clear under what conditions this mechanism took place, as it rarely occurred, but this is an indication that it is possible.

9.4 Effect of Column Drift

Whilst observations have been made of the behaviour of the resin columns in these structures, the contribution to energy absorption has yet to be quantified, whilst it was noted that they contribute a significant amount of additional weight to the structure also. It was therefore necessary to test the effectiveness of this mechanism to determine if any added benefit can outweigh the gain in mass. A novel test fixture was designed and created to enable the testing of movement of rigid objects through the foam core, to simulate the migration of the tufts. An acrylic test frame was created that could fit blocks of foam within it, whilst also allowing rigid pins to be inserted through the foam and mounted on to the test frame. Results of the testing revealed that a relatively small load was produced by the relative motion of the rigid pin and the foam block. This load increased linearly with the number of independent pins that were loaded, whilst it was also demonstrated that there was a notable increase when pins were able to collide and move together.

By investigating the energy absorbed by this mechanism it was noted that the direct contribution was small (an order of magnitude lower) when compared to the overall energy absorption of a tufted sandwich section. This therefore implies that the added benefit of this mechanism may be negatively outweighed by the significant increase in mass that excess resin will add to the structure. As such it may necessary to find a method to reduce or remove this excess resin, to enable the production of a more efficient structure. However further work is required to explore the contributions of other mechanisms within the global failure of a component, to understand if this is truly not significant.

9.5 Reclaimed Materials Case Study

To demonstrate the application of tufting within a sandwich panel, a case study was carried out exploring its use in conjunction with reclaimed materials. Due to the significant reduction in mechanical properties of a fully reprocessed reclaimed material, test coupons would fail catastrophically through facesheet buckling before a stable crushing mechanism could initiate. This resulted in a very poor specific energy absorption when compared to a more conventional virgin continuous fibre laminate. Through the addition of tufting, the facesheet-core interface was maintained in the reclaimed test coupons, and stable progressive crushing failure was able to occur. The resulting increase in specific energy absorption showed results comparable with virgin continuous test coupons that were also tufted, demonstrating a potential solution for the use of reclaimed materials and reducing process waste.

A significant observation made during this work was that SEA as a metric was difficult to apply to components that undergo significant fragmentation and mass loss during failure. This was noted due to a large discrepancy in the results for a normalised crush length test case against using the full data recorded for the component. It was noted that choosing one method over the other meant that the full detail observed during a test was not captured effectively to allow comparison between coupons.

9.6 Overall Conclusions

The aim of this work was to develop a deeper understanding in the field of tufted sandwich structures, to help influence and improve the future design of these components. This has been achieved through a series of novel experimental tests, aimed at looking at different aspects of these structures in close detail. The work carried out here further supports the use of tufting as a promising solution to reinforcing sandwich structures under dynamic in-plane loading, with the relevant mechanisms captured and analysed in detail.

Future work should look to build on this by developing analytical or numerical techniques to model these mechanisms thus enabling the selective positioning of tufts where they would be most effective, for increased manufacturing rates and higher structural efficiency.

Chapter 10 Future Work

Over the course of this and previous works, tufting has been demonstrated to be an effective technology for reinforcing sandwich structures through-thickness and thus improving the energy absorbing performance when loaded in edgewise compression. The crushing behaviour of these structures is better understood, as well as the role various design variables play within this. However, for this technology to be seriously considered in a commercial automotive production environment there are still several steps that must be overcome.

10.1 Manufacture

Whilst only touched upon briefly within this work, development of the manufacturing process for tufting is required for the technology to mature to a point that it could aid mass-produced components. Processing times for small lab scale demonstrator panels (0.3 m^2) can run to as much as several hours to complete using similar spacings as defined in this work. This greatly exceeds the target cycle times of only a few minutes that are expected in the automotive industry. A more selective placement of tufts could reduce processing time, but ultimately insertion rates must be reduced drastically, or multiple insertions would need to be made at once to meet expected production rates.

Following on from this, a more in-depth investigation into the link between manufacturing parameters and in-service mechanical performance is required. It was shown in section 8.6 that the needle insertion process can create defects within the structure, however what is not currently clear is the significance of these and whether they can affect the strength or stiffness. A significant amount of work still needs to be done to capture more cases of needle insertion and tuft formation in a manner akin to that presented in this work. A further step to be taken would be to directly compare preforms before and after infusion to capture the influence on typical laminate properties such as local volume fraction and porosity. A particularly interesting experiment would be to use a similar tufting rig that allows resin to be locally inserted into the preform simulating a larger infusion. With this, infusion process defects could be captured in-situ and direct links between mechanical performance and manufacturing parameters could begin to be drawn.

This would have to take on a renewed interest if insertion rates are increased, as the potential for a harsher process could lead to an increase in the observed defects within the

preform. Whilst the results presented suggested that an increased rate was beneficial to insertion quality, further work needs to be done to prove this, particularly looking in to what happens when the tuft itself is inserted, as well as what could happen if this is scaled up to a much larger component. With cost and production rates the key driver behind the automotive industry, this is likely to be the main challenge to overcome to allow this technology to succeed.

10.2 Performance

In addition to increasing manufacturing rates, there is still a need for a greater understanding of mechanical performance through additional load cases as well as additional design variables. Firstly, a consideration of varying test scales to greater levels than considered in this work is a must to understand the change in behaviour and performance and to give a closer link to an in-service component. Also testing at high loading rates could be improved by using higher capability equipment capable of greater loading speeds and higher impact loads. Further to this, transverse bending and shear loads are also important considerations for less harsh, everyday design cases. Whilst some work in this area has been considered elsewhere [127], fatigue is one load case that has not been investigated, and would play an important role in an automotive structural design.

However, more closely tied to this current work is the need to explore additional design variables to obtain a more optimal performance. These include the use of alternative materials and ply configurations. For example, previous work [45] has demonstrated the varying performance within different facesheet layups, as well as a change in performance with cores with varying strains to failure (ductile vs. brittle). Additionally, different resin systems and tuft materials could also play a role in performance. Further to this, the configurations of the tufts can also be modified in many ways. For example, changing the insertion angle of the tufts to line up closer to the loading direction could be an effective way of resisting the shear loads on the sandwich structure, whilst selectively placing the tufts within the structure could lead to a reduction in resin usage and weight, as well as potentially leading to faster processing times.

Relevant to both points above is the need to further characterise the reprocessed non-woven material explored in Chapter 7. Promising results were obtained for tufted coupons, but from this work it was apparent that failure of the reclaimed material test coupons is dominated by the material's poor mechanical properties. Some work has been done to investigate this area of research, but more is required to further characterise these materials

and understand how they behave, particularly for more relevant applications and load cases as outlined in this work. Furthermore, statistical variation in these properties needs to be understood, as there is a high chance of variability due to fabric construction, in addition to the varying history of the material before it is reprocessed into its current form. As interest and research output in this area has continued to grow, an increasing number of new reclaimed fabrics have become available with different processing characteristics. These too should also be explored to understand how they might behave under these load cases.

10.3 Modelling and Design Optimisation

Because of the complex failure mechanisms, the large number of process variables, and the significant costs associated with dynamic testing of composite structures, it is very difficult to see a clear route to optimum design without the use of numerical modelling tools to simulate the behaviour and performance of these types of structures. The observations made in several chapters indicate that improvements could be made by optimising the tuft insertion pattern, and a robust modelling technique would go a long way to identifying those strategies that could improve performance.

Whilst there have been a number of publications on the numerical analysis of composites in crash, using commercial finite element software packages [158–160], sandwich structures have been shown to be more difficult to model as the complexity is compounded by the interaction between skin and core. As a result, research in this area is still very limited.

One of the earliest papers published on the modelling of sandwich structures in crash situations was the work done by Kerth [161]. The author constructed a model using LS-DYNA consisting of a combination of shell and solid elements with homogeneous laminate properties. The shell elements were used for the skins whilst 3D elements were used to represent the core. Since then, Velecela and Soutis [146], and Mamalis et al. [162–164] have followed similar approaches to modelling the crush of sandwich structures. Advancements in the modelling technique included using the enhanced composite damage failure model for the FRP material, based on the Chang and Chang composite damage model [165]. This model accounts for degradation of the individual plies within the laminate before ultimate failure of the laminate when each ply has failed. Whilst the results of these studies were deemed satisfactory, there was some significant variation in the load-displacement diagram because of the simplifications required to reduce processing times.

More recently, Osmiani et al. [144] have demonstrated detailed finite-element modelling of tufts within a composite laminate to capture the delamination resistance.

By using a combination of the tufting modelling strategy, as well as improvements to existing to existing sandwich models could lead to an effective modelling strategy for tufted sandwich structures in the future.

Chapter 11 References

[1] Reducing CO2 emissions from passenger cars [Internet]. European Commision. [cited 2018 Jul 22]. Available from: https://ec.europa.eu/clima/policies/transport/vehicles/cars_en

[2] Wilson A. Vehicle weight is the key driver for automotive composites. Reinforced Plastics. 2017 Mar;61(2):100–2.

[3] China looks at plans to ban petrol and diesel cars [Internet]. BBC News. 2017 [cited 2017 Nov 17]. Available from: http://www.bbc.co.uk/news/business-41218243

[4] New diesel and petrol vehicles to be banned from 2040 in UK [Internet]. BBC News. 2017 [cited 2017 Nov 17]. Available from: http://www.bbc.co.uk/news/uk-40723581

[5] International Energy Agency (IEA). Global EV Outlook 2017. OECD; 2017.

[6] Volkswagen plans electric option for all models by 2030 [Internet]. BBC News. 2017 [cited 2017 Nov 17]. Available from: http://www.bbc.co.uk/news/business-41231766

[7] Materials for lithium-ion batteries could double range of electric vehicles The Engineer [Internet]. The Engineer. 2018 [cited 2018 May 20]. Available from: https://www.theengineer.co.uk/lithium-ion-batteries-electric-vehicles/

[8] Harman A. U.K. Seeds EV Battery R&D With £120 Million [Internet]. Wards Auto. 2017 [cited 2017 Dec 20]. Available from: http://wardsauto.com/engines/uk-seeds-ev-battery-rd-120-million

[9] Vaughan A. Energy storage leap could slash electric car charging times | Environment | The Guardian [Internet]. The Guardian. 2018 [cited 2018 May 20]. Available from: https://www.theguardian.com/environment/2018/feb/26/energy-storage-supercapacitors-electric-car-batteries-charging-times

[10] Leggett T. Why switching to fully electric cars will take time [Internet]. BBC News. 2017 [cited 2017 Nov 17]. Available from: http://www.bbc.co.uk/news/business-41268513

[11] Chady T. Airbus versus Boeing - Composite Materials: The sky's the limit [Internet]. Le Mauricien. 2013 [cited 2017 Jun 5]. Available from: http://www.lemauricien.com/article/airbus-versus-boeing-composite-materials-sky-s-limit

[12] Baraniuk C. Reaping the wind with the biggest turbines ever made [Internet]. BBC News. 2018 [cited 2018 Apr 18]. Available from: https://www.bbc.co.uk/news/business-43576226

[13] Sun HY, Li Liu Y, Li Zhou W. Carbon Fiber Reinforced Polymers (CFRP) Technique and Its Application in Bridge Engineering in The Future. In: International Conference on Education, Management, Commerce and Society. 2015.

[14] Olofin I, Liu R. The Application of Carbon Fibre Reinforced Polymer (CFRP) Cables in Civil Engineering Structures. International Journal of Civil Engineering. 2015;2(7):1–5.

[15] Beck M. Composites are taking off as a key material for outer space applications [Internet]. Composites Manufacturing. 2014 [cited 2017 Sep 25]. Available from: http://compositesmanufacturingmagazine.com/2014/10/composites-key-outer-space-applications-material/

[16] Polek G. Airbus Starts Fabricating First Fuselage Barrel for the A350 XWB [Internet]. AIN Online. 2010 [cited 2017 Dec 7]. Available from: https://www.ainonline.com/aviation-news/2010-12-07/airbus-starts-fabricating-first-fuselage-barrel-a350-xwb

[17] Airbus delivers first A350 XWB for Delta Air Lines [Internet]. Airbus. 2017 [cited 2017 Dec 7]. Available from: https://www.airbus.com/newsroom/press-releases/en/2017/07/airbus-delivers-first-a350-xwb-for-delta-air-lines.html

[18] Savage G. Formula 1 Composites Engineering. Engineering Failure Analysis. 2010 Jan;17(1):92–115.

[19] Woodard C. Watch the Backstory on How McLaren Built the World's First Carbon-Fiber F1 Car [Internet]. Road and Track. 2016 [cited 2017 Nov 24]. Available from: https://www.roadandtrack.com/motorsports/videos/a29037/how-mclaren-built-the-mp4-1/

[20] Stoffel Vandoorne, McLaren, Circuit de Catalunya, 2017 [Internet]. Race Fans. 2017 [cited 2017 Nov 24]. Available from: https://www.racefans.net/2017/03/05/pictures-bonus-gallery-first-f1-test-2017/mclaren-17/

[21] McLaren Technology Group. Case study: Carbon Fibre [Internet]. 2016 [cited 2016 Oct 26]. Available from: http://www.mclaren.com/technologygroup/case-studies/case-study-carbon-fibre/

[22] Jacob A. Lamborghini: 30 years of carbon fibre [Internet]. Materials Today. 2013 [cited 2016 Oct 26]. Available from: www.materialstoday.com/composite-applications/features/lamborghini-30-years-of-carbon-fibre/

[23] Feraboli P, Gasco F, Wade B, Maier S, Kwan R, Masini A, et al. Lamborghini "Forged Composite" Technology For The Suspension Arms Of The Sesto Elemento. In: 26th Technical Conference of the American Society of Composites. Montreal, Canada; 2011. p. 1012–24.

[24] Red C. Automotive CFRP: The shape of things to come [Internet]. Composites World. 2013 [cited 2014 Jun 10]. Available from: http://www.compositesworld.com

[25] Sloan J. BMW Leipzig: The epicenter of i3 production. Composites World. 2014;20(3):24–31.

[26] Sloan J. The making of the BMW i3 [Internet]. Composites World. 2014 [cited 2017 Dec 7]. Available from: https://www.compositesworld.com/blog/post/the-making-of-the-bmw-i3

[27] Gardiner G. Is the BMW 7 Series the future of autocomposites? [Internet]. Composites World. 2016 [cited 2017 May 31]. Available from: http://www.compositesworld.com/articles/is-the-bmw-7-series-the-future-of-

autocomposites

[28] Gordon Murray Design. iSTREAM - Gordon Murray Design [Internet]. 2017 [cited 2017 Nov 13]. Available from: http://www.gordonmurraydesign.com/en/istream.html

[29] Bright Lite Structures [Internet]. 2017 [cited 2017 Nov 13]. Available from: http://www.blstructures.com/

[30] Wheatley A, Warren D, Das S. Development of Low-Cost Carbon Fibre for Automotive Applications. In: Elmarakbi A, editor. Advanced Composite Materials for Automotive Applications: Structural Integrity and Crashworthiness. First Edit. John Wiley & Sons Ltd; 2014. p. 51–73.

[31] Elmarakbi A. Advanced Composite Materials for Automotive Applications: Structural Integrity and Crashworthiness. Elmarakbi A, editor. Advanced Composite Materials for Automotive Applications: Structural Integrity and Crashworthiness. Chichester, UK: John Wiley & Sons Ltd; 2013. 99–127 p.

[32] Mazumdar S, Karthikeyan D, Pichler D, Benevento M, Frassine R. State of the Composites Industry 2017. Composites Manufacturing. 2017.

[33] Gardiner G. Recycled carbon fiber update: Closing the CFRP lifecycle loop. Composites World. 2014;20(6):28–33.

[34] Snudden JP, Ward C, Potter KD. Reusing automotive composites production waste. Reinforced Plastics. 2014 Nov;58(6):20–7.

[35] Composites UK. End of Life Options for Composite Materials [Internet]. 2017 [cited 2017 Nov 13]. Available from: https://compositesuk.co.uk/composite-materials/properties/end-life-options

[36] Pimenta S, Pinho ST. Recycling carbon fibre reinforced polymers for structural applications: Technology review and market outlook. Waste Management. 2011 Feb;31(2):378–92.

[37] Reynolds N, Ramamohan AB. High-Volume Thermoplastic Composite

Technology for Automotive Structures. In: Elmarakbi A, editor. Advanced Composite Materials for Automotive Applications: Structural Integrity and Crashworthiness. First Edit. John Wiley & Sons Ltd; 2014. p. 29–50.

[38] Bernasconi A, Davoli P, Armanni C. Fatigue strength of a clutch pedal made of reprocessed short glass fibre reinforced polyamide. International Journal of Fatigue. 2010 Jan;32(1):100–7.

[39] Snudden JP. A Novel Approach to Reforming In-Process Scrap Carbon Fibre for High Value Applications: A Techno-Economic Study. University of Bristol; 2017.

[40] Carruthers JJ, Kettle AP, Robinson AM. Energy Absorption Capability and Crashworthiness of Composite Material Structures: A Review. Applied Mechanics Reviews. 1998;51(10):635.

[41] Ramakrishna S, Hamada H. Energy Absorption Characteristics of Crash Worthy Structural Composite Materials. Key Engineering Materials. 1998;141–143:585–622.

[42] Lukaszewicz D, Blok L, Kratz J, Ward C, Kassapoglou C. Experimental and numerical investigation of full scale impact test on fibre-reinforced plastic sandwich structure for automotive crashworthiness. International Journal of Automotive Composites. 2017;3(2/3/4):339–53.

[43] Global Registry. Global technical regulation on on pole side impact. 2014.

[44] Lukaszewicz D, Engel S, Boegle C. Testing of sandwich structures with CFRP skins in edgewise compression. In: 19th International Conference on Composite Materials. Montreal, Canada; 2013.

[45] Blok LG, Kratz J, Lukaszewicz D, Hesse SH, Ward C, Kassapoglou C. Improvement of the in-plane crushing response of CFRP sandwich panels by through-thickness reinforcements. Composite Structures. 2017 Feb;161:15–22.

[46] Lukaszewicz D. Automotive Composite Structures for Crashworthiness. In: Elmarakbi A, editor. Advanced Composite Materials for Automotive Applications: Structural Integrity and Crashworthiness. First Edit. John Wiley & Sons Ltd; 2014.

p. 99–127.

[47] Cetim, Momentive develop composite crashbox concept [Internet]. SAE International. 2014 [cited 2017 Dec 7]. Available from: http://articles.sae.org/13366/

[48] Dufour C, Boussu F, Wang P, Soulat D. Local strain measurements of yarns inside of 3D warp interlock fabric during forming process. International Journal of Material Forming. 2017;

[49] King D. BMW i3 called “most revolutionary car” since Ford Model T - [Internet]. Autoblog. 2015 [cited 2018 Jul 7]. Available from: https://www.autoblog.com/2015/01/16/bmw-i3-called-most-revolutionary-car-since-ford-model-t/#slide-97745

[50] Adams DF. Testing the crashworthiness of composite structures [Internet]. Composites World. 2012 [cited 2015 Aug 18]. Available from: http://www.compositesworld.com/articles/testing-the-crashworthiness-of-composite-structures

[51] ICONIC [Internet]. Iconic. 2018 [cited 2018 Aug 19]. Available from: https://blog.qub.ac.uk/wordpress/iconic/background/

[52] Crashworthiness of Carbon Fiber Composites [Internet]. Oak Ridge National Laboratory. 2017 [cited 2017 Nov 24]. Available from: http://energy.ornl.gov/CFCrush/test_method/test_method.cgi?nav=1

[53] Thornton PH. Energy Absorption in Composite Structures. Journal of Composite Materials. 1979 Jan 1;13(3):247–62.

[54] Hull D. Energy Absorption of Composite Materials Under Crash Conditions. In: 4th International Conference on Composite Materials. Tokyo, Japan; 1982.

[55] Farley GL. Energy absorption of composite material and structure. In: 43rd Annual Forum of the American Helicopter Society. St Louis, USA; 1987.

[56] Hull D. A unified approach to progressive crushing of fibre-reinforced composite

tubes. Composites Science and Technology. 1991 Jan;40(4):377–421.

[57] Farley GL, Jones RM. Crushing characteristics of continuous fiber-reinforced composite tubes. Journal of composite Materials. 1992;(1):37–50.

[58] Jacob GC, Starbuck JM, Fellers JF, Simunović S. Effect of fiber volume fraction, fiber length and fiber tow size on the energy absorption of chopped carbon fiber-polymer composites. Polymer Composites. 2005 Jun;26(3):293–305.

[59] Jacob GC, Starbuck JM, Fellers JF, Simunović S, Boeman RG. Crashworthiness of various random chopped carbon fiber reinforced epoxy composite materials and their strain rate dependence. Journal of Applied Polymer Science. 2006 Aug 5;101(3):1477–86.

[60] Feraboli P, Peitso E, Deleo F, Cleveland T, Stickler PB. Characterization of Prepreg-Based Discontinuous Carbon Fiber/Epoxy Systems. Journal of Reinforced Plastics and Composites. 2009 Jun 4;28(10):1191–214.

[61] Zenkert D. An Introduction to Sandwich Construction. London: Chameleon Press Ltd.; 1997.

[62] Karlsson KF, Tomas Åström B. Manufacturing and applications of structural sandwich components. Composites Part A: Applied Science and Manufacturing. 1997;28(2):97–111.

[63] Vinson JR. Sandwich Structures. Applied Mechanics Reviews. 2001 Aug 15;54(3):201.

[64] Laurin F, Vizzini AJ. Energy Absorption of Sandwich Panels with Composite-Reinforced Foam Core. Journal of Sandwich Structures and Materials. 2005 Mar 1;7(March 2005):113–32.

[65] Hou Y, Neville R, Scarpa F, Remillat C, Gu B, Ruzzene M. Graded conventional-auxetic Kirigami sandwich structures: Flatwise compression and edgewise loading. Composites Part B: Engineering. 2014 Mar;59:33–42.

[66] Kassapoglou C, Jonas P, Abbott R. Compressive Strength of Composite Sandwich

Panels After Impact Damage: An Experimental and Analytical Study. Journal of Composites Technology and Research. 1988;10(2):65.

[67] Sun CT, Wu CL. Low velocity impact of composite sandwich panels. In: 32nd Structures, Structural Dynamics, and Materials Conference. Reston, Virigina: American Institute of Aeronautics and Astronautics; 1991.

[68] Minguet P. A model for predicting the behavior of impact-damaged minimum gage sandwich panels under compression. In: 32nd Structures, Structural Dynamics, and Materials Conference. Reston, Virigina: American Institute of Aeronautics and Astronautics; 1991.

[69] Goldsmith W, Sackman JL. An experimental study of energy absorption in impact on sandwich plates. International Journal of Impact Engineering. 1992;12(2):241–62.

[70] Borazjani S, Belingardi G. Development of an innovative design of a composite-sandwich based vehicle roof structure. Composite Structures. 2017 May;168:522–34.

[71] Mamalis AG, Manolakos DE, Ioannidis MB, Kostazos PK. Axial crushing of hybrid square sandwich composite vehicle hollow bodyshells with reinforced core: Experimental. International Journal of Crashworthiness. 2001;6(3):363–76.

[72] Mamalis AG, Manolakos DE, Ioannidis MB, Papapostolou DP, Kostazos PK, Konstantinidis DG. On the compression of hybrid sandwich composite panels reinforced with internal tube inserts: Experimental. Composite Structures. 2002;56:191–9.

[73] Mamalis AG, Manolakos DE, Ioannidis MB, Papapostolou DP. On the crushing response of composite sandwich panels subjected to edgewise compression: Experimental. Composite Structures. 2005 Nov;71(2):246–57.

[74] Mamalis AG, Papapostolou DP. Experimental investigation of strain rate effects on the crushing characteristics of composite sandwich panels. International Journal of Crashworthiness. 2010 Dec 15;15(6):581–603.

[75] Torre L, Kenny JM. Evaluation of energy absorption properties of crashworthy sandwich structures. Advancing Affordable Materials Technology. 2001;33:1478–90.

[76] Velecela OJ, Soutis C. Crushing Morphology of Composite Sandwich Panels Under Edgewise Compression. Journal of Composite Materials. 2009;43(9):1035–49.

[77] Lindström A, Hallström S. Energy absorption of SMC/balsa sandwich panels with geometrical triggering features. Composite Structures. 2010 Oct;92(11):2676–84.

[78] Pitarresi G, Carruthers JJ, Robinson AM, Torre G, Kenny JM, Ingleton S, et al. A comparative evaluation of crashworthy composite sandwich structures. Composite Structures. 2007 Mar;78(1):34–44.

[79] Czaplicki MJ, Robertson RE, Thornton PH. Comparison of bevel and tulip triggered pultruded tubes for energy absorption. Composites Science and Technology. 1991 Jan;40(1):31–46.

[80] Dransfield K, Baillie C, Mai YW. Improving the delamination resistance of CFRP by stitching-a review. Composites Science and Technology. 1994;50(3):305–17.

[81] Mouritz AP. Review of z-pinned composite laminates. Composites Part A: Applied Science and Manufacturing. 2007 Dec;38(12):2383–97.

[82] Gnaba I, Legrand X, Wang P, Soulat D. Through-the-thickness reinforcement for composite structures: A review. Journal of Industrial Textiles. 2018 Apr 26;152808371877229.

[83] Palazotto AN, Gummadi LNB, Vaidya UK, Herup EJ. Low velocity impact damage characteristics of Z-fiber reinforced sandwich panels - an experimental study. Composite Structures. 1998;43:275–88.

[84] Marasco AI. Analysis and evaluation of mechanical performance of reinforced sandwich structures: X-Cor and K-Cor. Cranfield University; 2005.

[85] Rice MC, Fleischer CA, Zupan M. Study on the Collapse of Pin-Reinforced Foam Sandwich Panel Cores. Experimental Mechanics. 2006;46(2):197–204.

[86] Du L, Guiqiong J, Tao H. Z-pin Reinforcement on the Core Shear Properties of Polymer Foam Sandwich Composites. Journal of Composite Materials. 2009;43(3):289–300.

[87] Haldar S, Bruck HA. A New Methodology for Scaling the Mechanics of Pin-reinforcement in Composite Sandwich Structures under Compression using Digital Image Correlation. Experimental Mechanics. 2015 Aug 7;55:27–40.

[88] Marasco AI, Cartié DDR, Partridge IK, Rezai A. Mechanical properties balance in novel Z-pinned sandwich panels: Out-of-plane properties. Composites Part A: Applied Science and Manufacturing. 2006;37:295–302.

[89] Martakos G, Andreasen JH, Berggreen C, Thomsen OT. Experimental investigation of interfacial crack arrest in sandwich beams subjected to fatigue loading using a novel crack arresting device. Journal of Sandwich Structures & Materials. 2017 Jan;109963621769505.

[90] Martakos G, Andreasen JH, Berggreen C, Thomsen OT. Interfacial Crack Arrest in Sandwich Panels with Embedded Crack Stoppers Subjected to Fatigue Loading. Applied Composite Materials. 2017 Feb 18;24(1):55–76.

[91] Aktas A, Potluri P, Porat I. Development of Through-Thickness Reinforcement in Advanced Composites Incorporating Rigid Cellular Foams. Applied Composite Materials. 2013 Aug 16;20(4):553–68.

[92] Dell'Anno G, Treiber JWG, Partridge IK. Manufacturing of composite parts reinforced through-thickness by tufting. Robotics and Computer-Integrated Manufacturing. 2016 Feb;37:262–72.

[93] Potluri P, Kusak E, Reddy TY. Novel stitch-bonded sandwich composite structures. Composite Structures. 2003 Feb;59(2):251–9.

[94] Lascoup B, Aboura Z, Khellil K, Benzeggagh M. On the mechanical effect of stitch addition in sandwich panel. Composites Science and Technology. 2006;66:1385–98.

[95] Lascoup B, Aboura Z, Khellil K, Benzeggagh M. Impact response of three-

dimensional stitched sandwich composite. Composite Structures. 2010;92(2):347–53.

[96] Xia F, Wu X-Q. Study on impact properties of through-thickness stitched foam sandwich composites. Composite Structures. 2010 Jan;92(2):412–21.

[97] Xia F, Wu X-Q, Li J-L. Numerical Simulation of Impact Responses on Through-thickness Stitched Foam Core Sandwich Composite. Applied Composite Materials. 2013 Dec 24;20(6):1041–54.

[98] Ma J, Yan Y, Liu YJ, Yang L. Compression strength of stitched foam-core sandwich composites with impact induced damage. Journal of Reinforced Plastics and Composites. 2012 Aug 21;31(18):1236–46.

[99] Wang P, Lei Y, Yue Z. Experimental and numerical evaluation of the flexural properties of stitched foam core sandwich structure. Composite Structures. 2013 Jun;100:243–8.

[100] Shigang A, Yiqi M, Yongmao P, Daining F, Liqun T. Effect of stitching angle on mechanical properties of stitched sandwich panels. Materials and Design. 2013 Sep;50:817–24.

[101] Sickinger C, Herrmann A. Structural stitching as a method to design high-performance composites in future. Proceedings of the TechTextil Symposium. 2001;

[102] Wittig J. In-mold-reinforcement of preforms by 3-dimensional tufting. In: 47th International SAMPE Symposium and Exhibition. Long Beach, USA; 2002. p. 1043–51.

[103] Wittig J. Recent Developments in the Robotic Stitching Technology for Textile Structural Composites. Journal of Textile and Apparel, Technology and Management. 2001;2(1):1–8.

[104] Dell'Anno G, Cartié DDR, Partridge IK, Rezai A. Exploring mechanical property balance in tufted carbon fabric/epoxy composites. Composites Part A: Applied Science and Manufacturing. 2007;38(11):2366–73.

[105] Masa SK, Mallya AB, Dhanapal K, Ramachandra RV, Kishore. Post-failure Analysis and Fractography of In-plane Tension-Tested Tufted Carbon Fabric-Reinforced Epoxy Composite Laminates. Journal of Materials Engineering and Performance. 2015 Apr 12;24(4):1581–6.

[106] Cartié DDR, Dell'Anno G, Poulin E, Partridge IK. 3D reinforcement of stiffener-to-skin T-joints by Z-pinning and tufting. Engineering Fracture Mechanics. 2006;73:2532–40.

[107] Harman D, Grove S, Summerscales J. The economics of through-thickness fibre reinforcement using single sided robotic tufting. In: 16th European Conference on Composite Materials. Seville, Spain; 2014.

[108] Harman D. An economic evaluation of the robotic tufting process considering the application of a novel composite wing rib post. University of Plymouth; 2013.

[109] Wang Y, Soutis C. Modelling the effect of tufted yarns in composite T-joints. Engineering and Computational Mechanics. 2016 Dec;169(4):158–70.

[110] Clegg HM, Kratz J, Partridge I, Dell'Anno G. Evaluation of the effects of tufting on performance of composite T-joints. In: 17th European Conference on Composite Materials. Munich, Germany; 2016.

[111] Clegg H, Dell'Anno G, Partridge IK. Creating intersections in composites structures using tufted and 3D woven connectors. In: 7th International Symposium on Aircraft Materials (ACMA 2018). Compiègne, France; 2018. p. 189–96.

[112] Kratz J, Clegg HM, Dell'Anno G, Partridge IK. Improving the Damage Tolerance of Composite Joints with Tufting. In: 20th International Conference on Composite Materials. Copenhagen, Denmark; 2015.

[113] Scarponi C, Perillo AM, Cutillo L, Foglio C. Advanced TTT composite materials for aeronautical purposes: Compression after impact (CAI) behaviour. Composites Part B: Engineering. 2007;38(2):258–64.

[114] Colin de Verdiere M, Pickett AK, Skordos AA, Witzel V. Effect of tufting on the response of non crimp fabric composites. In: ECCOMAS Thematic Conference on

Mechanical Response of Composites. Porto, Portugal; 2007.

[115] Colin de Verdiere M, Pickett AK, Skordos AA, Witzel V. Evaluation of the mechanical and damage behaviour of tufted non crimped fabric composites using full field measurements. Composites Science and Technology. 2009;69(2):131–8.

[116] Colin de Verdiere M, Skordos AA, May M, Walton AC. Influence of loading rate on the delamination response of untufted and tufted carbon epoxy non crimp fabric composites: Mode I. Engineering Fracture Mechanics. 2012;96:11–25.

[117] Colin de Verdiere M, Skordos AA, May M, Walton AC. Influence of loading rate on the delamination response of untufted and tufted carbon epoxy non crimp fabric composites: Mode II. Engineering Fracture Mechanics. 2012;96:11–25.

[118] Wang P, Legrand X, Soulat D, Liu L, Tricaud M. Experimental Investigation of the Tufted 3-Dimensional Composite Reinforcement Forming. In: 21st International Conference on Composite Materials. Xi'an, China; 2017.

[119] Liu L, Zhang T, Wang P, Legrand X, Soulat D. Influence of the tufting yarns on formability of tufted 3-Dimensional composite reinforcement. Composites Part A: Applied Science and Manufacturing. 2015;78:403–11.

[120] Liu L, Wang P, Legrand X, Soulat D. Investigation of mechanical properties of tufted composites: Influence of tuft length through the thickness reinforcement. Composite Structures. 2017 Jul;172:221–8.

[121] Gnaba I, Wang P, Legrand X, Soulat D. Manufacturing and characterisation of tufted preform with complex shape. In: 7th International Symposium on Aircraft Materials (ACMA 2018). Compiègne, France; 2018. p. 167–75.

[122] Préau M, Treiber J, Partridge IK. Deformation and failure in a tufted carbon fabric/epoxy Ω – stiffener. In: Comptes Rendus des JNC 17. Poitiers, France; 2011.

[123] Martins AT, Aboura Z, Laksimi A, Khellil K, Harizi W. An experimental study of the mechanical behavior of omega stiffeners reinforced by tufting process. In: 7th International Symposium on Aircraft Materials (ACMA 2018). Compiègne, France; 2018. p. 157–65.

[124] Scott M, Dell'Anno G, Clegg H. Effect of Process Parameters on the Geometry of Composite Parts Reinforced by Through-the-Thickness Tufting. Applied Composite Materials. 2018 Jun 20;

[125] Deconinck P, Capelle J, Bouchart V, Chevrier P, Ravailler F. Delamination propagation analysis in tufted carbon fibre-reinforced plastic composites subjected to high-velocity impact. Journal of Reinforced Plastics and Composites. 2014 Jul 1;33(14):1353–63.

[126] French MA. Improved Damage Tolerance in Composite Armour through 3D Tufting. In: 28th International Symposium on Ballistics. Atlanta, USA; 2014.

[127] Henao A, Carrera M, Miravete A, Castejón L. Mechanical performance of through-thickness tufted sandwich structures. Composite Structures. 2010 Aug;92(9):2052–9.

[128] Henao A, Guzmán de Villoria R, Cuartero J, Carrera M, Picón J, Miravete A. Enhanced Impact Energy Absorption Characteristics of Sandwich Composites through Tufting. Mechanics of Advanced Materials and Structures. 2015 Dec 2;22(12):1016–23.

[129] Blok LG, Kratz J, Lukaszewicz D, Hesse SH, Kassapoglou C, Ward C. Improvement of the In-plane Crushing Response of CFRP Sandwich Panels by Through-thickness Reinforcements. In: 17th European Conference on Composite Materials. Munich, Germany; 2016.

[130] SGL Group. SIGRAFIL Continuous Carbon Fiber Tow. 2018.

[131] SGL Group. Textile Materials Made from Carbon, Glass, and Aramid Fibers. 2017.

[132] SGL Group. Recatex Carbon Fiber Nonwoven Complex. 2014.

[133] Momentive. EPIKOTE™ 935 Technical Data Sheet. 2006.

[134] Evonik Industries. Rohacell IG/IG-F Technical Information. 2014.

[135] Kratz J, Low YS, Fox B. Resource-friendly carbon fiber composites: combining

production waste with virgin feedstock. Advanced Manufacturing: Polymer & Composites Science. 2017 Oct 2;3(4):121–9.

[136] Blok LG. Testing and simulation of CFRP sandwiches with and without z-reinforcements during impact. Delft University of Technology; 2014.

[137] Tan G, Hartley JW, Withers E, Kratz J. Towards the Development of an Instrumented Test Bed for Tufting Visualisation. In: SAMPE Europe Conference. Amiens, France; 2015.

[138] Tan G. Exploring the effect on the tufting quality by the manufacturing characteristics in the tufting process. University of Bristol; 2015.

[139] Hartley J. Crash Simulation of Tufted Sandwich Components for Automotive Applications. University of Bristol; 2014.

[140] Hartley JW, Kratz J, Ward C, Partridge IK. Effect of tufting density and loop length on the crushing behaviour of tufted sandwich specimens. Composites Part B: Engineering. 2017 Mar;112:49–56.

[141] Treiber JWG. Performance of tufted carbon fibre/epoxy composites. Cranfield University; 2011.

[142] Siromani D, Henderson G, Mikita D, Mirarchi K, Park R, Smolko J, et al. An experimental study on the effect of failure trigger mechanisms on the energy absorption capability of CFRP tubes under axial compression. Composites Part A: Applied Science and Manufacturing. 2014 Sep;64:25–35.

[143] Warzok F, Allegri G, Gude M, Hallett SR. Experimental characterisation of fatigue damage in single Z-pins. Composites Part A: Applied Science and Manufacturing. 2016 Dec;91:461–71.

[144] Osmiani C, Mohamed G, Treiber JWG, Allegri G, Partridge IK. Exploring the influence of micro-structure on the mechanical properties and crack bridging mechanisms of fibrous tufts. Composites Part A: Applied Science and Manufacturing. 2016 Dec;91:409–19.

[145] ASTM International. C364 - Standard Test Method for Edgewise Compressive Strength of Sandwich Constructions. In: Annual Book of ASTM Standards. 1999. p. 1–2.

[146] Velecela OJ, Soutis C. Prediction of crushing morphology of GRP composite sandwich panels under edgewise compression. Composites Part B: Engineering. 2007 Oct;38(7–8):914–23.

[147] Farley GL, Dickinson LC. Removal of Surface Loop from Stitched Composites Can Improve Compression and Compression-after-Impact Strengths. Journal of Reinforced Plastics and Composites. 1992 Jun 18;11(6):633–42.

[148] Hartley JW, Tse G, Kratz J, Ward C, Partridge IK. Column interaction in tufted sandwich structures under edgewise loading. In: 17th European Conference on Composite Materials. Munich, Germany; 2016.

[149] Tse G. Exploring tufted sandwich structures in edgewise compression by novel failure control. University of Bristol; 2016.

[150] Stanley LE, Adams DO. Development and Evaluation of Stitched Sandwich Panels. 2001.

[151] Hartley JW, Ward C. Improving the Understanding of Tufted Energy Absorbing Sandwich Structures. In: American Society for Composites 2017. Lancaster, PA: DEStech Publications, Inc.; 2017. p. 2260–73.

[152] Hartley J, Dyson M, Ward C. Improving the Performance of Tufted Composite Sandwich Structures. In: 21st International Conference on Composite Materials. Xi'an, China; 2017.

[153] Dyson M. Exploring the effects of column interaction in tufted sandwich cores. University of Bristol; 2017.

[154] Makabe C, Murdani A, Kuniyoshi K, Irei Y, Saimoto A. Crack-growth arrest by redirecting crack growth by drilling stop holes and inserting pins into them. Engineering Failure Analysis. 2009 Jan;16(1):475–83.

[155] Hartley J, Bogucki P, Snudden J, Withers E, Ward C, Kratz J. Reclaiming in-process composite waste for use in energy absorbing sandwich structures. In: International SAMPE Technical Conference. 2016.

[156] Bogucki P. Reclaiming in-process composite waste for use in energy absorbing sandwich structures. University of Bristol; 2016.

[157] Singh P, Saponara V La. Experimental Investigation on Performance of Angle-Stitched Sandwich Structures. In: 45th AIAA/ASME/ASCE/AHS/ASC Structures, Structural Dynamics & Materials Conference. Palm Springs, USA; 2004.

[158] Obradovic J, Boria S, Belingardi G. Lightweight design and crash analysis of composite frontal impact energy absorbing structures. Composite Structures. 2012 Jan;94(2):423–30.

[159] Greve L, Pickett AK. Delamination testing and modelling for composite crash simulation. Composites Science and Technology. 2006 May;66(6):816–26.

[160] Barnes G, Nixon S, Schrank M. Composite Crush Simulation - Emerging Technologies and Methodologies. 2009.

[161] Kerth S, Maier M, Nohr M. Modeling of the Crash Behaviour of Edge Loaded Sandwich Structures with Fibre Reinforced Polymer Faces. Mechanics of Sandwich Structures. 1998;37–44.

[162] Mamalis AG, Manolakos DE, Ioannidis MB, Kostazos PK, Papapostolou DP. Axial collapse of hybrid square sandwich composite tubular components with corrugated core: Numerical modelling. Composite Structures. 2002 Dec;58(4):571–82.

[163] Mamalis AG, Spentzas KN, Papapostolou DP, Pantelelis N. Finite element investigation of the influence of material properties on the crushing characteristics of in-plane loaded composite sandwich panels. Thin-Walled Structures. 2013 Feb;63:163–74.

[164] Mamalis AG, Manolakos DE, Ioannidis MB, Kostazos PK. Crushing of hybrid square sandwich composite vehicle hollow bodyshells with reinforced core subjected to axial loading: Numerical simulation. Composite Structures. 2003

Aug;61(3):175–86.

[165] Chang FK, Chang KY. A Progressive Damage Model for Laminated Composites Containing Stress Concentrations. Journal of Composite Materials. 1987;21:834–55.